

## **Distribution Agreement**

In presenting this thesis or dissertation as a partial fulfillment of the requirements for an advanced degree from Emory University, I hereby grant to Emory University and its agents the non-exclusive license to archive, make accessible, and display my thesis or dissertation in whole or in part in all forms of media, now or hereafter known, including display on the world wide web. I understand that I may select some access restrictions as part of the online submission of this thesis or dissertation. I retain all ownership rights to the copyright of the thesis or dissertation. I also retain the right to use in future works (such as articles or books) all or part of this thesis or dissertation.

Signature:

---

**Kelly R. Morrison**

---

Date

**Complementary Approaches to Combat Antibacterial Resistance: Metal-binding Small Molecules  
and Quaternary Ammonium Compounds**

By

Kelly R. Morrison  
Doctor of Philosophy

Chemistry

---

William, M. Wuest, Ph.D.  
Advisor

---

Simon B. Blakey, Ph.D.  
Committee Member

---

David G. Lynn, Ph.D.  
Committee Member

Accepted:

---

Lisa A. Tedesco, Ph.D.  
Dean of the James T. Laney School of Graduate Studies

---

Date

**Complementary Approaches to Combat Antibacterial Resistance: Metal-binding Small Molecules  
and Quaternary Ammonium Compounds**

By

Kelly R. Morrison

B.S., St. Bonaventure University, 2013

M.S., Rochester Institute of Technology, 2015

Advisor: William M. Wuest, Ph.D.

An abstract of

A dissertation submitted to the Faculty of the  
James T. Laney School of Graduate Studies of Emory University  
in partial fulfillment of the requirements for the degree of  
Doctor of Philosophy in Chemistry

2020

## Abstract

### **Complementary Approaches to Combat Antibacterial Resistance: Metal-binding Small Molecules and Quaternary Ammonium Compounds**

By Kelly R. Morrison

Antibiotic resistance is a complex problem that has a far-reaching and destructive impact on life including health care, agriculture, and food-handling industries. All classes of antibiotics currently in use inhibit the same few biological targets allowing for rapid bacterial resistance development. With this in mind, my dissertation focuses on synthesizing and investigating natural products and small molecules that may inhibit bacteria in new ways. One area of my research is focused on investigating siderophores which are small iron-binding secondary metabolites that contribute to bacteria's pathogenicity. Alternatively, a general method for sterilization is still needed for surfaces to keep food production centers and hospitals clean. Quaternary Ammonium Compounds (QACs) provide a broad-spectrum class of antibiotics that allow for bacterial killing without hitting a specific metabolic target by perturbing and lysing phospholipid membranes leading to cell death. Unfortunately, resistance to QACs are also on the rise and as such warrant further investigation into resistance mechanisms and the development of more potent compounds with novel structures.



**Complementary Approaches to Combat Antibacterial Resistance: Metal-binding Small Molecules  
and Quaternary Ammonium Compounds**

By

Kelly R. Morrison

B.S., St. Bonaventure University, 2013

M.S., Rochester Institute of Technology, 2015

Advisor: William M. Wuest, Ph.D.

A dissertation submitted to the Faculty of the  
James T. Laney School of Graduate Studies of Emory University  
in partial fulfillment of the requirements for the degree of  
Doctor of Philosophy in Chemistry

2020

Acknowledgements:

First and foremost, I thank God for his grace and mercy. Without Him, I would not be here.

Second, I thank my amazing parents. Throughout my whole life they have shown me patience and love. I never once doubted their faith in me. They constantly encouraged me to keep perusing my goals no matter how tough it was. Thank you for believing in me, for listening to my fears, and for giving me courage. Dad, thank you for all your sacrifices and for instilling in me that education is a gift, not to be taken for granted – this one's for you!

I thank my amazing fiancé, Rick. His support and confidence in me is what gets me through the day-to-day. Thank you for being with me on this crazy graduate school journey. Thank you for moving with me, to Atlanta, around Atlanta, and finally back to Philly! Thank you for agreeing to adopt Stella-Beer with me, the cutest and snuggliest of all puppers. Most importantly, thank you for loving me for who I am, always.

Thank you to my adopted family, my friends who are always there to support me, to pick me up when I'm down, or to make me laugh until I cry. Amanda, Michala, Maggie, Dawn, Bill, Joe, Brendan, Michelle, and Nick you are all amazing people and I am so thankful for your presence in my life.

Bill, thank you for taking a chance on a master's student from Rochester, and thank you for the continued support through the bumpy graduate school experience.

Thank you to the amazing Wuest lab members both past and present. Alex Koval, thank you for being my first friend in the lab and the best mentor. Thank you to the Temple crew who moved with me to Atlanta, for both laughing and crying with me as we all transitioned to a new environment. Thank you to my year-mate, Amy, for helping me to not take life too seriously and making goofy bird calls to liven everyone's day. Thank you Ingrid, Guillaume, Ryan, and Sean for being amazing office mates and friends. Thank you Justin, Ryan, and Savannah for being invaluable teammates. Thank you to the rest of my friends in the Wuest lab, you have all made the graduate school experience fun and full of laughter. Also, a big thank you to Maddie and Chris for being the best roommates while writing this!

Thank you to the Emory community for their encouragement and support, especially my committee members Dr. Blakey and Dr. Lynn, as well as Steve, Claire, Fred, and Kira.

# Table of Contents

1	Introduction.....	1
2.	Synthesis and Biological Investigation of Iron-binding Natural Products.....	1
2.1	Bacterial Iron Acquisition and Storage.....	1
2.2	Iron Uses and Functions.....	2
2.3	Siderophores .....	4
2.3.1.	Pyochelin.....	5
2.4	Ulba ctins .....	7
2.4.1.	Isolation.....	7
2.4.2.	Biosynthetic Route to Ulba ctin .....	9
2.4.3.	First Total Synthesis of Ulba ctin F .....	11
2.4.4.	Metal-binding studies.....	17
2.4.5.	Biological Investigation of Ulba ctin F.....	21
2.4.6.	Analog Design and Synthesis .....	23
2.5	Watasemy cins and Thiazostatins .....	25
2.5.1.	Isolation of Thiazostatins and Watasemy cins .....	25
2.5.2.	Progress Towards the Total Synthesis of Watasemy cins and Thiazostatins.....	27
2.6	Conclusion .....	38
2.7	References.....	38
3.	Quaternary Ammonium Compounds .....	1
3.1	General QAC Structure and Mechanism of Action .....	1
3.2	Polymeric Quaternary Ammonium Compounds (polyQACs).....	3
3.2.1.	The Haldar Group .....	3
3.2.2.	The Finn Group.....	5
3.2.3.	The Tiller Group .....	6
3.3	QACs as small molecules .....	9
3.3.1.	Commercial QACs.....	9
3.3.2.	Aminosterols as QACs.....	9
3.3.3.	Repurposing Known Antibiotics.....	12
3.3.2.1	Vancomycin Analogs by the Boger Lab .....	12
3.3.2.2.	Polymyxin B Analogs with the Pires Lab.....	14
3.3.2.	Minbiole-Wuest Labs: Collaborative QAC Development .....	20
3.3.3.1.	TMEDA Inspired QACs: the start of a beautiful thing .....	21
3.4.	QAC Resistance .....	32

3.5. QAC activity against clinically isolated bacteria .....	37
3.5.1. Acinetobacter baumannii .....	39
3.5.2. Pseudomonas aeruginosa .....	42
3.5.3. Future Experimentation.....	44
3.6 Conclusions.....	47
3.7 References.....	47
4. Supporting Information.....	55

## List of Figures:

### Chapter 2:

Figure 2.1: Iron acquisition pathways in Gram-negative and Gram-positive bacteria .....	2
Figure 2.2: TCA cycle highlighting iron-bound aconitase.....	3
Figure 2.3: Common siderophore moieties responsible for metal binding .....	4
Figure 2.4: Structural diversity of siderophores and their producing organisms .....	5
Figure 2.5: Mislin et al. first generation analogs .....	6
Figure 2.6: Mislin et al. second generation analogs for fluorescent tracking .....	7
Figure 2.7: Location and structure of ulbactins F and G by Igarashi et al. ....	8
Figure 2.8: The ulbactin family as reported in a Japanese patent .....	8
Figure 2.9: Crystal structures of ulbactins F and G as reported by Igarashi et al.....	8
Figure 2.10: NRPS biosynthesis of ulbactins F and G as proposed by Igarashi et al. ....	10
Figure 2.11: Structural comparison of ulbactins F and G to yersiniabactin and micacocidin A.....	11
Figure 2.12: Crystal structure and assignment of epi-ulbactin F .....	16
Figure 2.13: Thought experiment to explain lack of ulbactin G synthesis .....	17
Figure 2.14: Colorimetric binding assays with two iron(III) sources .....	18
Figure 2.15: CAS media assay to test qualitative iron binding of ulbactin F and epi-ulbactin F .....	19
Figure 2.16: Fluorescence titration curves for Fe(III), Cu(II), Al(III), Ni(II), Zn(II), and relative metal selectivity plot.....	20
Figure 2.17: Computational modeling of ulbactin F-Fe(III) binding.....	21
Figure 2.18: Proposed analogs of ulbactin F and their relative CLogP values .....	24
Figure 2.19: Structures of thiazostatins and watasemycins with their relative isolation amounts .....	26

### Chapter 3:

Figure 3.1 Generally accepted QAC mechanism of action.....	2
Figure 3.2: Geng et al. polyQACs.....	5
Figure 3.3: General PBI structure and activity against select bacteria.....	7
Figure 3.4: General structure of self-deactivating polyQACs .....	7
Figure 3.5: General structures for ciprofloxacin-polyQAC chimeras.....	8
Figure 3.6: Common commercial QACs .....	9
Figure 3.7: Aminosterol structures and biological activities .....	11
Figure 3.8: Aminosterol structures and biological activities .....	13
Figure 3.9: Overview of Boger lab QAC-vancomycin analogs and their activity against VanA E. faecalis .....	14
Figure 3.10: Polymyxin B structure highlighting the conserved cyclic peptide core for Pires lab analogs	15
Figure 3.11: Polymyxin B-QAC analogs synthesized by Pires lab .....	16
Figure 3.12: General structure and design of TMEDA-based QACs .....	21
Figure 3.13: General structure and design of bis-, tris-, and tetraQACs.....	22
Figure 3.14: Conceptual design of bisQACs for core rigidity investigation.....	26
Figure 3.15: Depiction of the QacR-QacA resistance mechanism .....	34
Figure 3.16: Mono- and Tris-dye QACs used for QacR binding experiments .....	35
Figure 3.17: Best in class QACs for testing against clinically isolated bacteria.....	38

Figure 3.18: General scope of the <i>A. baumannii</i> panel from Walter Reed Medical Center .....	39
Figure 19: General scope of the <i>P. aeruginosa</i> panel from Walter Reed Medical Center.....	42
Figure 3.20: An example of observed MICs in QAC assays .....	45

## List of Schemes:

### Chapter 2:

Scheme 2.1: First synthesis of pyochelin by Ankenbauer et al.....	6
Scheme 2.2: Retrosynthetic analysis of ulbactins F and G .....	12
Scheme 2.3: Synthesis of phenol-thiazoline intermediate .....	12
Scheme 2.4: Parallel routes to form protected thiazolidine intermediate <b>2.40</b> .....	13
Scheme 2.5: First generation end-game route to ulbactins F and G .....	13
Scheme 2.6: Second generation cascade route to ulbactins F and G .....	15
Scheme 2.7: Attempt to form aldehyde <b>2.16</b> through bisulfite salt .....	16
Scheme 2.8: Synthetic route to stereospecific synthesis of ulbactin F.....	24
Scheme 2.9: Retrosynthetic analysis of watasemycins and thiazostatin .....	27
Scheme 2.10: Masterson method to synthesize $\alpha$ -methyl cysteine derivatives .....	28
Scheme 2.11: Kedrowski method towards $\alpha$ -methyl cysteine derivatives.....	29
Scheme 2.12: Attempt at adapting Kedrowski method to watasemycins and thiazostatin synthesis .....	30
Scheme 2.13: Pattenden method towards synthesis of $\alpha$ -methyl cysteine derivatives.....	30
Scheme 2.14: Attempts towards N-methyl- $\alpha$ -methyl cysteine through Pattenden method .....	31
Scheme 2.15: Smith et al. $\alpha$ -methyl amino acid synthetic method .....	32
Scheme 2.16: Chakraborty method to synthesize amino acids .....	33
Scheme 2.17: Nickel(II) catalysis to yield $\alpha$ -methyl cysteine.....	34
Scheme 2.18: Camphorsultam method for synthesis of $\alpha$ -methyl cysteine .....	35
Scheme 2.19: Proposed synthesis of N-methyl- $\alpha$ -methyl cysteine based on the method reported by Alezra et al.....	35
Scheme 2.20: Proposed route to N-methyl- $\alpha$ -methyl cysteine .....	36
Scheme 2.21: Threonine substitution method developed by Morell et al. and Ge et al.....	37
Scheme 2.22: Initial attempts at threonine substitution .....	37
Scheme 2.23: Synthesis of $\beta$ -methyl cysteine.....	38

### Chapter 3:

Scheme 3.1: Haldar lab general synthesis of amide QAC polymers .....	4
Scheme 3.2: Synthesis of hybrid bisQACs .....	23
Scheme 3.3: Synthesis of amide-containing hybrid bisQACs .....	24
Scheme 3.4: Synthesis of piperazine-based bisQACs.....	26
Scheme 3.5: Synthesis of amide-containing piperazine bisQACs .....	27
Scheme 3.6: Synthesis of DABCO-core bisQACs and amide-containing DABCO bisQACs .....	27
Scheme 3.7: Synthesis of pyridinium based -ane, -ene, -yne core bisQACs. ....	29
Scheme 3.8: Synthesis of amide-containing alkyne bisQACs .....	30



List of Tables:

Chapter 2:

Table 2.1: Comparison of important <sup>1</sup> H NMR signals to distinguish ulbactins F, G, and epi-F .....	15
Table 2.2: Cancer activity of ulbactin F and G reported by Igarashi et al. ....	22
Table 2.3: Antibiotic activity of watasemycins A and B as reported by Sasaki et al. ....	26

Chapter 3:

Table 3.1: MICs of Geng et al. polyQACs .....	6
Table 3.2: Squalamine as a chemosensitizer of common antibiotics. Squalamine dosed at 1/5 MIC per bacteria strain. (Squalamine MICs were: AG100 2 mg/L; AG100Atet 2 mg/L; PAO1 16 mg/L; PA124 16 mg/L; ATCC13048 8 mg/L; CM-64 8 mg/L.).....	10
Table 3.3: MICs of Polymyxin B-QAC Analogs (E. coli data collected by Pires lab).....	17
Table 3.4: MICs of hybrid bisQACs.....	25
Table 3.5: MICs of first-generation rigidity bisQACs.....	28
Table 3.6: MICs of the -ane, -ene, -yne core rigidity bisQACs.....	31
Table 3.7: MICs of select QACs against qac gene containing SA strains .....	36
Table 3.8: Biological activity of best in class QACs against commercial strains.....	39
Table 3.9: MICs of Best in Class QACs against easiest to kill clinical AB strains .....	40
Table 3.10: MICs of Best in class QACs against hardest to kill clinical AB strains .....	41
Table 3.11: MICs of Best in Class QACs against easiest to kill clinical PA strains.....	43
Table 3.12: MICs of Best in Class QACs against hardest to kill clinical PA strains.....	43

List of Graphs:

Chapter 2:

Graph 2.1: Growth promotion assay of *P. aeruginosa* (PAO1) treated with ulbactin F-Fe<sup>3+</sup> complex ..... 22

Chapter 3:

Graph 3.1: IC<sub>50</sub> data of polymyxin B analogs against CA-MRSA ..... 19

Graph 3.2: IC<sub>50</sub> data of polymyxin B analogs against *P. aeruginosa*..... 19

Graph 3.3: IC<sub>50</sub> data of polymyxin B analogs against *A. baumannii* ..... 20

Abbreviations:

AB	<i>Acinetobacter baumannii</i>
EDC	<i>1-ethyl-3-(3-dimethylaminopropyl)carbodiimide</i>
DMAP	<i>4-dimethylaminopyridine</i>
IC50	<i>50% Inhibition of Growth</i>
A(cys)	<i>Adenylation domain for cysteine incorporation</i>
A	<i>adenylation domain of NRPS</i>
ABC	<i>ATP-binding cassette</i>
BEC	<i>benzethonium chloride</i>
BAC	<i>benzyl alkonium chloride</i>
BAC-12	<i>benzyl alkonium chloride (n = 12)</i>
BGC	<i>biosynthetic gene cluster</i>
CPC	<i>cetyl pyridinium chloride</i>
CTAB	<i>cetyltrimethylammonium bromide</i>
CAS	<i>chrome azurol S</i>
CA-MRSA	<i>Community Acquired Methicillin-Resistant S. aureus</i>
CCCP	<i>cyanide 3-chlorophenylhydrazone</i>
Cy	<i>cyclization domain of NRPS</i>
CF	<i>Cystic Fibrosis</i>
ExbB	<i>cytoplasmic membrane protein</i>
ExbD	<i>cytoplasmic membrane protein</i>
DMP	<i>Dess-Martin Periodinane</i>
DAB	<i>diaminobutryl</i>
DDAC	<i>didecyldimethylammonium chloride</i>
DECP	<i>diethylcyanophosphonate</i>
DIPEA	<i>diisopropylethyl amine</i>
DMSO	<i>dimethyl sulfoxide</i>
DTT	<i>dithiothrietol</i>

Dps	<i>DNA-binding protein that protects against oxidative stress</i>
EC	<i>E. coli</i>
EPA	<i>Environmental Protection Agency</i>
EDTA	<i>ethylenediaminetetraacetic acid</i>
GPP	<i>geranyl pyrophosphate</i>
HA-MRSA	<i>Hospital Acquired Methicillin-Resistant S. aureus</i>
Fe(acac) <sub>3</sub>	<i>Iron(III) acetylacetonate</i>
KP	<i>Klebsiella pneumoniae</i>
LPS	<i>lipopolysaccharide</i>
MgAB	<i>Magnesium dimethylaminoborohydride</i>
MS	<i>Mass Spectrometry</i>
TonB	<i>membrane-bound energy-transducing protein</i>
MT	<i>methyltransferase domain of NRPS</i>
MIC	<i>minimum inhibitory concentration</i>
MDR	<i>multidrug resistant</i>
TMEDA	<i>N,N,N',N'-tetramethylethylenediamine</i>
NDM-1	<i>New Delhi metallo-β-lactamase-1</i>
NRPS	<i>non-ribosomal peptide synthetase</i>
OD <sub>600</sub>	<i>optical density at 600 nm</i>
PA14	<i>P. aeruginosa strain</i>
PAO1	<i>P. aeruginosa strain</i>
PMB	<i>para-methoxybenzyl</i>
PBP	<i>periplasmic binding proteins</i>
PLE	<i>Pig Liver Esterase</i>
PEI	<i>poly(ethylene imine)</i>
PKS	<i>polyketide synthase</i>
polyQAC	<i>polymeric Quaternary Ammonium Compound</i>
PVC	<i>polyvinyl chloride</i>

PA	<i>Pseudomonas aeruginosa</i>
QAC	<i>quaternary ammonium compounds</i>
ROS	<i>reactive oxygen species</i>
SA	<i>S. aureus</i>
SMR	<i>small multidrug efflux pump</i>
SAR	<i>structure-activity relationship</i>
Boc	<i>tert-butyloxycarbonyl</i>
TLC	<i>Thin-Layer Chromatography</i>
TE	<i>thioesterase domain of NRPS</i>
T	<i>thiolation domain of NRPS</i>
TCA cycle	<i>tricarboxylic acid cycle</i>
NEt <sub>3</sub>	<i>triethylamine</i>
TFA	<i>trifluoroacetic acid</i>
TIPSH	<i>Triisopropylsilane</i>
Trt	<i>trityl</i>
VISA	<i>vancomycin-intermediate-resistant Staphylococcus aureus</i>
VREs	<i>vancomycin-resistant Enterococcus faecalis (VanB phenotype)</i>
VREm	<i>vancomycin-resistant Enterococcus faecium (VanA phenotype)</i>
VBNCs	<i>viable but non-culturable cells</i>
WWTPs	<i>Waste Water Treatment Plants</i>

# 1. Introduction

**Stop referring to a coming post-antibiotic era – it’s already here.** You and I are living in a time when some miracle drugs no longer perform miracles and families are being ripped apart by a microscopic enemy. The time for action is now and we can be part of the solution.

- U.S. Center for Disease Control and Prevention, *Antibiotic Resistance Threats in the United States*, **2019**.

This is the first step of four in the CDC’s recent report on antibiotic resistance. This statement certainly is concerning to say the least, and we can only hope that it’s effect is felt by more than just the proverbial choir. The CDC report continues with three additional steps that we, as a community, need to do to stop antibiotic resistance. They are:

- 1) Stop playing the blame game,
- 2) Stop relying *only* on new antibiotics, and
- 3) Stop believing that antibiotic resistance is a problem “over there.”<sup>1</sup>

Essentially, we will only be able to combat antibiotic resistance through a change of attitude and perspective. The work disclosed within this dissertation aims to do just that by developing and researching two distinct pathways to investigate pathogenic bacteria and then use that information to better inform the community about the antibiotic issue at hand.

In the first chapter, we start our journey through a bottom-up approach wherein we leverage privileged structural characteristics to justify our hypotheses about activity of novel compounds. We began that journey through synthesis of novel small molecules hypothesized to be relevant to pathogenic bacteria, followed by extensive characterization of their properties and relevance to pathogenic bacteria. In this approach we are using synthetic organic techniques to build new molecules that at minimum provide us with insight into how bacteria interact with the host through iron acquisition.

The second chapter describes a biological investigation into the activity of novel biocides based on existing commercial active ingredients. Through collaborative efforts, we have designed and investigated compounds against some of the most common pathogenic bacteria that humans and animals come in contact with. Additionally, we are attempting to add a level of real-world context to our research by looking at the effects these compounds have on clinically isolated bacteria, not just common lab strains. We hope that these projects will help inform the community about the necessity for a change in our disinfection practices.

- (1) Frieden, T. CDC. Antibiotic Resistance Threats in the United States. *Centers Dis. Control Prev.* **2019**, 1–148. <https://doi.org/CS239559-B>.

## 2. Synthesis and Biological Investigation of Iron-binding Natural Products

To maintain a competitive growth advantage, bacteria must devise methods to obtain nutrients. This desperate battle is especially crucial in an infection state within a mammalian host. Iron is a crucial resource necessary for bacterial cell composition, metabolism, and in general, for iron-containing proteins to function. Unsurprisingly, humans bind this precious resource very tightly in hemoglobin, transferrin, and lactoferrin leaving the free ferric iron concentration at  $10^{-24}$  M.<sup>1</sup> This prohibits easy access to such a precious resource, at least without specific a mechanism of acquisition. More recent findings suggest that the presence of siderophores, or iron-binding small molecules, in the lungs can trigger an increase in the HIF-1 $\alpha$  signal, causing bacteria to be spread to the spleen where the infection can persist.<sup>2</sup> Additionally, siderophores and the role they play in iron acquisition, have been shown to greatly impact the severity of bacterial infections in the gastro-intestinal tract.<sup>3</sup>

### 2.1 Bacterial Iron Acquisition and Storage

Since iron is so tightly held within cells, bacteria must acquire iron through transferrin, lactoferrin, hemoglobin, or siderophores. Transferrin and lactoferrin are large glycoproteins, whereas hemoglobin and siderophores are small molecules, all of which bind iron reversibly, but at high binding constants. In Gram-negative bacteria, all four of these iron-carriers are too large to fit through the cell membrane porins that facilitate passive diffusion, and therefore need to be actively transported into the cell through a series of outer-membrane receptors, periplasmic binding proteins (PBP), and ATP-binding cassette (ABC) transporters (**Figure 2.1**). Each method of transport also requires the participation of TonB (a membrane-bound energy-transducing protein), ExbB, and ExbD (are both cytoplasmic membrane proteins). Gram-positive bacteria, with their lack of outer-membrane, is facilitated by a membrane-anchored binding protein, permease proteins, and ABC transporter (**Figure 2.1**, inset).<sup>4</sup>



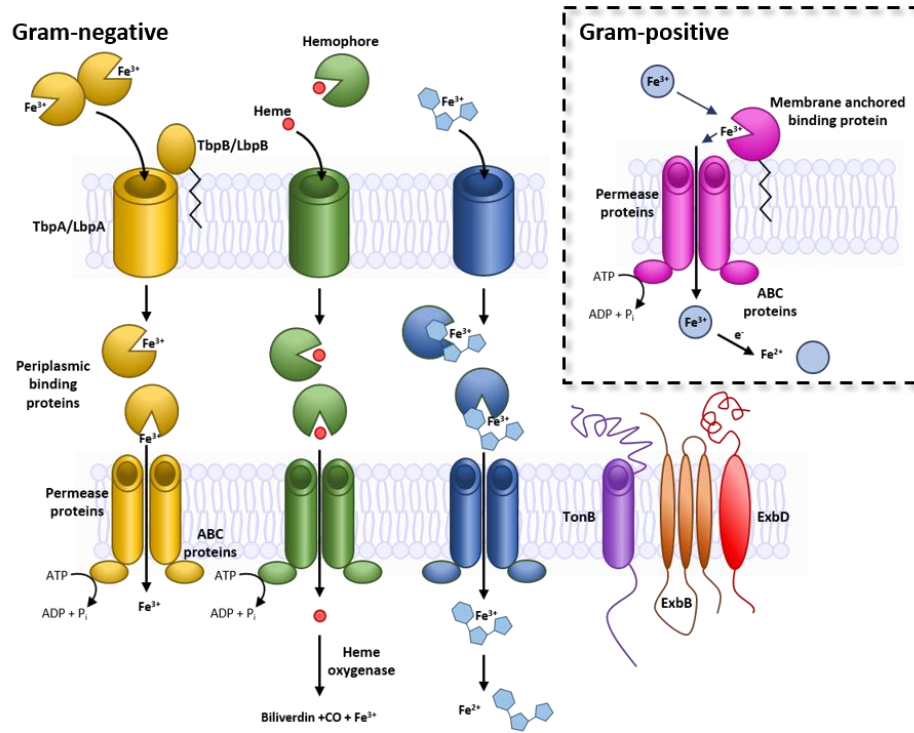


Figure 2.1: Iron acquisition pathways in Gram-negative and Gram-positive bacteria

When iron is in excess, bacteria can create stores to draw on later by depositing iron in storage proteins: ferritins, bactoferritins, and Dps proteins. Ferritins can be found in both eukaryotes and prokaryotes and are used strictly as an iron source for continual growth even in periods of iron scarcity. Bactoferritin function other than iron storage is less understood, but are unique to bacteria and only contain heme-bound iron. Dps proteins are DNA-binding proteins found only in prokaryotes and non-specifically bind DNA to protect it from redox-related destruction.<sup>5,6</sup>

## 2.2 Iron Uses and Functions

Iron has several uses both in bacteria and in higher order organisms like humans. Bacteria use iron to regulate cell composition, metabolism, and protein structure and function. A lack of sufficient iron in bacteria can change cell morphology as well as inhibit growth and sporulation, a process which is essential for preserving genetic material.

Iron can affect the act of metabolism, but also what products are made during the metabolic process. For example, iron is essential to the tricarboxylic acid (TCA) cycle and the electron transport chain. During

the TCA cycle, citrate is converted to isocitrate by the aconitase enzyme where the iron-sulfur cluster directly reacts with the substrate, citrate (**Figure 2.2**). Throughout the TCA cycle and electron transport chain there are many other proteins that contain iron-sulfur clusters that are necessary for function, like succinate dehydrogenase, but their iron-sulfur clusters do not make direct binding contacts with the substrate like aconitase.<sup>7</sup>

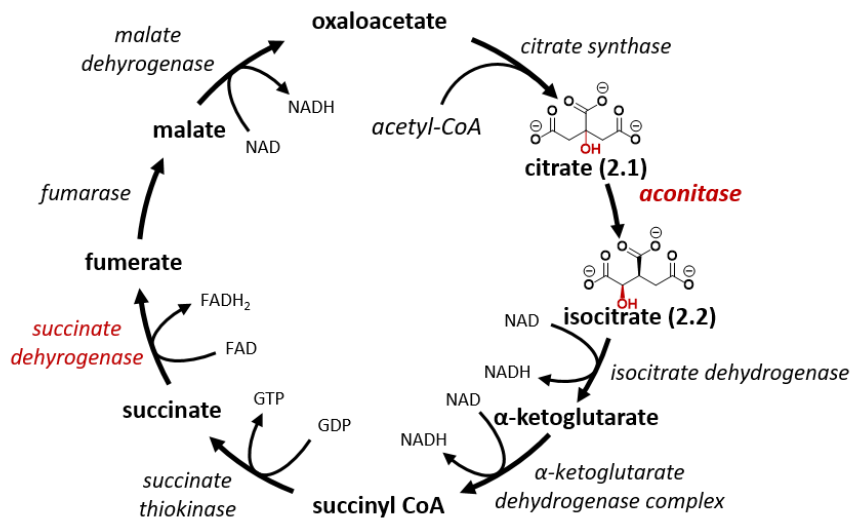


Figure 2.2: TCA cycle highlighting iron-bound aconitase

Iron is also essential to the electron transport chain where cytochromes and non-heme components shuttle electrons back and forth. Additionally, iron is crucial in nitrogen fixation and oxidative phosphorylation. All of this together indicates that a lack of iron can force a cell to switch from metabolism to glycolysis pathways for survival. Furthermore, iron plays a role regulating the production of porphyrins, toxins, vitamins, antibiotics, hydroxamates, cytochromes, pigments, siderophores, aromatic compounds, DNA, and RNA.<sup>8</sup> Iron also plays a role in protecting or damaging the cell from oxidation through the Fenton reaction which converts unstable ferrous iron into ferric ion, which is then converted into insoluble iron(III) hydroxide for cellular protection, and radical oxygen species (ROS).<sup>4</sup>



While several methods of iron acquisition, storage and usage have been discussed, the primary focus of the research disclosed will be in relation to siderophores.

### 2.3 Siderophores

Siderophores are small molecules with a high affinity for ferric iron, and are bacteria's secret weapon for stealing iron from their hosts. These crucial small molecules generally have an high iron-binding stability constants of  $10^{10}$  to  $10^{49}$ .<sup>9</sup> Siderophore structural characteristics are varied and diverse, but often have a few common moieties that are responsible for iron binding (**Figure 2.3**).

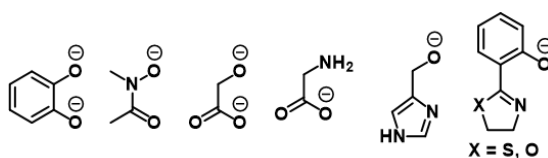


*Figure 2.3: Common siderophore moieties responsible for metal binding*

Siderophore structure allows them to bind iron with high thermodynamic stability and preference for the higher oxidation state of iron, compared to other biological iron binders which have a preference for iron(II). The attraction to iron(III) and lack of binding ability of iron(II) contributes to ability of chelators to release iron cargo once inside the cell. Much of this preference can be explained with hard acid base theory, in that the hard acid iron(III) is preferentially linked with a hard base like oxygen. The three-dimensionality of the ligand also allows for proper octahedral geometric arrangement about iron(III).<sup>10</sup>

While siderophores must maintain certain characteristics to effectively bind and release iron, they are very diverse structurally from organism to organism. **Figure 2.4** showcases some of these structures and the organisms they originated from. A focus on the color-coded metal binding functional groups may lead the reader to assume that siderophores all look alike, but a closer look will allow a view of the subtle changes in structure outside of the metal binding moiety that allow for specificity and recognition between bacteria. This recognition element not only allows bacteria to import their siderophores, but some have evolved to accept siderophores made by other bacteria, giving them a competitive advantage.<sup>11</sup>

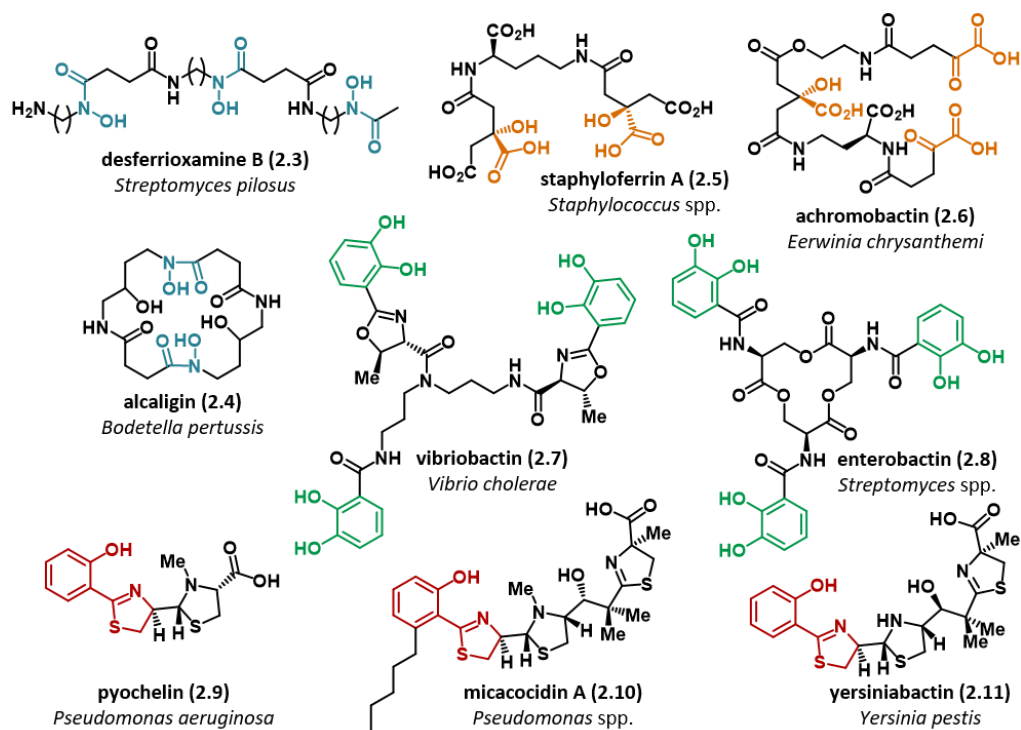
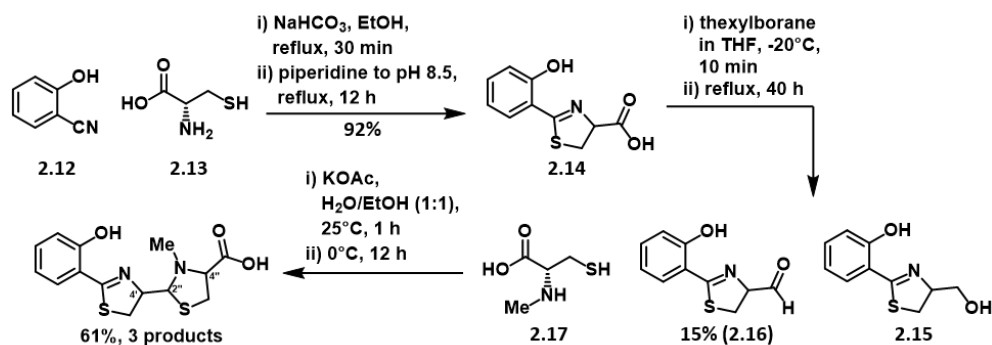


Figure 2.4: Structural diversity of siderophores and their producing organisms

### 2.3.1. Pyochelin

Pyochelin was originally isolated by Cox and colleagues in 1981 and was identified as an iron-chelator that was able to promote the growth of *P. aeruginosa* (PA). In their studies, pyochelin was first treated with ferric chloride and then the complex was exposed to several different strains of PA. In all cases, even with clinically isolated bacteria, the iron-pyochelin complex promoted bacterial growth indicating the small molecule could assist in iron acquisition.<sup>12</sup> In 1988, pyochelin was synthesized by Ankenbauer and coworkers and the biological activity was investigated further (**Scheme 2.1**).



*Scheme 2.1: First synthesis of pyochelin by Ankenbauer et al.*

Though their synthesis was not stereospecific and was low yielding due to reduction from acid **2.14** to aldehyde **2.16**, it was still pioneering and matched the NMR spectra of isolated pyochelin. The synthesized pyochelin mix was also capable of mimicking the growth promotion of isolated pyochelin.<sup>13</sup>

Similarly, the first “stereo-controlled” synthesis of pyochelin was completed in 2000 by Zamri and Abdallah. They optimized the first condensation of 2-hydroxybenzotrile (**2.12**) and L-cysteine (**2.13**) by using a 1:1 ratio of methanol and pH 6.4 phosphate buffer and heating for four days. However, the most important change in their synthesis was optimizing the reduction of acid **2.14** to aldehyde **2.16**. Instead of reducing the acid to the aldehyde directly, they converted the acid to a Weinreb amide and then reduced using lithium aluminum hydride. At the end of their synthesis, Zamri and Abdallah were able to isolate four stereoisomers of pyochelin by first converting it to the methyl ester form and then performing purification.<sup>14</sup> Further stereochemical information was reported by Schlegel and coworkers. They chose to isolate the different stereoisomers of pyochelin instead of synthesizing them. After extensive analysis, Schlegel was able to conclude that the stereochemistry at the C-2’ position (**Figure 2.5**) can isomerize through a ring-opening mechanism, facilitated by the lone pair on the nitrogen or the sulfur under aqueous conditions.<sup>15</sup>

The Mislin group followed up these initial studies by making analogs that could be further functionalized to form Trojan horse-type antibiotic-siderophore conjugates, or to track pyochelin as it is incorporated by bacteria. In a 2006 paper, they started by synthesizing an analog library with substitution at the 4 position of the phenol all in decent overall yields (30-45%) (**Figure 2.5**). Unfortunately, the mix of stereoisomers were challenging to separate so no biological testing was performed at this juncture.<sup>16</sup>

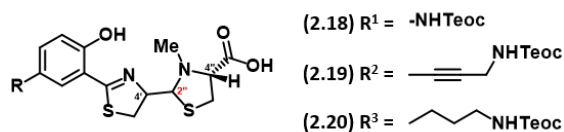


*Figure 2.5: Mislin et al. first generation analogs*

Though the synthesis and yields of these compounds were successful, Mislin and colleagues instead began to focus on synthesizing analogs that could be used to track pyochelin in biological systems. They decided to add the fluorescent 4-nitrobenzo[1,2,5]oxadiazole group to the amine of the thiazolidine (**Figure 2.6**). With these two analogs in hand, researchers were able to fluorescently track pyochelin within *P. aeruginosa* cells using the piperazine linked analog.<sup>17</sup>

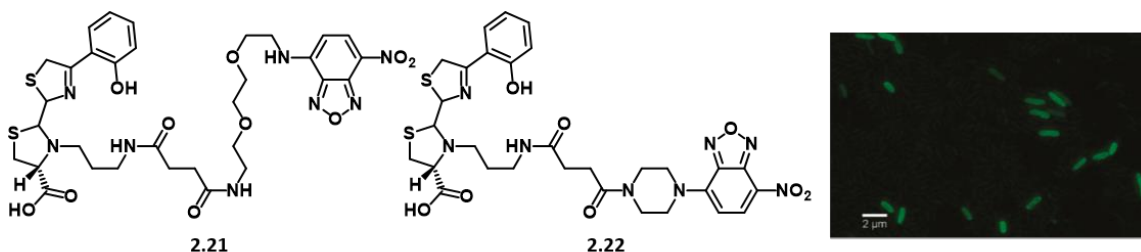


Figure 2.6: Mislin et al. second generation analogs for fluorescent tracking

## 2.4 Ulbactins

### 2.4.1. Isolation

In 2016, Igarashi and colleagues isolated a diastereomeric pair of natural products, ulbactin F and G. These compounds were isolated from a strain of *Brevibacillus* sp. (TP-B0800) that was living on an unidentified marine sponge off the coast of Iwate, Japan.<sup>18</sup> The bacteria was cultured in several different types of media, metabolites were extracted with 1-butanol, purified with HPLC, and analyzed for UV absorption properties. During this final test, peaks were observed at 204, 251, and 316 nm which is typical of the privileged phenol-thiazoline scaffold, commonly found in siderophores. With this in mind, further isolation and characterization of this fraction was completed to yield the structures of ulbactin F and G (**Figure 2.7**).

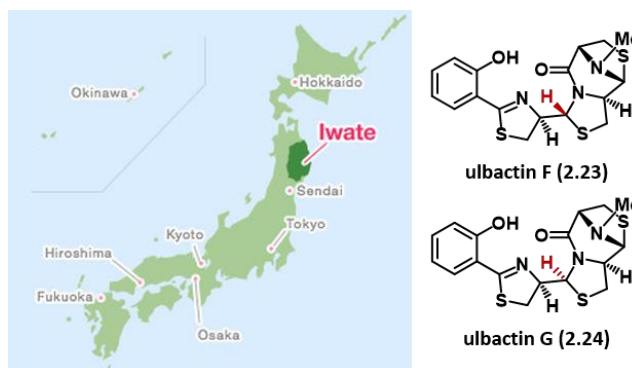


Figure 2.7: Location and structure of ulbactins F and G by Igarashi et al.

These structures were found to contain the phenol-thiazoline scaffold as predicted by UV absorption, but also an unusual tricyclic moiety derived from cysteine. A Japanese patent previously described the structures of other ulbactins that were used for their UV absorptive properties in cosmetics; however, no stereochemical assignments were made (**Figure 2.8**).<sup>19</sup>

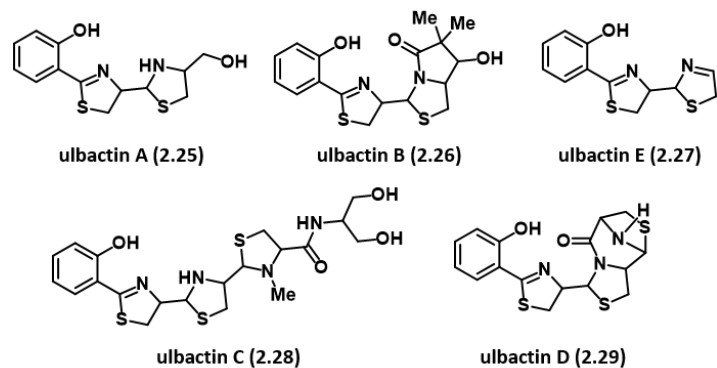


Figure 2.8: The ulbactin family as reported in a Japanese patent

The UV absorptive properties as well as the uncommon tricyclic moiety and potential biological function made ulbactins F and G desirable targets for total synthesis. In the isolation paper, crystal structures were reported suggesting that ulbactin F, with its single stereochemical difference from ulbactin G, wraps up on itself and provides a potential pocket for metal binding (**Figure 2.9**). This information, combined with the presence of the phenol-thiazoline siderophore motif, spurred the hypothesis that ulbactins may be siderophores for marine bacteria, and as such, could be used as xenosiderophores for terrestrial bacteria.

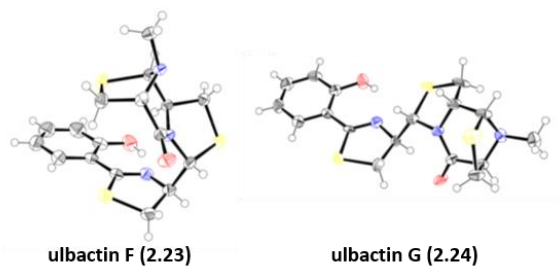


Figure 2.9: Crystal structures of ulbactins F and G as reported by Igarashi et al.

#### 2.4.2. Biosynthetic Route to Ulbactin

Given the uniqueness of ulbactins F and G, Igarashi and coworkers set out to sequence the biosynthetic gene cluster (BGC) within the *Brevibacillus* sp. TP-B0800 producing strain. They began by sequencing the entire genome of TP-B0800 which was a total of 6,280,149 base pairs. Then, the non-ribosomal peptide synthetase (NRPS) clusters and polyketide synthase (PKS) clusters were identified for further study.<sup>20</sup> PKSs and NRPSs are modular proteins responsible for the production of many complex natural products. NRPSs, specifically, are not reliant on messenger RNA and can synthesize only one product. They are commonly responsible for production of natural products that contain D-amino acids and complex cyclic structures, like that of ulbactins F and G.

NRPSs have multiple domains that are essential to small molecule production. For example, every NRPS must contain an adenylation (**A**) domain where the amino acid or starting materials are reacted with ATP to form a thioester bond with the thiolation domain (**T**). This allows the starting materials to be held in position for further catalytic reactions. Additionally, a condensation or cyclization domain (**Cy**) is used to form an amide bond between two loaded small molecules. Finally, once the synthesis is complete, NRPSs use a single termination domain (**TE**) in which an additional thioesterase reacts to cleave the final product from the penultimate protein domain.<sup>21,22</sup>

Igarashi and coworkers were able to identify three NRPS gene clusters and three hybrid PKS/NRPS gene clusters.<sup>20</sup> Two of these gene clusters were identified as those that produce known natural products, but the four remaining clusters were suspected to be novel. Researchers looked to the Walsh group's research which had already identified the BGC of the similar natural product, pyochelin.<sup>23</sup> From this work, Igarashi and colleagues were able to determine that one particular NRPS gene cluster was likely to contain the synthesis of ulbactins based on the number of thiazoline cyclization domains, as well as adenylation domains that commonly integrate salicylic acid and cysteine.

Armed with this information, the NRPS gene cluster of ulbactins F and G was determined (**Figure 2.10**). Salicylic acid is loaded through a thiolation domain (**T**) and cysteine is loaded through adenylation



(A(cys)). These two compounds then react to form a thiazoline facilitated by a cyclization (Cy) domain. This process is reiterated twice more, followed by a reduction of thiazoline to thiazolidine catalyzed by a separate, an off-pathway thiazoline reductase. The ulbactin precursor is then methylated by the methyltransferase domain (MT) and placed on the final thiolation domain.<sup>20</sup>

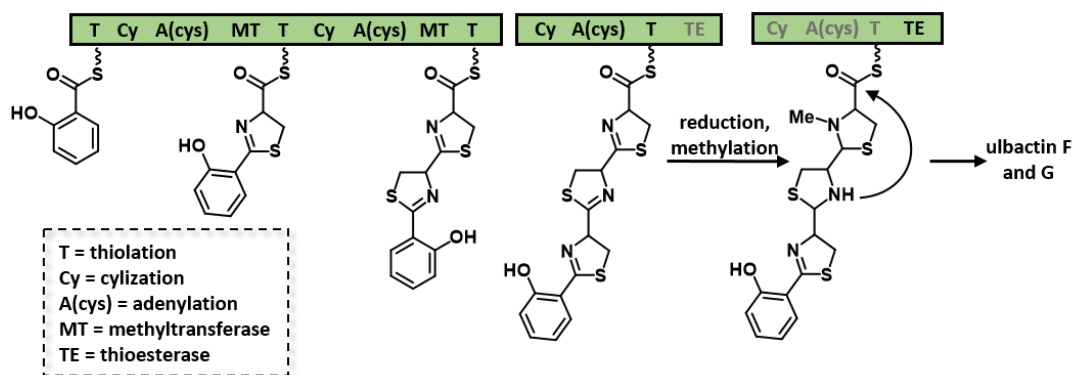


Figure 2.10: NRPS biosynthesis of ulbactins F and G as proposed by Igarashi et al.

At this point the only remaining domain is that of the thioesterase which releases ulbactin from the NRPS. Researchers found no evidence of a cyclase that would facilitate the condensation of the secondary amine onto the thioester; however, the favorability of ulbactin F over ulbactin G in a 17: 1 ratio suggests that the final TE domain may play a role in diastereoselectivity.<sup>18</sup> This has led to the hypothesis that reduction and methylation allows for enough conformational flexibility and thermodynamic instability that the secondary amine condenses to form the final tricycle moiety.

The hypothesis that thermodynamic control is exerted during biosynthesis is further supported by looking at the structures of yersiniabactin and micacocidin A (**Figure 2.11**). Both of these compounds share phenol-thiazoline-thiazolidine pattern with ulbactins, but then have a secondary hydroxyl and gem-dimethyl moiety before the final thiazoline ring and acid. It is likely that this interrupted pattern may prohibit the cyclization of yersiniabactin and micacocidin A,<sup>24</sup> which is further supported by the NRPS BGS of yersiniabactin which shares common precursors with ulbactins up until the installation of the hydroxyl and gem-dimethyl groups.<sup>25</sup> It is also likely that the secondary binding contribution of the right

(red) side of yersiniabactin (**2.11**) and micacocidin (**2.10**) is enhanced by contortion of the structure through the Thorpe-Ingold effect, whereas the wrapping up of the tricycle places secondary iron binders closer in ulbactins F and G.

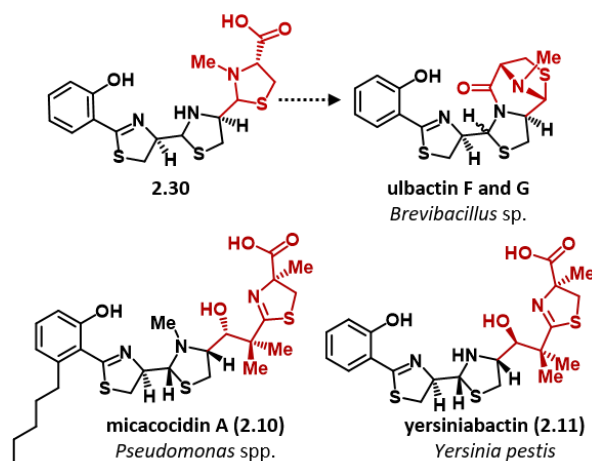


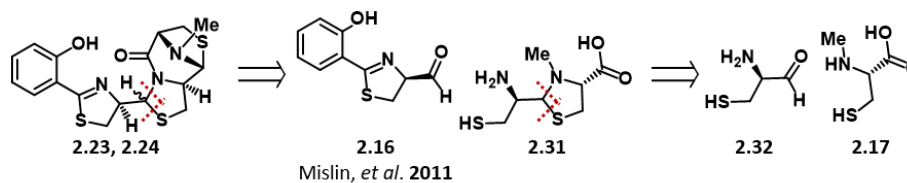
Figure 2.11: Structural comparison of ulbactins F and G to yersiniabactin and micacocidin A

#### 2.4.3. First Total Synthesis of Ulbactin F

Shapiro, J. A.†; Morrison, K. R.†; Chodisetty, S. S.; Musaev, D. G.; Wuest, W. M. Biologically Inspired Total Synthesis of Ulbactin F, an Iron-Binding Natural Product. *Org. Lett.* **2018**, 20 (18), 5922–5926. <https://doi.org/10.1021/acs.orglett.8b02599>.

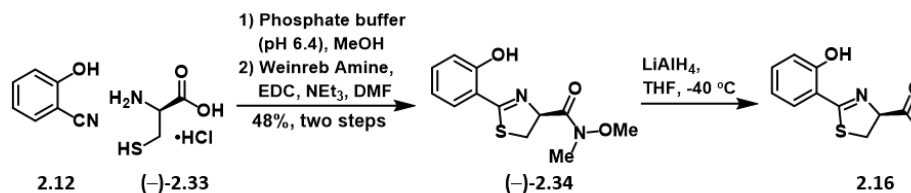
† Both authors contributed equally: Initial synthetic efforts and route exploration was completed by K.R.M., J.A.S. was instrumental in route optimization and metal binding studies. Both researchers worked collaboratively to complete the synthesis and analyze the results, often passing materials back and forth. S.S.C. (undergraduate) assisted in scale-up of starting materials as a first experience in organic synthesis.

With the knowledge of previous syntheses of pyochelin and the biosynthetic route in mind, the total synthesis of ulbactins F and G was undertaken.<sup>26</sup> Starting from ulbactin, we envisioned breaking the molecule apart into two main fragments: phenol-thiazoline aldehyde (**2.16**) and thiazolidine (**2.31**) (Scheme 2.2). The phenol-thiazoline intermediate is shared with the synthesis of pyochelin and has been optimized by Mislin and coworkers.<sup>17</sup> The thiazolidine piece can be derived from two equivalents of cysteine, one is converted from D-cysteine to an aldehyde (**2.32**) and the other is an N-methyl derivative (**2.17**) of L-cysteine.



*Scheme 2.2: Retrosynthetic analysis of ulbactins F and G*

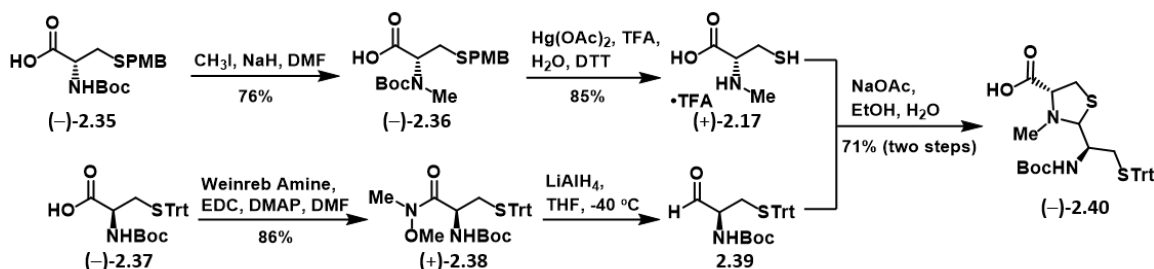
Synthesis of the two key intermediates, **2.16** and **2.31**, were completed in three parallel pathways. Starting from the pH 6.4 buffered condensation of 2-hydroxybenzoxonitrile and D-cysteine hydrochloride salt, the phenol-thiazoline acid precursor was formed (**Scheme 2.3**). The acid was then converted to a Weinreb amide through coupling with EDC and triethylamine ( $\text{NEt}_3$ ) in 48% over two steps. The amide **2.34** was then reduced using lithium aluminum hydride in THF at  $-40^\circ\text{C}$ . The resulting aldehyde was not stable to column chromatography and therefore was used immediately in successive reactions.



*Scheme 2.3: Synthesis of phenol-thiazoline intermediate*

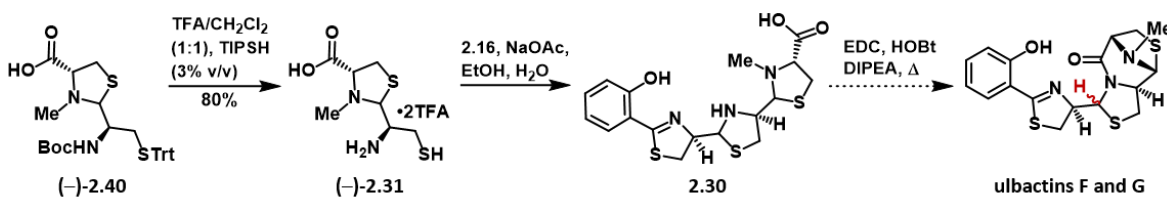
Synthesis of the thiazolidine fragment began with the N-methylation of N-Boc-S-PMB protected L-cysteine through a procedure originally reported by Malkov (**Scheme 2.4**).<sup>27</sup> In this reaction, the first equivalents of sodium hydride deprotonate and chelate the acid functionality, the second equivalent then deprotonates and chelates the carbamate nitrogen which is then methylated by methyl iodide to form **2.36**. Global deprotection then proceeded with trifluoroacetic acid (TFA) and mercury(II) diacetate, followed by reaction quench and addition of dithiothreitol (DTT) to reduce disulfide bonds between cysteines.<sup>28</sup> N-methyl-L-cysteine **2.17** was isolated as a TFA salt through centrifugation, filtering, and lyophilization in 85% yield (**Scheme 3.4**). At the same time, N-Boc-S-Trt-D-cysteine is reacted the Weinreb amine through amide coupling with EDC and DMAP to form **2.38** in 86% yield. Similar to the phenol-thiazoline reduction, Weinreb amide **2.38** was reduced with lithium aluminum hydride to form the protected cysteine aldehyde.

Again, due to aldehyde stability issues, the aldehyde is reacted immediately with N-methyl-L-cysteine in a condensation reaction to form thiazolidine **2.40** in 71% yield over two steps. This procedure was adapted from work completed by Mislin and coworkers during pyochelin synthesis.<sup>17</sup>



Scheme 2.4: Parallel routes to form protected thiazolidine intermediate **2.40**

With thiazolidine **2.40** prepared in the protected form, a global deprotection was employed with a 1:1 ratio of TFA and dichloromethane with 3% v/v of triisopropylsilane (TIPSH) to act as a disulfide bond reducing agent. The deprotected thiazolidine **2.31** was isolated as a di-TFA salt in 80% yield after concentration, dissolving in water and filtration to remove protecting group byproducts, and lyophilization. The final two steps of the synthesis were proposed to be a condensation between phenol-thiazoline aldehyde **2.16** and deprotected thiazolidine **2.31**, followed by intramolecular amide coupling with coupling partners and base (**Scheme 2.5**). Unfortunately, the final condensation between these two intermediates was unsuccessful. Suspicious that phenol-thiazoline aldehyde stability was contributing to reaction failure, we attempted to isolate the phenol-thiazoline aldehyde through crystallization as well as traditional purification methods, but ultimately unsuccessful.



Scheme 5: First generation end-game route to ulbactins F and G



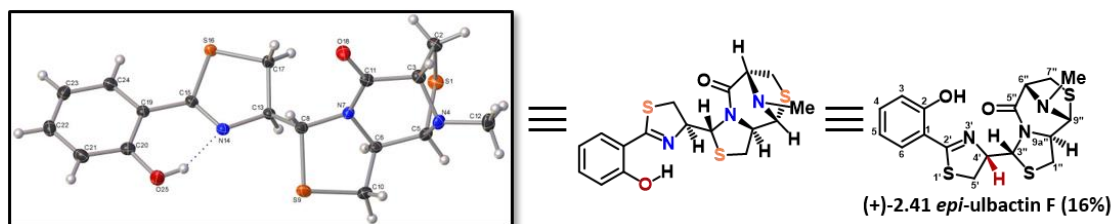
Scheme 2.6: Second generation cascade route to ulbactins F and G

After careful analysis, we were able to assign the structure of *epi*-ulbactin F (**2.41**). Prior studies by Schlegel determined that thiazolidines like **2.31** can interconvert through a ring opening-closing mechanism in aqueous media allowing the formation of diastereomers.<sup>15</sup> However, in order for the tricycle ring to form, the acid and primary amine must be *syn* to each other meaning that only one isomer of thiazolidine **2.31** would be able to react to form the conserved tricycle structure observed across all stereoisomers isolated. This allowed us to conclude that ulbactin F and the unknown compound were not diastereomeric at that position. Additionally, the two most distinguishing characteristics in the <sup>1</sup>H NMR of ulbactin F and G correspond to positions 3'' and 4' (**Figure 2.12**); therefore, a comparison of those signals with the analogous signals of *epi*-ulbactin F was conducted (**Table 2.1**).

Table 2.1: Comparison of important <sup>1</sup>H NMR signals to distinguish ulbactins F, G, and *epi*-F

	3''			4'		
Position	Splitting	Shift (ppm)	Integration	Splitting	Shift (ppm)	Integration
G	d	4.94	1	ddd	6.25	1
F	d	5.76	1	ddd	4.87	1
<i>epi</i> -F	d	5.65	1	dd	4.92	1

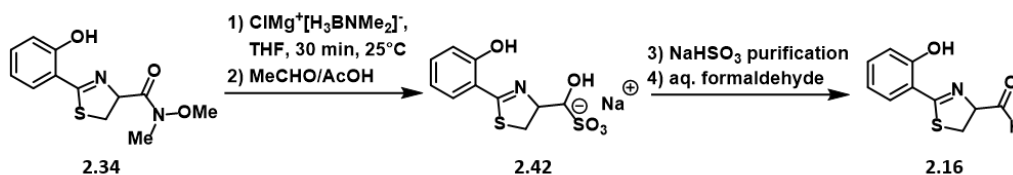
While there were some minor differences in splitting patterns between ulbactin F and *epi*-ulbactin F, their shifts were very similar especially compared those of ulbactin G. In order to confirm the structure and absolute configuration of *epi*-ulbactin F, a recrystallization was completed in hexanes and dichloromethane and the resulting crystal was given to Dr. John Basca and Dr. Thomas Pickel for X-ray analysis. With their help, the stereochemical structure was confirmed to be a diastereomer of ulbactin F at the 4' position (**Figure 2.12**).



Resolved by Dr. John Basca and Dr. Thomas Pickel at the Emory X-ray Crystallography Facility

Figure 2.12: Crystal structure and assignment of *epi*-ulbactin F

Now that the structure of *epi*-ulbactin F was confirmed, we set out to understand its origin. A dig through prior art on the synthesis of aldehyde fragment **2.16** found references to enantiomer formation during the amidation reaction in Zamri's pyochelin synthesis, and in much improved ratios in Mislin's synthesis of pyochelin analogs.<sup>14,17</sup> Zamri's pyochelin synthesis reported a ratio of 3:7 desired to undesired enantiomer, while Mislin reported 10% of his yield of aldehyde **2.16** was the undesired enantiomer. In an attempt to further modify conditions to alleviate the amount of undesired enantiomer, we screened common and available reducing reagents, including those that would lead to over-reduction to the primary alcohol. After oxidation back up to the aldehyde, none of these conditions were able to achieve the yields or selectivity that the current Weinreb reduction method did. Not satisfied with these results, we attempted a more novel reduction procedure using chloromagnesium dimethylaminoborohydride (MgAB) which would allow for the isolation of the desired aldehyde as a bisulfite salt (**Scheme 2.7**).<sup>29</sup> Unfortunately, these conditions could not be optimized to form product in for the desired substrate.



Scheme 2.7: Attempt to form aldehyde **2.16** through bisulfite salt

Unfortunately, ulbactin G was never observed throughout our experimentation and reaction optimizations. Initial hypotheses suggested that perhaps the mechanism of intramolecular ring-closing proceeded through association of the phenol with the acid, followed by attack of the secondary amine to the pseudo-ester and release of the phenol (**Figure 2.13**). While a phenol is not likely to form a formal bond with an acid, there is the potential for an intramolecular hydrogen-bond network that could increase the electrophilicity of the acid carbonyl, thereby promoting attack of the secondary amine without the assistance of an amide coupling reagent. If one follows through with this logic, two potential “macrocycles” can be proposed. If the linear acid assumes the stereochemistry corresponding to ulbactin G, then any

association between phenol and acid would prohibit final ring closure due to steric clash (**Figure 2.13**, top). The central thiazolidine ring is forced into a conformation where the sulfur and methylene blocks the approach of the nucleophilic secondary amine to acid carbonyl. However, when the linear acid adopts the stereochemistry of ulbactin F and the same association between phenol and acid is assumed, the nucleophilic secondary amine is positioned such that its sigma orbitals have favorable overlap with the antibonding pi orbitals of the acid carbonyl (**Figure 2.13**, bottom).

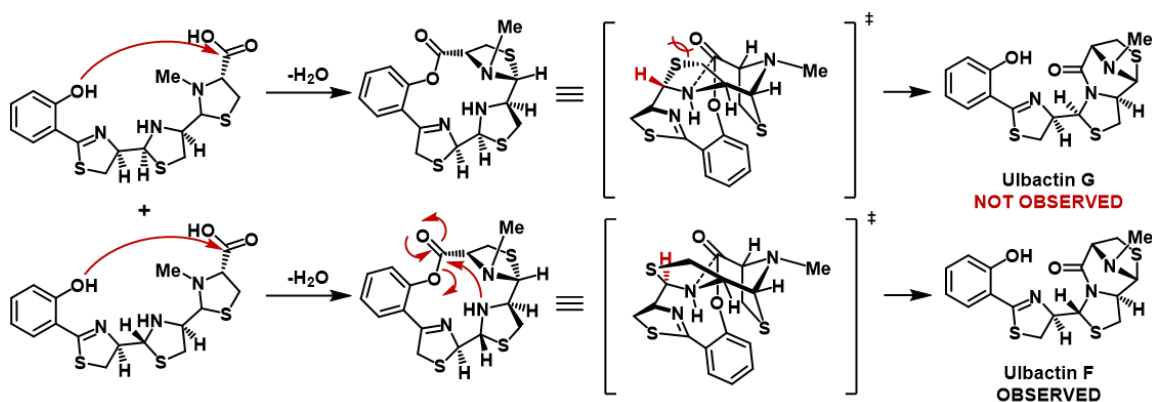


Figure 2.13: Thought experiment to explain lack of ulbactin G synthesis

#### 2.4.4. Metal-binding studies

Now that ulbactin F and *epi*-ulbactin F were synthesized, investigations into the iron-binding hypothesis were conducted. Given the knowledge that ulbactins tend to be UV absorbers, a preliminary colorimetric test was conducted in which equal concentrations of either ulbactin F, *epi*-ulbactin F, or neither were added to iron(III) acetylacetonate ( $\text{Fe}(\text{acac})_3$ ) in methanol (**Figure 2.14**, left). In this test, the orange color of the iron complex was observed in each vial indicating that no ligand exchange had occurred. Though this was originally concerning, we reasoned that  $\text{Fe}(\text{acac})_3$  has a high binding affinity given its octahedral geometry and six iron-oxygen bonds. As an alternative, a test with iron(III) chloride was conducted in the same manner as described previously. In this experiment, the dark green solution in methanol lightened when combined with an equal concentration of ulbactin F indicating a potential ligand exchange (**Figure 2.14**, right). Interestingly, no iron binding was observed in either case for *epi*-ulbactin F indicating that the 4' stereocenter, or the resulting conformational change to the molecule as a whole, prohibits *epi*-ulbactin F's



ability to bind iron. While these two tests provided some insight into possible binding, further tests were needed to be conclusive.

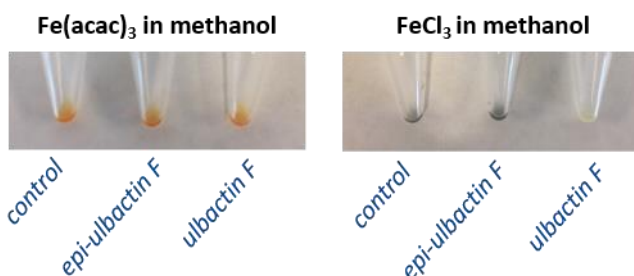
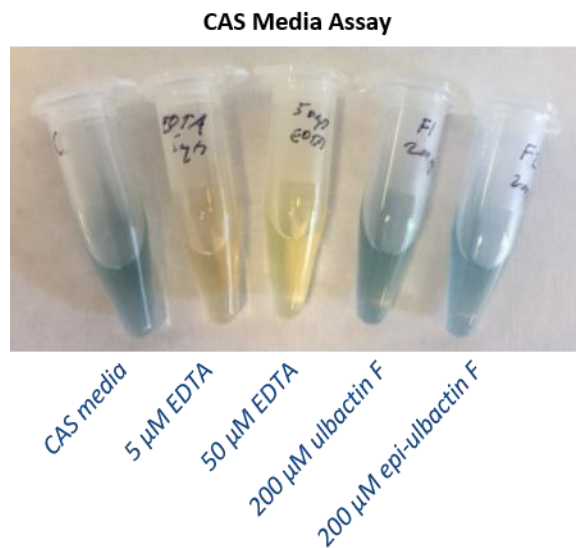


Figure 2.14: Colorimetric binding assays with two iron(III) sources

A common assay performed in biological communities is the use of chrome azurol S (CAS) media or agar. In this assay, blue CAS media was prepared according to Louden and colleagues, allowing researchers to observe a blue to yellow color change when iron is bound by the added compound instead of the CAS media.<sup>30</sup> Solutions of varying concentrations of ethylenediaminetetraacetic acid (EDTA), a known iron chelator, were made to act as a positive, dose-response control. Two additional vials were made with either ulbactin F or *epi*-ulbactin F. In this manner a slight color change was observed for ulbactin F, though not as drastic as with EDTA complexation. Again, no color change was observed for *epi*-ulbactin F (**Figure 2.15**). Though we were excited by the possibility of ulbactin F chelating iron, we needed quantitative experimentation to parse out the murky results from the qualitative colorimetric assays.



*Figure 2.15: CAS media assay to test qualitative iron binding of ulbactin F and epi-ulbactin F*

Again, knowing that ulbactins tend to be UV absorbers was the key piece of information that allowed us to complete fluorescent titration assays to quantitatively assess iron binding. In these assays 1.4  $\mu$ L aliquots of 10 mM  $\text{FeCl}_3$  in methanol was added to 350  $\mu$ L of 400  $\mu$ M solution of ulbactin F in methanol. These concentrations and amounts were chosen such that the stoichiometry of iron to ulbactin F could be assessed with ease. As amounts of  $\text{FeCl}_3$  solution were added, the fluorescence spectrum was collected. As can be seen by the  $\text{FeCl}_3$  graph shown below, at a 1:1 ratio of ulbactin F to  $\text{FeCl}_3$  the fluorescence is quenched indicating a one-to-one stoichiometric binding event between those two species (**Figure 2.16**,  $\text{FeCl}_3$ ). While some quenching does occur with other biologically relevant metal species, it is clear that ulbactin F does indeed preferentially bind  $\text{FeCl}_3$  as is indicated by taking the ratio of relative fluorescence at the start and end of each titration plotted for the reader's convenience on the Relative Metal Selectivity graph (**Figure 2.16**).

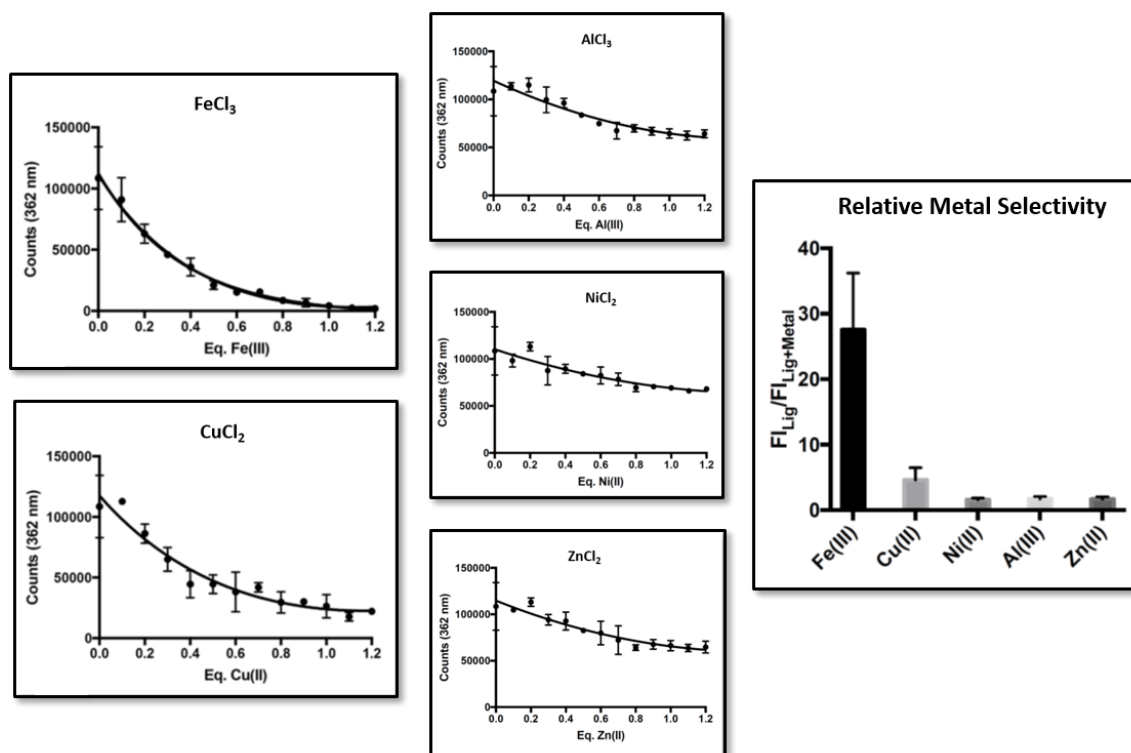


Figure 2.16: Fluorescence titration curves for Fe(III), Cu(II), Al(III), Ni(II), Zn(II), and relative metal selectivity plot

Satisfied that ulbactin F could bind iron in a one-to-one ratio, we sought the assistance of Dr. Musaev at the Cherry Emerson Computational Center for assistance in explaining the preference seen for FeCl<sub>3</sub> binding over Fe(acac)<sub>3</sub>. Through a series of computational experiments, Dr. Musaev was able to confirm that the predicted enthalpy and entropy values for ulbactin F binding with Fe(acac)<sub>3</sub> were both positive and therefore unfavorable. However, when ulbactin F was modelled with FeCl<sub>3</sub> both enthalpy and entropy values were negative and therefore indicated a favorable binding event (**Figure 2.17**). These computational results were also exciting because they predicted which atoms were contributing to metal binding. As was expected, the phenol-thiazoline motif acted as the strongest binding partners with predicted bond lengths of 1.865 (O-Fe) and 2.064 (N-Fe), but two other binding partners were also observed. Based on the wrapping of the tricycle region, it was calculated that the amide nitrogen and one of the thiazolidine sulfurs also contribute to metal-ligand stabilization with predicted bond lengths of 3.417 and 4.655 respectively. Instead of acting as formal bonds, it is suspected that these two atoms act through loose coordination. This may also explain why ulbactin F binds only FeCl<sub>3</sub>. It may be as simple as the steric

bulk of the tricycle prohibits the iron binding when it is chelated by the large acetylacetonate groups, but more likely these secondary binding atoms are unable to outcompete the acetylacetonate groups. This is also supported by the increased conformational flexibility and hydrogen bond donor-acceptor character of pyochelin which is capable of binding iron(III) acetylacetonate.

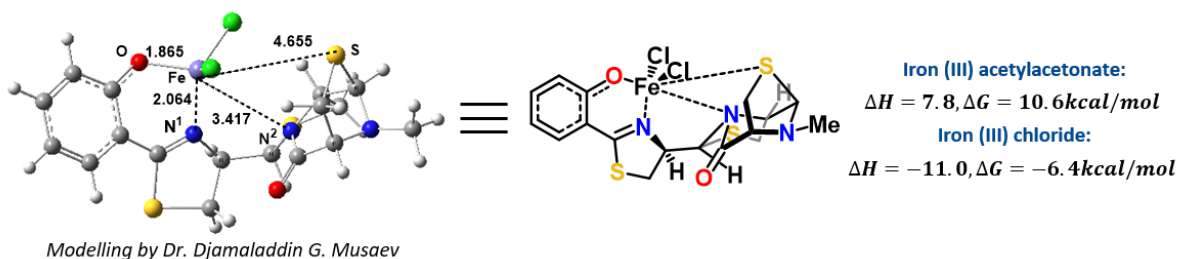


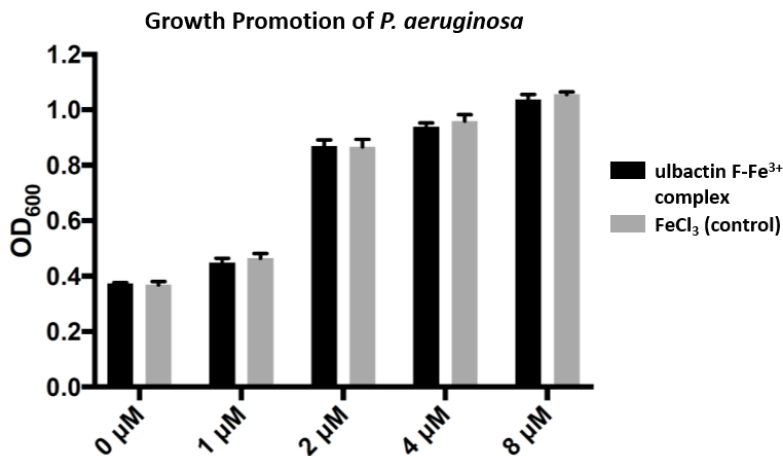
Figure 2.17: Computational modeling of ulbactin F-Fe(III) binding

While we are assured that ulbactin F is capable of binding iron at least weakly, we were unable to obtain a binding constant due to solubility issues. Pyochelin's binding affinity has been measured previously in a 10% methanol/water solution,<sup>31</sup> but unfortunately ulbactin F precipitates out of solution in anything less than 50% methanol or dimethylsulfoxide (DMSO) and water. This is likely due to the reduction in hydrogen bond donors and acceptors as compared to pyochlelin whose secondary binders consist of a tertiary nitrogen and acid moieties.

#### 2.4.5. Biological Investigation of Ulbactin F

Since the metal-binding properties of ulbactin F were established, researchers continued to test their hypothesis that ulbactin F may be able to act as a siderophore for a bacterial species like PA. A bacterial growth assay was conducted in M9 minimal media supplemented with 2,2'-dipyridyl (a known iron chelator commonly used in these assays). This type of experiment is designed such that there is no iron available to the bacteria unless it is acquired from the dosed compound. In order to control for this effect,  $\text{FeCl}_3$  is dosed into one row of wells at various concentrations for comparison. Ideally, the bacteria would be able to acquire iron from the ulbactin F- $\text{Fe}^{3+}$  complex more efficiently due to enzymatic recognition pathways than from just  $\text{FeCl}_3$ . This would result in an increase in growth which is measured by optical density ( $\text{OD}_{600}$ ).<sup>32</sup> Unfortunately, no statistically relevant difference in growth was observed between naked  $\text{FeCl}_3$  treatment

or ulbactin F-Fe<sup>3+</sup> treatment (**Graph 2.1**). This could be due to a lack of recognition by PA for the non-native ulbactin F structure, or to solubility issues with the ulbactin F-Fe<sup>3+</sup> complex. It is possible that while PA is our bacteria of interest due to its implications in Cystic Fibrosis and burn infections, ulbactin F may be recognized by bacteria that is native to the marine environment it was isolated from like *Vibrio* species that have relevance to both marine and human health.



Graph 2.1: Growth promotion assay of *P. aeruginosa* (PAO1) treated with ulbactin F-Fe<sup>3+</sup> complex

Though bacterial activity has yet to be confirmed, ulbactin F and G are reported to have anticancer activity. Igarashi *et al.* reported migratory inhibition of epidermoid carcinoma, antimetastatic migration inhibition for esophageal squamous carcinoma, and antimetastatic inhibition of tumor cell invasion in murine colon carcinoma (**Table 2.2**).<sup>18</sup> Samples of ulbactin F and epi-ulbactin F have been sent to collaborators at the Winship Cancer Institute at Emory Hospital to confirm activity and access the role of iron-ulbactin interactions in these cancers.

Table 2.2: Cancer activity of ulbactin F and G reported by Igarashi *et al.*

Cancer type	Cell line	Inhibition type	IC <sub>50</sub> (μM)	
			ulbactin F	ulbactin G
epidermoid	A431	migration	6.4	6.1
esophageal squamous	EC109	migration	2.1	NT
		tumor cell invasion	1.7	NT
murine colon	26-L5	invasion	1.7	NT

#### 2.4.6. Analog Design and Synthesis

*The following work was conducted by K.R.M.*

At the conclusion of the biological investigations of ulbactin F, we identified that one of the primary issues with discovering more conclusive information about the molecule was its inherent insolubility. Still curious about its potential applications to pathogenic bacteria, a new series of analogs were proposed that would retain the iron-binding functionality, but improve solubility. To enable rapid analog production and take advantage of the thermodynamic control of tricycle formation, a new synthetic route was proposed.

Three analogs are proposed with the intent to increase hydrogen bond donor-acceptor character and aqueous solubility. To retain the iron binding pocket formed by the phenol-thiazoline and tricycle, hydrogen bond donor-acceptor groups could only be added to the benzene ring. It was also important that any group added to the benzene would not prohibit the already existing hydroxyl group from binding iron. With this in mind, ulbactin F – 2,6-diol (**2.44**) and ulbactin F – 2,4-diol (**2.45**) were designed such that the additional hydroxyl groups could help solubilize the molecule, but any rotation of the phenol would not prohibit native coordination to iron (**Figure 2.18**, CLogP values estimated by ChemDraw). Additionally, ulbactin F – pyridine was designed such that the additional nitrogen could increase solubility, without adding steric constraints. It is possible that rotation of the phenol would affect the binding sites for this analog, but given the six-membered hydrogen bonding ring formed by the phenol-thiazoline motif and resonance contributors, there would probably be a preference for the conformation shown over any other.

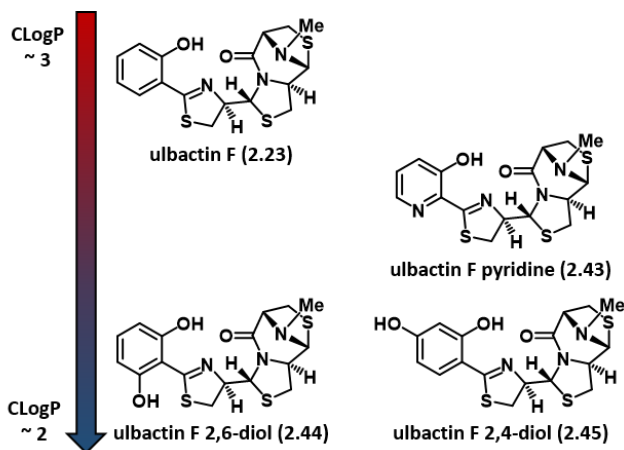
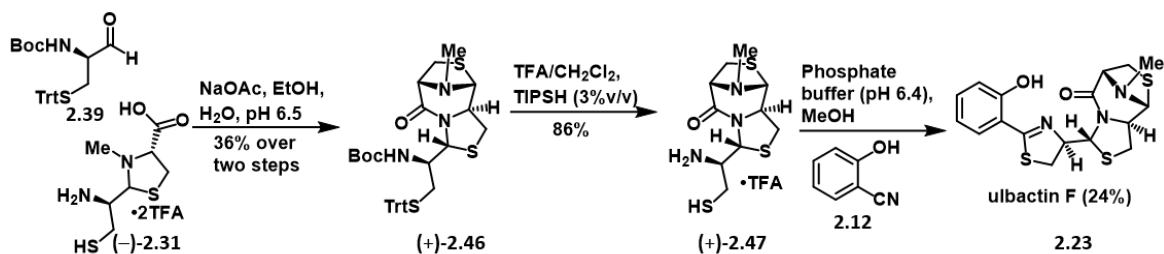


Figure 2.18: Proposed analogs of ulbactin F and their relative CLogP values

If the current route to synthesize ulbactin F were used to make the proposed analogs, it would necessitate optimizing conditions for the synthesis of three different phenol-thiazoline aldehydes which has already proven to be a challenging molecule to work with. It would also potentially allow the synthesis of stereoisomers like *epi*-ulbactin F, which have no iron binding capability and are therefore less interesting for this specific investigation. With this in mind, a new synthesis was proposed and carried out that takes advantage of thermodynamic control on tricycle formation and allows incorporation of analogous phenols in the final step of the reaction (**Scheme 2.8**).



Scheme 2.8: Synthetic route to stereospecific synthesis of ulbactin F

Starting from two intermediates previously utilized in the biosynthetic-mimic route, deprotected thiazolidine **2.31** and D-cysteine aldehyde **2.39** are combined in a condensation reaction with sodium acetate at pH 6.5. This reaction facilitates the formation of three bonds and two rings in one step. It is theorized that thermodynamic control allows synthesis of only one stereoisomer in 36% yield over two steps from

reduction of the cysteine aldehyde. Tricycle **2.46** can then be deprotected using a 1:1 ratio of TFA and dichloromethane with an added 3% v/v of TIPS<sub>3</sub>S<sub>2</sub> disulfide reducing agent in 86% yield. A final condensation with 2-hydroxybenzotrile forms only ulbactin F in 24% yield. Though this route is one step longer and therefore slightly lower yielding compared to the initial route, it optimizes the stereochemical diversity seen in the previous route and avoids the use of the phenol-thiazoline aldehyde intermediate which is unstable and promotes the production of stereoisomers. All three analogs can be made through the same pathway from their corresponding nitriles with the exception of the 2,6-diol analog.<sup>33,34</sup> This particular compound will need to be added to the reaction as 2-hydroxy-6-methoxybenzotrile to combat phenolic oxidative reactivity during the reaction. The methoxy group will then need to be deprotected to yield the final 2,6-diol analog **2.44**.<sup>35</sup>

## 2.5 Watasemycins and Thiazostatins

*The following work was designed and led by K.R.M. with invaluable assistance from Ryan A. Allen.*

During literary research for the ulbactin project, we discovered watasemycins and thiazostatins; two sets of diastereomers with similar structures and proposed functions to pyochelin and ulbactins. These quickly became compounds of interest due to their synthetic challenge and potential for specificity in biological function that neither pyochelin nor ulbactin was previously able to satisfy.

### 2.5.1. Isolation of Thiazostatins and Watasemycins

In 1989 and 2002 two molecules of interest were isolated, one from soil and one from a marine environment, with only one methyl to differentiate them. Naturally, we were intrigued by the drastic difference one methyl or one stereocenter could make on the biological activity of these small molecules. Thiazostatins A and B were isolated in 1989 by Shindo and colleagues from a soil sample from Yamaguchi-city, Japan.<sup>36</sup> They were able to determine that thiazostatins A and B were produced by a strain of *Streptomyces toluosus* (1368-MT1) (**Figure 2.19**). Initially, researchers were screening for new antioxidant compounds due to their ability to be useful in treatment of arteriosclerosis (hardening of arterial walls) and ischemia (restriction of blood supply/oxygen supply to tissues). Through extensive spectroscopic analysis, researchers identified the structure of thiazostatins A and B as diastereomers at position 2", though not the



absolute stereochemistry. They were also able to confirm that the compounds have an IC<sub>50</sub> of 3 μM against erythrocyte hemolysis caused by 2,2'-azobis(amidinopropane)dihydrochloride (a radical producing compound) which is less active than the standard of care at the time, vitamin E (1 μM).<sup>36</sup>

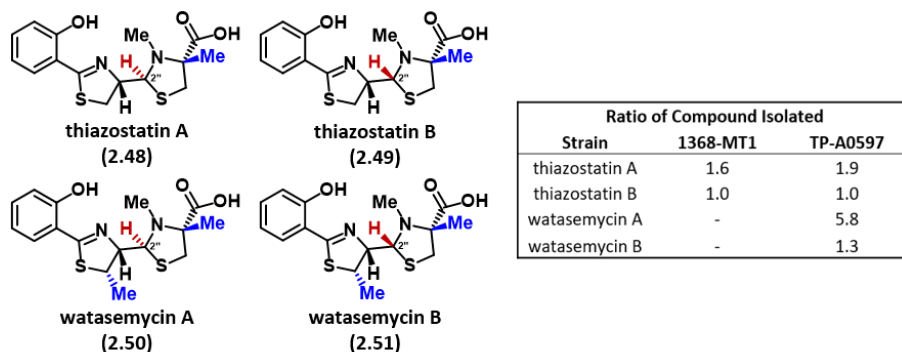


Figure 2.19: Structures of thiazostatins and watasemycins with their relative isolation amounts

Later, in 2002, watasemycins A and B were isolated from a seawater sample from Toyama Bay, Japan. The producing species was determined to be *Streptomyces* sp. (TP-A0597) which upon further investigation, was also found to produce thiazostatins A and B allowing researchers to assign the absolute configuration to all four compounds (Figure 2.19).<sup>37</sup> Unlike the thiazostatins, watasemycins have an additional methyl group and were reported to have antibiotic activity (Table 2.3).

Table 2.3: Antibiotic activity of watasemycins A and B as reported by Sasaki et al.

Compound	Minimum Inhibitory Concentration (μg/mL)				
	<i>S. aureus</i> 209P-JC-1	<i>B. subtilis</i> ATCC 6633	<i>E. coli</i> NIHJ JC-2	<i>Proteus mirabilis</i> ATCC 21100	<i>Pseudomonas aeruginosa</i> A3
watasemycin A	12.5	25.0	100	0.39	>100
watasemycin B	25.0	50.0	>100	6.25	>100

All of this data together raises many intriguing questions:

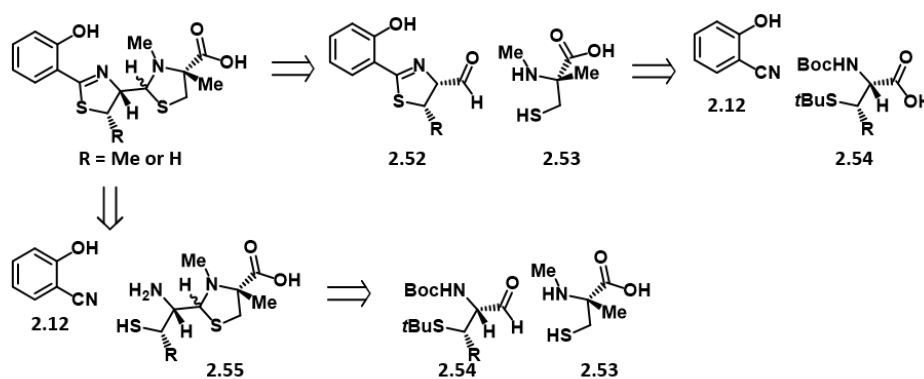
- 1) Why does the organism make all four compounds, do they have different functions?
- 2) Given that all four are presumably biosynthetically made by NRPS machinery in a manner similar to that of pyochelin and ulbactin, and that synthesizing β-methyl and α-methyl cysteines is energetically more taxing than simply using native cysteine, what purpose do they serve?

- 3) How is it that a  $\beta$ -methyl cysteine moiety confers antibiotic properties, but the same molecule without that methyl is not active?
- 4) How is it that watasemycin A, different from watasemycin B at one stereocenter, has better antibiotic activity?

These are the primary questions that we have set out to answer through the first total synthesis of these four compounds.

### 2.5.2. Progress Towards the Total Synthesis of Watasemycins and Thiazostatins

Retrosynthesis of watasemycins and thiazostatins could be thought of in two different routes. Either route consists of three main building blocks: 2-hydroxybenzotrile,  $\beta$ -methyl-L-cysteine (**2.54**), and N-methyl- $\alpha$ -methyl-L-cysteine (**2.53**). The first route mimics prior syntheses of pyochelin by first forming the phenol-thiazoline aldehyde **2.52** and N-methyl- $\alpha$ -methyl-L-cysteine **2.53**. Further disconnection leads to 2-hydroxybenzotrile and  $\beta$ -methyl-L-cysteine (**Scheme 2.9**, top). However, armed with the knowledge that phenol-thiazoline aldehydes are notorious for stereoconversion alpha to the acid moiety and are generally unstable, we have devised an alternate route that could potentially alleviate that concern. In the second route, the first disconnection forms 2-hydroxybenzotrile and thiazolidine **2.55**. The thiazolidine can then be further broken apart into the two cysteine building blocks **2.54** and **2.53** (**Scheme 2.9**, bottom).



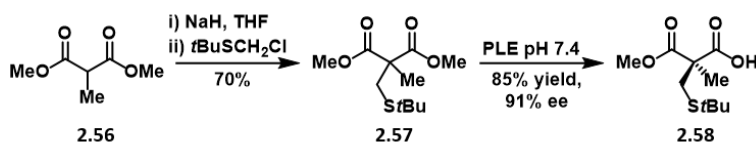
*Scheme 2.9: Retrosynthetic analysis of watasemycins and thiazostatins*

### 2.5.2.1. Completed Attempts at N-methyl- $\alpha$ -methyl-L-cysteine Synthesis

The synthesis of N-methyl- $\alpha$ -methyl-L-cysteine building block has proven to be quite challenging. This synthetic journey is still ongoing and while many of the known methods have worked in specific situations, many fail to take into account the reactivity of thioethers both in the chemistry that happens at adjacent groups, but also their resilience to deprotection to unveil the desired thiol. A brief survey of the attempts at synthesis and those yet to be attempted are addressed in the following sections.

#### 2.5.2.1.1. The Masterson Method

In 2008, the Masterson lab published their synthesis to  $\alpha$ -methyl cysteine through the use of chiral enzymatic resolution. Their work demonstrated that a prochiral malonic ester **2.56** could be alkylated with *tert*-butyl(chloromethyl)sulfane after exposure to sodium hydride. This racemic mixture could then be hydrolyzed by a commercially available Pig Liver Esterase (PLE) enzyme at pH 7.4 which would enantioselectively hydrolyze one of the methyl esters in decent yield (69-85%) and enantioselectivity (*R*: 70-91% ee) (**Scheme 2.10**).<sup>38</sup> Unfortunately, our attempts at repeating this synthesis were unsuccessful in hydrolyzing the methyl ester using PLE causing researchers to abandon this method in exchange for more direct synthetic options.

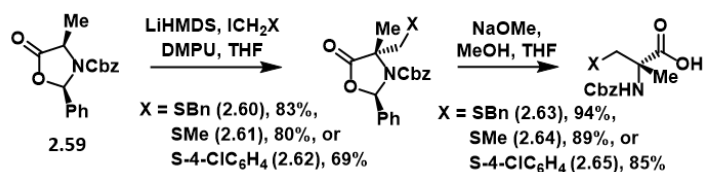


*Scheme 2.10: Masterson method to synthesize  $\alpha$ -methyl cysteine derivatives*

#### 2.5.2.1.2. The Kedrowski Method

The following method was originally developed by Kedrowski in 2002 and consists of protecting alanine and then alkylating with a thioether. Using common alkylating conditions, N-Cbz-oxazolidine **2.59** is deprotonated with lithium bis(trimethylsilyl)amide then alkylated with various alkyl halides containing a thioether. The product is then ring opened with sodium methoxide to give the protected cysteine derivative (**Scheme 2.11**). This procedure is appealing due to its rapid synthesis from commercially available

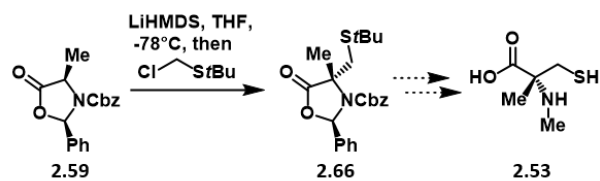
materials to yield a protected version of  $\alpha$ -methyl cysteine in two steps. While work would still need to be completed to N-methylate and deprotect the thioether moiety, it seemed a promising and direct place to start.



Scheme 2.11: Kedrowski method towards  $\alpha$ -methyl cysteine derivatives

Before proceeding with the synthesis, we examined potential deprotection conditions for the thioether groups used by Kedrowski.<sup>39</sup> One pitfall of amino acid chemistry, and specifically cysteine chemistry, is the polar nature of deprotected compounds and the difficulty associated with purifying them. As a result, whenever a deprotection step is needed, great effort is exerted to ensure that it is a global deprotection that contains a disulfide reducing reagent within the deprotection reaction. This allows for rapid, clean, and productive synthesis of cysteine-derived compounds. Unfortunately, the thioethers utilized by Kedrowski require a two-step deprotection which only unveils the thiol instead of removing all protecting groups, or use of neat hydrofluoric acid and anisole.<sup>40,41</sup>

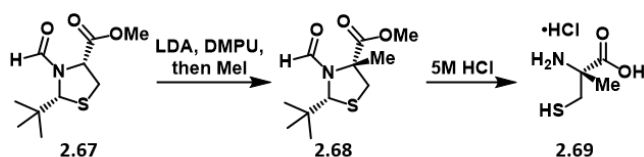
For the synthesis of watasemycins and thiazostatins, researchers searched for an alkylating agent that would allow one step, global deprotection immediately following alkylation. Recalling the Masterson lab alkylating reagent and the facile deprotection conditions reported by Nishimura for *tert*-butyl thioethers, researchers elected to use their alkylating reagent on this system. The Nishimura deprotection conditions consisted of mercury(II) diacetate, TFA or aqueous acetic acid, and anisole as a scavenger which readily revealed thiols.<sup>42</sup> Unfortunately, the *tert*-butyl(chloromethyl)sulfane alkylation was unsuccessful after several attempts including increasing equivalents of base used, preparing fresh batches of the alkylating reagent, increasing the equivalents of alkylating reagent, and allowing the reaction to warm during the course of the reaction (**Scheme 2.12**). In most cases, researchers recovered unreacted starting material, except for when temperatures were warmed, in which case only decomposition was observed.



Scheme 2.12: Attempt at adapting Kedrowski method to watasemycins and thiazostatin synthesis

### 2.5.2.1.3. The Pattenden Method

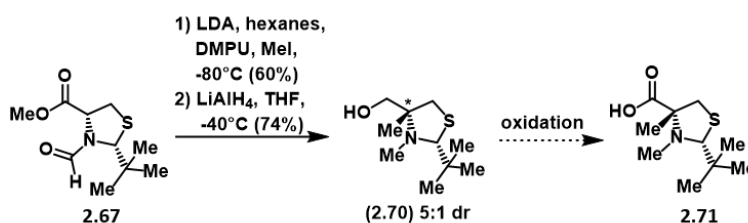
Based off procedures published by the Pattenden group in 1993, N-formyl-methyl ester-thiazolidine **2.67** can be methylated with LDA, DMPU, and methyl iodide at -90°C, stereoselectively (**Scheme 2.13**). In this reaction the *tert*-butyl and methyl ester functionalities are located on the same face of the thiazolidine, thereby forcing a single ring conformation. After deprotonation, the *tert*-butyl group continues to direct the facial selectivity for attack on the electrophilic methyl iodide. Their literature reports that this transformation occurs in 56% yield and complete diastereoselectivity confirmed through X-ray crystallography.<sup>43</sup> The next step in their synthesis was to globally deprotect with 5M hydrochloric acid to unveil  $\alpha$ -methyl-L-cysteine as a hydrochloride salt.



Scheme 2.13: Pattenden method towards synthesis of  $\alpha$ -methyl cysteine derivatives

Learning from the Pattenden group, we chose to adapt this route to the synthesis of watasemycins and thiazostatins. Unfortunately, if the literature procedure were to be completed as shown, then the resulting  $\alpha$ -methyl-L-cysteine HCl salt would have to be reprotected in order to selectively methylate the amine without causing side reactions at the thiol or acid functionalities. With this in mind, and recognizing that the nitrogen can be thought of as protected earlier in the synthesis as a formamide (**2.68**), plans were made to transform the formyl group to a methyl through reductive amination and then global deprotection to give the desired N-methyl- $\alpha$ -methyl-L-cysteine.

Repetition of the Pattenden synthetic route began productively with the methylation with LDA proceeding in 60% yield. Unfortunately, traditional reductive amination conditions, and selective formyl reduction conditions with sodium cyanoborohydride were unsuccessful. After a screen of reducing reagents and conditions, it was determined that lithium aluminum hydride provided the best yields without deteriorating the diastereomeric excess (**Scheme 2.14**). Though researchers were disappointed that the methyl ester was also reduced to the primary alcohol, they were optimistic that oxidation to the acid would be possible.



*Scheme 2.14: Attempts towards N-methyl-α-methyl cysteine through Pattenden method*

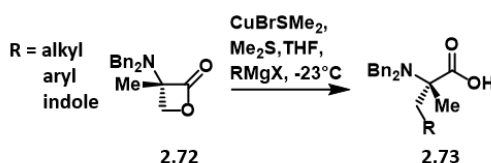
Literature searches towards this goal suggested oxidation directly from alcohol to acid in one step using either ruthenium trichloride and sodium metaperiodate or TEMPO, sodium chlorite and sodium hypochlorite.<sup>44</sup> Both procedures were shown to proceed at greater than 80% yields on (2*S*,5*S*)-*N*-Boc-5-*tert*-butylprolinol. Importantly, this substrate and any substrates found did not contain a thioether functionality. Upon further research into thioether reactivity, it was discovered that any reaction containing a ruthenium catalyst, sodium metaperiodate, or radical oxidant would likely oxidize the thioether to a sulfoxide.<sup>44-46</sup> Likewise, the Jones oxidation, while previously shown to work in the presence of a thioacetate<sup>47</sup> can also promote oxidation of a thioether, especially when acid is also present.<sup>48</sup> The idea of a stepwise oxidation was briefly proposed when researchers realized that Swern oxidations may be amenable to the strict reactive requirements of the substrate. Unfortunately, this would only allow the synthesis of an aldehyde with few options for oxidation from aldehyde to acid.

### 2.5.2.2. Future Directions towards N-methyl- $\alpha$ -methyl-L-cysteine

At this point, we took a step back to reassess the options available. There remain a few options for synthesis of this particular component, and while synthesis of N-methyl- $\alpha$ -methyl-L-cysteine is still possible using the routes above, they would involve multiple protecting group manipulations. Though this would not sacrifice the goal of analyzing the biological effects of the desired natural products, it is also our goal to use a concise and elegant route for synthesis of these molecules. This would further develop our chemical and biological skills sets. At this juncture five future routes are proposed and assessed for usefulness.

#### 2.5.2.2.1. $\beta$ -Lactone Method

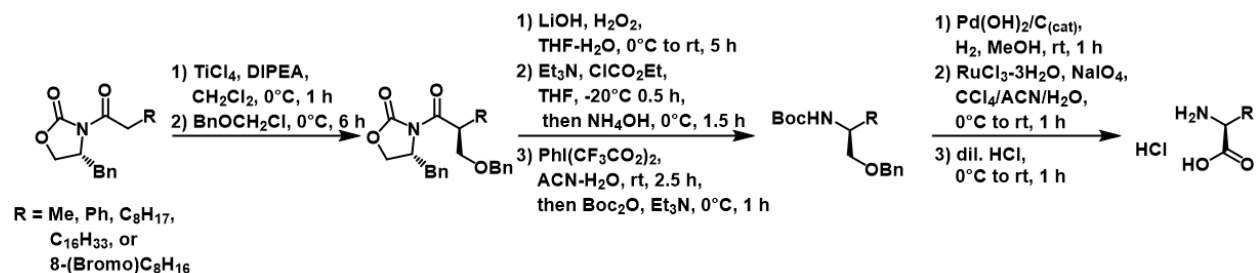
In 2005, Smith and coworkers published their route to form  $\alpha$ -methyl amino acids through a  $\beta$ -lactone intermediate derived from  $\alpha$ -methyl serine. Using cuprate alkylating reagents, they were able to synthesize a range of  $\alpha$ -methyl amino acids (**Scheme 2.15**).<sup>49</sup> While this work is incredibly valuable for synthesized amino acids when the side chain consists of an alkyl, aryl or indole functionality, the nature of the reaction conditions is not suitable for application to cysteine. This method is also cost prohibitive given that the starting material is made from  $\alpha$ -methyl-L-serine which is \$308.50/250 mg from Fisher Scientific (1/18/2020). This expense also makes converting  $\alpha$ -methyl-L-serine to  $\alpha$ -methyl-L-cysteine through a Mitsunobu reaction sequence also cost prohibitive.<sup>50</sup>



*Scheme 2.15: Smith et al.  $\alpha$ -methyl amino acid synthetic method*

#### 2.5.2.2.2. Evans Auxillary Method

In 2002, Chakraborty and Ghosh published a route to synthesized chiral amino acids through the use of Evans's auxiliary.<sup>51</sup> While their route is successful in a small substrate scope, it is a lengthy synthesis and was never utilized to form a quaternary center alpha to the acid of the resulting amino acid (**Scheme 2.16**). Additionally, many of the steps in their synthesis are not amenable to a thioether.

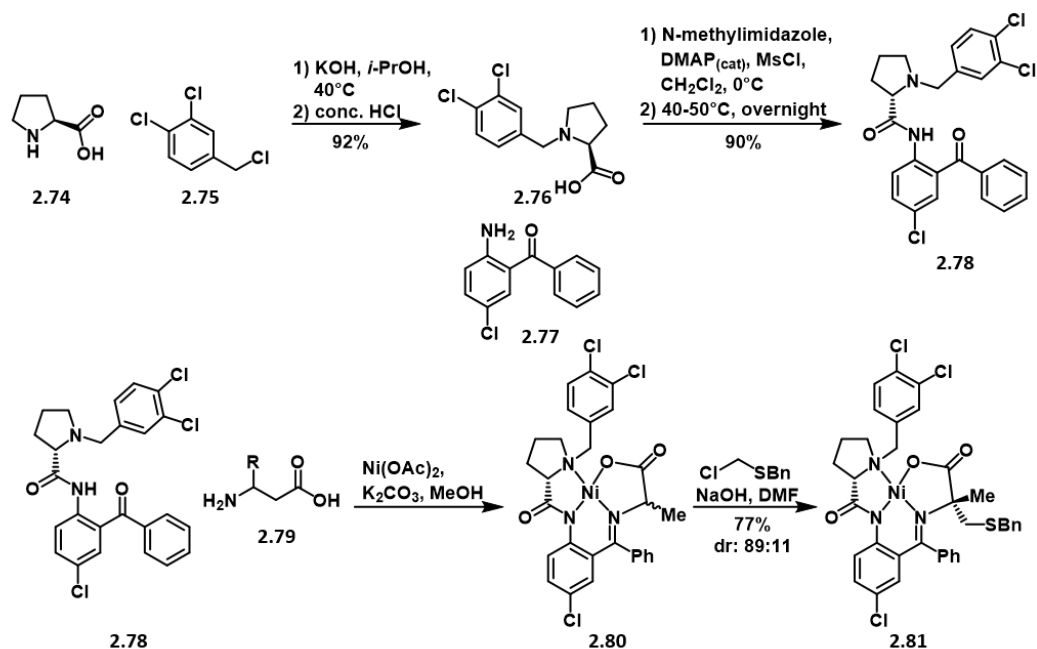


Scheme 2.16: Chakraborty method to synthesize amino acids

### 2.5.2.2.3. Nickel-Catalyst Method

In 2014, Zhou and coworkers developed a nickel catalyst that allowed kinetic resolution of  $\beta$ -substituted  $\beta$ -amino acids. The synthesis for their ligand is shown below with the only chiral component being derived from proline.<sup>52</sup> Later, Yamamoto and colleagues were able to use that chiral ligand to synthesize  $\alpha$ -methyl cysteine through nickel(II) catalysis.<sup>53</sup> This method has several advantages in that the chiral ligand and cysteine product can be recovered through exposure to acid and then a series of pH adjustments in separate aliquots. They achieve relatively good yields and enantiomeric excess of up to 98% (Scheme 2.17). The only flaw in their route is the use of a benzyl protected thiol. As has been discussed previously, the removal of a benzyl group from a thiol can only be completed in a two-step route or use of neat hydrofluoric acid. While neither of these conditions are ideal, it may be possible to replicate this work through the use of a *para*-methoxybenzene protecting group which has been shown is readily removed in the presence of TFA and mercury(II) acetate.<sup>26</sup>

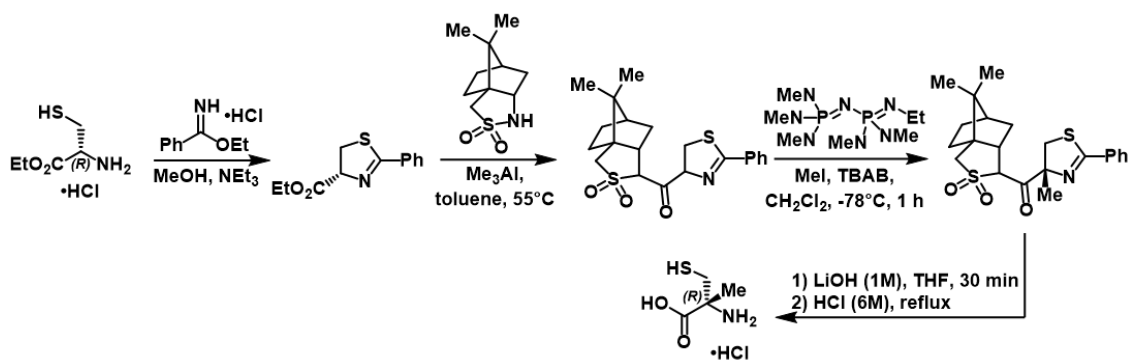




Scheme 2.17: Nickel(II) catalysis to yield  $\alpha$ -methyl cysteine

#### 2.5.2.2.4. Camphorsultam Method

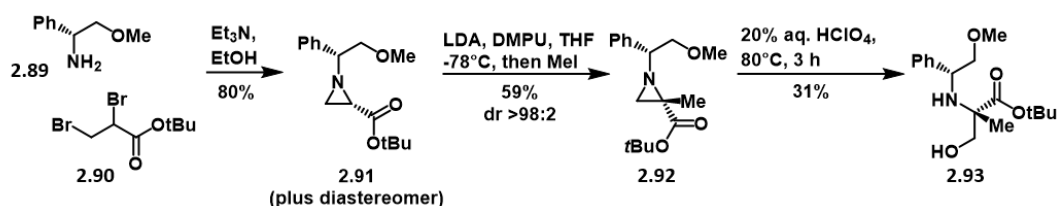
An additional option available to synthesize  $\alpha$ -methyl-L-cysteine is through the work published by Johnston and Hulme in 2013. Starting from ethyl ester cysteine, they first formed a phenyl thiazoline intermediate through condensation with a benzimidate. Next, they exposed this precursor to a camphorsultam which when exposed to stoichiometric amounts of P2-Et phosphazene base to generate a “naked” enolate. Directed facially by the camphorsultam, enolate attack of methyl iodide proceeded readily in 99% yield to give a single diastereomer. Cleavage of the camphorsultam auxiliary was performed with lithium hydroxide and recovered. The phenyl-thiazoline system was deconstructed in the presence of hydrochloric acid to give  $\alpha$ -methyl cysteine in 89% over two steps (Scheme 2.18).<sup>54</sup> While this method seems like a relatively efficient and highly stereoselective, the camphorsultam auxiliary and phosphazene base are expensive (camphorsultam: \$228/5 g; phosphazene: \$621/5 mL Sigma-Aldrich, 01/18/20) and both are used stoichiometrically.



Scheme 2.18: Camphorsultam method for synthesis of  $\alpha$ -methyl cysteine

#### 2.5.2.2.5. Aziridine Method

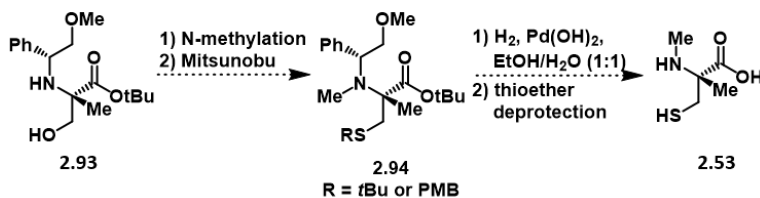
The final method proposed, and the most desirable, was published in 2001 by Alezra and coworkers consisting of a route to quaternary amino acid derivatives through a chiral aziridine. First, researchers combined *tert*-butyl-2,3-dibromopropanoate with 2-methoxyphenylethanamine to prepare the aziridine-*tert*-butylesters which when treated with lithium diisopropylamine form the aziridine enolate. Nucleophilic attack of the enolate was performed against a range of electrophiles including methyl iodide all in reasonable yield. High diastereoselectivity promoted by the steric clash and facial selectivity of the phenyl group on the auxiliary was observed in most cases. Aziridine opening was then completed with aqueous perchloric acid and heating to yield the serine derivative. Their procedure continued with auxiliary removal and deprotection of the acid functionality to give a series of serine derivatives (Scheme 2.19).<sup>55</sup>



Scheme 2.19: Proposed synthesis of *N*-methyl- $\alpha$ -methyl cysteine based on the method reported by Alezra et al.

We currently propose a divergence from their procedure after the aziridine opening so that *N*-methylation can occur followed by a Mitsunobu reaction to install an appropriate thioether such as *tert*-butyl, *para*-methoxybenzene,<sup>50</sup> or potassium thioacetate.<sup>56</sup> The *N*-methylation could occur through mildly basic conditions and treatment with methyl iodide.<sup>57</sup> Precedence indicates that in the presence of a benzyl amine, primary alcohol, and the *tert*-butyl ester group will not interfere with this process. Treatment with

palladium hydroxide and hydrogen gas would reveal the amine and acid moieties,<sup>55</sup> and deprotection of the thiol will unveil the desired intermediate (**Scheme 2.19**).



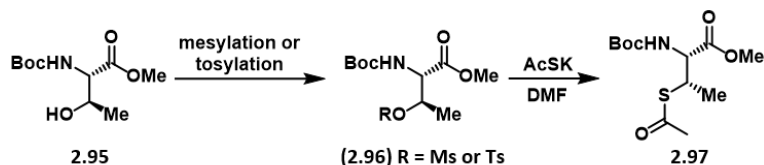
*Scheme 2.20: Proposed route to N-methyl- $\alpha$ -methyl cysteine*

This route above all the others discussed, seems to be the most applicable to the desired building block for watasemycins and thiazostatins syntheses due to its relative ease of synthesis, stereocontrol, and flexibility to allow for N-methylation (**Scheme 2.20**). While the starting materials are expensive, *tert*-butyl-2,3-dibromopropanoate can be synthesized through bromination of the very cost effective *tert*-butyl acrylate (\$51/100 mL, Sigma-Aldrich 01/23/20).<sup>58</sup> Additionally, the chiral auxiliary can be prepared with the desired stereospecificity from (*R*)-(-)-2-phenylglycinol (\$76.10/5g, Sigma-Aldrich 01/23/20) treated with sodium hydride and methyl iodide.<sup>59</sup> Unfortunately, the one drawback is the acquisition of the chiral auxiliary is not recovered at the end of the synthesis.

#### 2.5.2.2. $\beta$ -Methyl Cysteine Synthesis

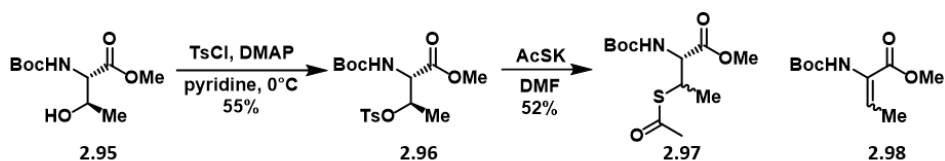
*The following work was pioneered by K.R.M. and optimized by teammate, R.A.A.*

While challenging in its own right, synthesizing a  $\beta$ -methyl derivative of cysteine proved to be more direct than  $\alpha$ -methylation. Starting from threonine and performing a Mitsunobu reaction seem the most direct pathway at the outset, but unfortunately modifications to reaction conditions and extensive trials were all unsuccessful. However, beginning with Morell in 1976,<sup>60</sup> and later repeated by Ge and colleagues in 2009,<sup>61</sup> a pathway was designed in which threonine was mesylated or tosylated and then exchanged for a thioacetate through a substitution reaction to yield a protected version of  $\beta$ -methyl cysteine (**Scheme 2.21**).



*Scheme 2.21: Threonine substitution method developed by Morell et al. and Ge et al.*

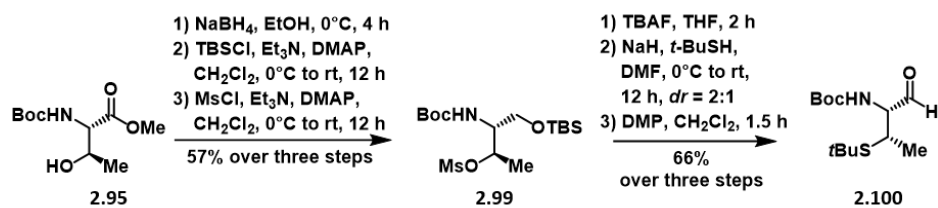
Initial attempts to replicate this work were moderately successful, but were plagued by selectivity issues during the substitution reaction (**Scheme 2.22**). As is common with  $S_N2$  reactions, completing elimination pathways can often cause byproduct formation.



*Scheme 2.22: Initial attempts at threonine substitution*

An alternate route was proposed and carried out to alleviate alpha hydrogen acidity by first reducing the acid to the alcohol.

First, the methyl ester of N-Boc-L-threonine is reduced with sodium borohydride and the resulting primary alcohol is selectively protected with a silyl group over the secondary alcohol, which is then mesylated.<sup>62</sup> At this point, initial routes proceeded with the substitution of mesylate for thioether, but the yields were poor. After some initial troubleshooting, Allen was able to discern that deprotection of the primary alcohol first allowed for enhanced yields during the subsequent substitution reaction. The final step oxidizes alcohol to aldehyde **2.100** with Dess-Martin Periodinane (DMP) to give our  $\beta$ -methyl cysteine intermediate in a modest dr of 2:1 (**Scheme 2.23**). While this diastereomeric ratio is not optimized yet, the two compounds are separable and may be advantageous in future analog studies, should the project reach that point. Allen is currently working to optimize the diastereomeric ratio by lowering the temperature of the substitution reaction for the synthesis of watasemycins. While the step count is longer than desirable, the chemistry itself can be performed rapidly and is highly reproducible.



Scheme 2.23: Synthesis of  $\beta$ -methyl cysteine

## 2.6 Conclusion

Over the course of the two projects discussed within this chapter, we have been able to complete the first total synthesis of ulbactin F, learned about its metal binding capabilities, proposed analogs for future studies, and have fully immersed ourselves in complex cysteine chemistry in an effort to complete the first total synthesis of watasemycins and thiazostatins. Though we have not yet completed the total synthesis of the latter two molecules, we have made significant progress and look forward to its completion in the hands of Ryan Allen.

## 2.7 References

- (1) Martin, R. B.; Savory, J.; Brown, S.; Bertholf, R. L.; Willis, M. R. Transferrin Binding of Al<sup>3+</sup> and Fe<sup>3+</sup>. *Clin. Chem.* **1987**, *33* (3), 405–407.
- (2) Behnsen, J.; Raffatellu, M. Siderophores: More than Stealing Iron. *MBio* **2016**, *7* (6), e01906-16. <https://doi.org/10.1128/mBio.01906-16>.
- (3) Ellermann, M.; Arthur, J. C. Siderophore-Mediated Iron Acquisition and Modulation of Host-Bacterial Interactions. *Free Radic. Biol. Med.* **2017**, *105*, 68–78. <https://doi.org/10.1016/j.freeradbiomed.2016.10.489>.
- (4) Krewulak, K. D.; Vogel, H. J. Structural Biology of Bacterial Iron Uptake. *Biochem. Biophys. Acta* **2008**, *1778*, 1781–1804. <https://doi.org/10.1016/j.bbamem.2007.07.026>.
- (5) Andrews, S. C.; Robinson, A. K.; Rodríguez-Quñones, F. Bacterial Iron Homeostasis. *FEMS Microbiol. Rev.* **2003**, *27*, 215–237. [https://doi.org/10.1016/S0168-6445\(03\)00055-X](https://doi.org/10.1016/S0168-6445(03)00055-X).
- (6) Keohane, C. E.; Steele, A. D.; Fetzer, C.; Khowsathit, J.; Van Tyne, D.; Moynié, L.; Gilmore, M. S.; Karanicolas, J.; Sieber, S. A.; Wuest, W. M. Promysalin Elicits Species-Selective Inhibition of *Pseudomonas Aeruginosa* by Targeting Succinate Dehydrogenase. *J. Am. Chem. Soc.* **2018**, *140* (5), 1774–1782. <https://doi.org/10.1021/jacs.7b11212>.
- (7) Sun, F.; Huo, X.; Zhai, Y.; Wang, A.; Xu, J.; Su, D.; Bartlam, M.; Rao, Z. Crystal Structure of Mitochondrial Respiratory Membrane Protein Complex II. *Cell* **2005**, *121* (7), 1043–1057. <https://doi.org/10.1016/j.cell.2005.05.025>.
- (8) Messenger, A. J. M.; Barclay, R. Bacteria, Iron and Pathogenicity. *Biochem. Educ.* **1983**, *11* (2), 54–63.
- (9) Johnstone, T. C.; Nolan, E. M. Beyond Iron: Non-Classical Biological Functions of Bacterial

- Siderophores. *Dalt. Trans.* **2015**, *44* (14), 6320–6339. <https://doi.org/10.1039/c4dt03559c>.
- (10) Neilands, J. B. Siderophores: Structure and Function of Microbial Iron Transport Compounds. *J. Biol. Chem.* **1995**, *270* (45), 26723–26726. <https://doi.org/10.1074/jbc.270.45.26723>.
  - (11) Endicott, N. P.; Lee, E.; Wencewicz, T. A. Structural Basis for Xenosiderophore Utilization by the Human Pathogen *Staphylococcus Aureus*. *ACS Infect. Dis.* **2017**, *3* (7), 542–553. <https://doi.org/10.1021/acsinfecdis.7b00036>.
  - (12) Boukhalfa, H.; Crumbliss, A. L. Chemical Aspects of Siderophore Mediated Iron Transport. *BioMetals* **2002**, *15*, 325–339.
  - (13) Ankenbauer, R. G.; Toyokuni, T.; Staley, A.; Rinehart, K. L.; Cox, C. D. Synthesis and Biological Activity of Pyochelin , a Siderophore of *Pseudomonas Aeruginosa*. *J. Bacteriol.* **1988**, *170* (11), 5344–5351.
  - (14) Zamri, A.; Abdallah, M. A. An Improved Stereocontrolled Synthesis of Pyochelin, Siderophore of *Pseudomonas Aeruginosa* and *Burkholderia Cepacia*. *Tetrahedron* **2000**, *56* (47), 249–256. [https://doi.org/10.1016/S0040-4020\(00\)00875-9](https://doi.org/10.1016/S0040-4020(00)00875-9).
  - (15) Schlegel, K.; Taraz, K.; Budzikiewicz, H. The Stereoisomers of Pyochelin, a Siderophore of *Pseudomonas Aeruginosa*. *BioMetals* **2004**, *17* (4), 409–414. <https://doi.org/10.1023/B:BIOM.0000029437.42633.73>.
  - (16) Rivault, F.; Schons, V.; Liébert, C.; Burger, A.; Sakr, E.; Abdallah, M. A.; Schalk, I. J.; Mislin, G. L. A. Synthesis of Functionalized Analogs of Pyochelin, a Siderophore of *Pseudomonas Aeruginosa* and *Burkholderia Cepacia*. *Tetrahedron* **2006**, *62* (10), 2247–2254. <https://doi.org/10.1016/j.tet.2005.12.012>.
  - (17) Noël, S.; Guillon, L.; Schalk, I. J.; Mislin, G. L. A. Synthesis of Fluorescent Probes Based on the Pyochelin Siderophore Scaffold. *Org. Lett.* **2011**, *13* (5), 844–847. <https://doi.org/10.1021/ol1028173>.
  - (18) Igarashi, Y.; Asano, D.; Sawamura, M.; In, Y.; Ishida, T.; Imoto, M. Ulbactins F and G, Polycyclic Thiazoline Derivatives with Tumor Cell Migration Inhibitory Activity from *Brevibacillus Sp.* *Org. Lett.* **2016**, *18*, 1658–1661. <https://doi.org/10.1021/acs.orglett.6b00531>.
  - (19) Kiluchi, K.; Chen, C.; Adachi, K.; Nishijima, M.; Nishida, F.; Takadera, T.; Sano, H. No Title. 049492, 1997.
  - (20) Komaki, H.; Hosoyama, A.; Ichikawa, N.; Igarashi, Y. Gene Reports Draft Genome Sequence of a Sponge-Derived *Brevibacillus Sp.* TP-B0800 , a Producer of Ulbactins with Tumor Cell Migration Inhibitory Activity. *Gene Reports* **2016**, *5*, 140–143. <https://doi.org/10.1016/j.genrep.2016.10.006>.
  - (21) Alberto Martínez-Núñez, M.; Eric Lopez y Lopez, V. Nonribosomal Peptides Synthetases and Their Applications in Industry. *Sustain. Chem. Process.* **2016**, *4* (13), 1–8. <https://doi.org/10.1186/s40508-016-0057-6>.
  - (22) Winn, M.; Fyans, J. K.; Zhuo, Y.; Micklefield, J. Recent Advances in Engineering Nonribosomal Peptide Assembly Lines. *Nat. Prod. Rep.* **2016**, *33*, 317–347. <https://doi.org/10.1039/c5np00099h>.
  - (23) Quadri, L. E. N.; Keating, T. A.; Patel, H. M.; Walsh, C. T. Assembly of the *Pseudomonas Aeruginosa* Nonribosomal Peptide Siderophore Pyochelin : In Vitro Reconstitution of Aryl-4 , 2-Bisthiazoline Synthetase Activity. *Biochemistry* **1999**, *38*, 14941–14954.

<https://doi.org/10.1021/bi991787c>.

- (24) Ino, A.; Hasegawa, Y.; Murabayashi, A. Total Synthesis of the Antimycoplasma Antibiotic Micacocidin. *Tetrahedron Lett.* **1998**, *39*, 3509–3512.
- (25) Pfeifer, B. A.; Wang, C. C. C.; Walsh, C. T.; Khosla, C. Biosynthesis of Yersiniabactin, a Complex Polyketide-Nonribosomal Peptide, Using *Escherichia coli* as a Heterologous Host. *Appl. Environ. Microbiol.* **2003**, *69* (11), 6698–6702. <https://doi.org/10.1128/AEM.69.11.6698>.
- (26) Shapiro, J. A.; Morrison, K. R.; Chodisetty, S. S.; Musaev, D. G.; Wuest, W. M. Biologically Inspired Total Synthesis of Ulbactin F, an Iron-Binding Natural Product. *Org. Lett.* **2018**, *20* (18), 5922–5926. <https://doi.org/10.1021/acs.orglett.8b02599>.
- (27) Malkov, A. V.; Vranková, K.; Černý, M.; Kočovský, P. On the Selective N-Methylation of BOC-Protected Amino Acids. *J. Org. Chem.* **2009**, *74* (21), 8425–8427. <https://doi.org/10.1021/jo9016293>.
- (28) Macmillan, D.; Anderson, D. W. Rapid Synthesis of Acyl Transfer Auxiliaries for Cysteine-Free Native Glycopeptide Ligation. *Org. Lett.* **2004**, *6* (25), 4659–4662. <https://doi.org/10.1021/ol048145o>.
- (29) Bailey, C. L.; Clary, J. W.; Tansakul, C.; Klabunde, L.; Anderson, C. L.; Joh, A. Y.; Lill, A. T.; Peer, N.; Braslau, R.; Singaram, B. Reduction of Weinreb Amides to Aldehydes under Ambient Conditions with Magnesium Borohydride Reagents. *Tetrahedron Lett.* **2015**, *56*, 706–709. <https://doi.org/http://dx.doi.org/10.1016/j.tetlet.2014.12.066>.
- (30) Loudon, B. C.; Haarmann, D.; Lynne, A. M. Use of Blue Agar CAS Assay for Siderophore Detection. *J. Microbiol. Biol. Educ.* **2011**, *12*, 51–53. <https://doi.org/10.1128/jmbe.v12i1.249>.
- (31) Cox, C. D.; Graham, R. Isolation of an Iron-Binding Compound from *Pseudomonas aeruginosa*. *J. Bacteriol.* **1979**, *137* (1), 357–364.
- (32) Shapiro, J. A.; Wenczewicz, T. A. Structure-Function Studies of Acinetobactin Analogs. *Metallomics* **2017**, *9* (5), 463–470. <https://doi.org/10.1039/c7mt00064b>.
- (33) Noël, S.; Hoegy, F.; Rivault, F.; Rognan, D.; Schalk, I. J.; Mislin, G. L. A. Synthesis and Biological Properties of Thiazole-Analogues of Pyochelin, a Siderophore of *Pseudomonas aeruginosa*. *Bioorg. Med. Chem. Lett.* **2014**, *24*, 132–135. <https://doi.org/https://doi.org/10.1016/j.bmcl.2013.11.054>.
- (34) Bergeron, R. J.; Wiegand, J.; Dionis, J. B.; Egli-karmakka, M.; Frei, J.; Huxley-tencer, A.; Peter, H. H. Evaluation of Desferrithiocin and Its Synthetic Analogues Chelators Orally Effective Iron. *J. Med. Chem.* **1991**, *34* (7), 2072–2078.
- (35) Santos, F. S.; Zanutto, G. M.; Argomedo, L. M. Z.; Darbem, M. P.; Gonçalves, P. F. B.; Stefani, H. A.; Rodembusch, F. S. Dyes and Pigments Synthesis, Experimental and Theoretical Photophysical Study of Proton Transfer Based Oxazoline Fluorophores. Potential Tailor Made Optical Sensors for Enantiomeric Detection in Solution. *Dye. Pigment.* **2019**, *165*, 372–382. <https://doi.org/https://doi.org/10.1016/j.dyepig.2019.02.047>.
- (36) Shindo, K.; Takenaka, A.; Nogushi, T.; Hayakawa, Y.; Seto, H. Thiazostatin A and Thiazostatin B, New Antioxidants Produced by *Streptomyces Tolurosus*. *J. Antibiot.* **1989**, *42* (10), 1526–1529.
- (37) Sasaki, T.; Igarashi, Y.; Saito, N.; Furumai, T. Watasemycins A and B, New Antibiotics Produced by *Streptomyces* Sp. TP-A0597. *J. Antibiot.* **2002**, *55* (3), 249–255.

- (38) Masterson, D. S.; Roy, K.; Rosado, D. A.; Fouche, M. A Divergent Approach to the Preparation of Cysteine and Serine Analogs. *J. Pept. Sci.* **2008**, *14*, 1151–1162.
- (39) Kedrowski, B. L.; Heathcock, C. H. Thiazoline Ring Formation from 2-Methylcysteines and 2-Halomethylalanines. *Heterocycles* **2002**, *58*, 601–634.
- (40) Akaji, K.; Tatsumi, T.; Yoshida, M.; Kimura, T.; Fujiwara, Y.; Kiso, Y. Synthesis of Cystine-Peptide by a New Disulphide Bond-Forming Reaction Using the Silyl Chloride-Sulphoxide System. *J. Chem. Soc., Chem. Commun.* **1991**, 167–168.
- (41) Sakakibara, S.; Shimonishi, Y.; Kishida, Y.; Okada, M.; Sugihara, H. Use of Anhydrous Hydrogen Fluoride in Peptide Synthesis. I. Behavior of Various Protective Groups in Anhydrous Hydrogen Fluoride. *Bull. Chem. Soc. Jpn.* **1967**, *40* (9), 2164–2167. <https://doi.org/10.1246/bcsj.40.2164>.
- (42) Nishimura, O.; Kitada, C.; Fujino, M. New Method for Removing the S-p-Methoxybenzyl and S-t-Butyl Groups of Cysteine Residues with Mercuric Trifluoroacetate. *Chem. Pharm. Bull.* **1978**, *26* (5), 1576–1585.
- (43) Pattenden, G.; Thorn, S. M.; Jones, M. F. Enantioselective Synthesis of 2-Alkyl Substituted Cysteines. *Tetrahedron* **1993**, *49* (10), 2131–2138.
- (44) Halab, L.; Belec, L.; Lubell, W. D. Improved Synthesis of (2S,5S)-5-Tert-Butylproline. *Tetrahedron* **2001**, *57* (30), 6439–6446. [https://doi.org/10.1016/S0040-4020\(01\)00535-X](https://doi.org/10.1016/S0040-4020(01)00535-X).
- (45) Gore, E. S. Ruthenium Catalysed Oxidations of Organic Compounds. *Platin. Met. Rev.* **1983**, *27* (3), 111–125.
- (46) Schoneich, C.; Aced, A.; Asmus, K. Mechanism of Oxidation of Aliphatic Thioethers to Sulfoxides by Hydroxyl Radicals . The Importance of Molecular Oxygen. *J. Am. Chem. Soc* **1993**, *115* (24), 11376–11383.
- (47) Jiang, Z.; Liu, X.; Qiu, X.; Qing, F. Asymmetric Synthesis of Both Enantiomers of Syn - ( 3-Trifluoromethyl ) Cysteine Derivatives. *J. Fluor. Chem.* **2005**, *126*, 499–505. <https://doi.org/10.1016/j.jfluchem.2004.11.009>.
- (48) Xu, L.; Cheng, J.; Trudell, M. L. Chromium ( VI ) Oxide Catalyzed Oxidation of Sulfides to Sulfones with Periodic Acid. *J. Org. Chem.* **2003**, *68*, 5388–5391. <https://doi.org/10.1021/jo03003>.
- (49) Smith, N. D.; Wohlrab, A. M.; Goodman, M. Enantiocontrolled Synthesis of  $\alpha$ -Methyl Amino Acids via Bn 2N- $\alpha$ -Methylserine- $\beta$ -Lactone. *Org. Lett.* **2005**, *7* (2), 255–258. <https://doi.org/10.1021/ol047761h>.
- (50) Siebum, A. H. G.; Woo, W. S.; Raap, J.; Lugtenburg, J. Access to Any Site-Directed Isotopomer of Methionine, Selenomethionine, Cysteine, and Selenocysteine - Use of Simple, Efficient Modular Synthetic Reaction Schemes for Isotope Incorporation. *Eur. J. Org. Chem.* **2004**, *2004* (13), 2905–2913. <https://doi.org/10.1002/ejoc.200400063>.
- (51) Chakraborty, T. K.; Ghosh, A. Synthesis of Chiral Alpha-Amino Acids. *Tetrahedron Lett.* **2002**, *43*, 9691–9693.
- (52) Zhou, S.; Wang, J.; Chen, X.; Aceña, J. L.; Soloshonok, V. A.; Liu, H. Chemical Kinetic Resolution of Unprotected  $\beta$ -Substituted  $\beta$ -Amino Acids Using Recyclable Chiral Ligands. *Angew. Chem. Int. Ed.* **2014**, *53* (30), 7883–7886. <https://doi.org/10.1002/anie.201403556>.



- (53) Yamamoto, J.; Kawashima, A.; Kawamura, A.; Abe, H.; Moriwaki, H.; Shibata, N.; Soloshonok, V. A. Operationally Convenient and Scalable Asymmetric Synthesis of (2S)- and (2R)- $\alpha$ -(Methyl)Cysteine Derivatives through Alkylation of Chiral Alanine Schiff Base NiIII Complexes. *Eur. J. Org. Chem.* **2017**, *2017* (14), 1931–1939. <https://doi.org/10.1002/ejoc.201700018>.
- (54) Johnston, H. J.; Hulme, A. N. A Facile, Inexpensive and Scalable Route to Thiol Protected Alpha-Methyl Cysteine. *Synlett* **2013**, *24* (5), 591–594. <https://doi.org/10.1055/s-0032-1318316>.
- (55) Alezra, V.; Bonin, M.; Micouin, L.; Policar, C.; Husson, H. P. The Origin of Chemical and Configurational Stability of Chiral Nonracemic Tert-Butyl Aziridinecarboxylate Anions. *Eur. J. Org. Chem.* **2001**, *2001* (13), 2589–2594. [https://doi.org/10.1002/1099-0690\(200107\)2001:13<2589::AID-EJOC2589>3.0.CO;2-Y](https://doi.org/10.1002/1099-0690(200107)2001:13<2589::AID-EJOC2589>3.0.CO;2-Y).
- (56) Park, J. D.; Kim, D. H. Cysteine Derivatives as Inhibitors for Carboxypeptidase A: Synthesis and Structure-Activity Relationships. *J. Med. Chem.* **2002**, *45* (4), 911–918. <https://doi.org/10.1021/jm010272s>.
- (57) Morlot, M.; Gourand, F.; Perrio, C. Deoxyradiofluorination Reaction from  $\beta$ -Hydroxy- $\alpha$ -Aminoesters: An Entry to [18F]Fluoroaminoesters under Mild Conditions. *Eur. J. Org. Chem.* **2019**, *2019* (23), 3751–3762. <https://doi.org/10.1002/ejoc.201900300>.
- (58) Casiraghi, A.; Valoti, E.; Suigo, L.; Artasensi, A.; Sorvillo, E.; Straniero, V. How Reaction Conditions May Influence the Regioselectivity in the Synthesis of 2,3-Dihydro-1,4-Benzoxathiine Derivatives. *J. Org. Chem.* **2018**, *83* (21), 13217–13227. <https://doi.org/10.1021/acs.joc.8b02012>.
- (59) Howson, S. E.; Allan, L. E.; Chmel, N. P.; Clarkson, G. J.; Deeth, R. J.; Faulkner, A. D.; Simpson, D. H.; Scott, P. Origins of Stereoselectivity in Optically Pure Phenylethanaminopyridine Tris-Chelates  $M(\text{NN}\zeta)_3 \text{N}^+$  ( $M = \text{Mn, Fe, Co, Ni and Zn}$ ). *Dalt. Trans.* **2011**, *40*, 10416–10433. <https://doi.org/10.1039/c1dt11184a>.
- (60) Morell, J. L.; Fleckenstein, P.; Gross, E. Stereospecific Synthesis of (2S,3R)-2-Amino-3-Mercaptobutyric Acid - an Intermediate for Incorporation into Beta-Methylanthionine-Containing Peptides. *J. Org. Chem.* **1977**, *42* (2), 355–356.
- (61) Ge, W.; Clifton, I. J.; Howard-Jones, A. R.; Stok, J. E.; Adlington, R. M.; Baldwin, J. E.; Rutledge, P. J. Structural Studies on the Reaction of Isopenicillin N Synthase with a Sterically Demanding Depsipeptide Substrate Analogue. *ChemBioChem* **2009**, *10* (12), 2025–2031. <https://doi.org/10.1002/cbic.200900080>.
- (62) Nakamura, Y.; Shin, C. Facile Syntheses of (S,S)-2,3-Diaminobutyric Acid and the Acid Containing N-Terminal Tripeptide of Antrimycins. *Chem. Lett.* **1992**, *21* (1), 49–52. <https://doi.org/10.1246/cl.1992.49>.

### 3. Quaternary Ammonium Compounds

Leitgeb, A.J.; Feliciano, J.A.; Sanchez, H.; Allen, R.A.; **Morrison, K.R.**; Sommers, K.J.; Carden, R. Wuest, W.M.; Minbiolo, K.P.C. “Further Investigation into Rigidity-Activity Relationships in BisQAC Amphiphilic Antiseptics” *ChemMedChem*, **2020**, *accepted*.

Invited digest: **Morrison, K.R.**; Allen, R.A.; Minbiolo, K.P.C.; Wuest, W.M., “More QACs, More Questions: Recent Advances in Structure Activity Relationships and Hurdles in Understanding Resistance Mechanisms” *Tetrahedron Lett.* **2019**, *60*, 150935.

Kontos, R.C.; Schallenhammer, S.A.; Bentley, B.S.; **Morrison, K.R.**; Feliciano, J.A.; Tasca, J.A.; Kaplan, A.R.; Bezpalko, M.W.; Kassel, S.W.; Wuest, W.M.; Minbiolo, K.P.C. “An Investigation into Rigidity-Activity Relationships in bisQAC Amphiphilic Antiseptics” *ChemMedChem* **2018**, *13*, 1.

Schallenhammer, S.A.; Duggan, S.M.; **Morrison, K.R.**; Bentley, B.S.; Wuest, W.M.; Minbiolo, K.P.C. “Hybrid BisQACs: Potent Biscationic Quaternary Ammonium Compounds Merging the Structure of Two Commercial Antiseptics” *ChemMedChem* **2017**, *12*, 1931.

The above listed publications were conducted in collaboration with the Minbiolo Lab at Villanova University where the aforementioned lab synthesized the compounds. Any and all biological data was conducted in the Wuest Lab with Morrison acting as primary scientist with valued support from Allen and Kaplan.

Blanchet, M. Borselli, D.; Rodallec, A.; Peiretti, F.; Vidal, N.; Bolla, J.-M.; Digiorgio, C.; **Morrison, K.R.**; Wuest, W.M.; Brunel, J.M., “Claramines: A New Class of Broad-Spectrum Antimicrobial Agents with Bimodal Activity.” *ChemMedChem*, **2018**, *13*, 1018.

The publication listed above was an additional collaborative effort by Morrison and Wuest with the Brunel lab in France. This publication includes editorial effects and intellectual contributions on biological results by Morrison and Wuest. Biological assays were conducted by Morrison but are not ultimately included in the publication.

Ongwae, G.; **Morrison, K.R.**; Allen, R.; Kim, S.; Im, W.; Wuest, W.M.; Pires, M.M. “Broadening Activity of Polymyxin by Quaternary Ammonium Grafting.” *ACS ID*, **2020**, *submitted*.

Our publication with the Pires lab was a collaborative effort by Morrison, Allen, and Wuest. Biological assays with the exception of *E. coli*, and analysis of that data were completed by Morrison and Allen.

#### 3.1 General QAC Structure and Mechanism of Action

Quaternary ammonium compounds (QACs), or small molecules with a positively charged nitrogen and long alkyl chains have been investigated and used to disinfect surfaces since the early 1900s.<sup>1-4</sup> Found in all manner of hygiene products and surface disinfectants, these ubiquitous molecules have allowed people to sanitize their homes, businesses, and hospitals.<sup>5-7</sup> QACs are active against a wide array of microbes

including bacteria, fungi, and viruses due to their non-discriminatory mechanism of action of cellular membrane disruption.

Initial interactions between a QAC and cell membrane occur as the positively charged hydrophilic head associates with the negatively charged phospholipid head. After first contact, the hydrophobic tail of the QAC intercalates into the membrane, associating with the fatty acid tail of the phospholipids. It has been observed recently through computation methods that charged lipids in the membranes closely associate to the QACs as they intercalate into the membrane.<sup>8</sup> At this point, the QAC can act in a number of ways to kill a microbe. First, multiple molecules can interact with the membrane independently causing fissures that promote the disruption of ion gradients across the cell membrane. Alternatively, QAC molecules can aggregate in the membrane leading to cell component leakage or pore formation and cell lysis (**Figure 3.1**). Additional data has found that cell death may be more sophisticated than just breaking the membrane apart, and that death may be caused by either an autolytic response to QACs or interactions with membrane-bound proteins.<sup>9</sup> In all cases these interactions and methods of killing are closely linked with QAC structure leaving researchers with many avenues to investigate.

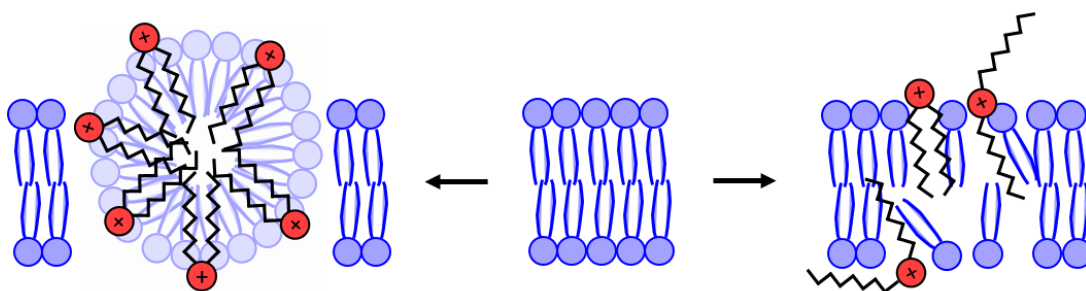


*Figure 3.20 Generally accepted QAC mechanism of action*

With antibiotics becoming less effective and bacteria gaining momentum through rapid resistance acquisition, QAC research and development continues to be a crucial area for chemists and biologists alike. The following sections will provide a brief overview of the field of QAC polymers and QAC small molecules, including work completed with collaborators from the Brunel, Pires, and Minbiole labs.

### 3.2 Polymeric Quaternary Ammonium Compounds (polyQACs)

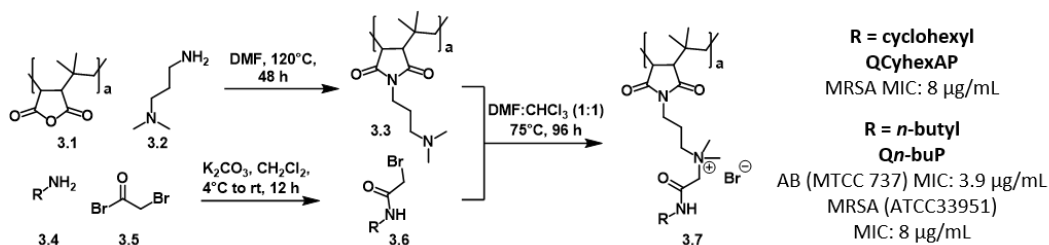
Several key research groups have emerged as pioneers at incorporating QACs into materials. Some of the key findings in recent years are highlighted in the following sections. (For additional information see the following reviews.<sup>10-12</sup>) Though small molecule QACs have a long and potent history, recent advances have shown that polyQACs can complement them, and together form very potent agents for disinfection. For example, traditional QACs can be wiped from surfaces through contact or other cleaning practices, thereby requiring repeated application. This leads to accumulation in Waste Water Treatment Plants (WWTPs) and the environment, causing an increase in resistance development.<sup>13</sup> Advantageously, polyQACs require only one application and therefore minimize the environmental stress.<sup>14</sup> There have also been recent advances that reduce the ability of proteins and cells from adhering to surfaces.<sup>15</sup> Furthermore, there have been several advances in the use of polyQACs *in vivo*.<sup>16,17</sup>

#### 3.2.1. The Haldar Group

One group that has been particularly active in the field of QAC materials research in the Haldar group at Jawaharlal Nehru Centre for Advanced Scientific Research. Over the years they have developed several exciting technologies, both in polyQACs and small molecule QACs with a focus on coatings for medical devices, like catheters. In 2016, they developed a series of polymeric amide QACs that demonstrated potent activity against methicillin-resistant *Staphylococcus aureus* (MRSA) and more significantly *A. baumannii* (AB).<sup>18</sup> AB is a Gram-negative pathogen found almost exclusively in hospitals, and is capable of surviving on surfaces longer than other bacteria due to biofilm formation. It is also more apt to acquire resistance due to its extended lifespan, and has been implicated in complex infections in immunocompromised individuals like burn victims, particularly soldiers who fought in the Iraq War, and Cystic Fibrosis (CF) patients.<sup>18-20</sup>

Over several iterations of investigation, the Haldar lab was able to demonstrate their proficiency at developing AB and MRSA active polymers. Initial forays into this area yielded four polymers with activity against resistant strains of AB (R674 and R676) in the range of 3.9 – 7.8 µg/mL.<sup>18</sup> Later studies expanded

the analog scope to the more active cyclohexyl amide polymer (**3.7**),<sup>21</sup> investigated the importance of hydrophobic group spacing,<sup>22</sup> and hydrogen bonding in these potential disinfectants.<sup>23–25</sup> A sample synthesis used by the Haldar lab is shown in **Scheme 3.1** demonstrating the ease of synthesis of these potent and effect membrane perturbers.



*Scheme 3.24: Haldar lab general synthesis of amide QAC polymers*

One mechanism of action proposed was through membrane permeabilization as would be expected from a QAC. However, further studies into polyQAC activity against biofilms showed the potential for lipopolysaccharide (LPS) neutralization. Using a series of analogs, fluorescence quenching experiments were conducted using BODIPY dye-LPS conjugates. In this experiment, BODIPY dye fluorescence is quenched as the LPS aggregates to it. When treated with polyQACs, the LPS aggregate is disrupted, promoting leakage of the dye and therefore an increase in the fluorescence signal dependent on the side chain structure of the polymer used. It was determined that polymers containing amide side chains demonstrated more aggregation with LPS, leading to the theory that amide moieties of the QAC are capable of hydrogen bonding with the ester moieties of LPS to promote interactions between the two types of polymers.<sup>26</sup>

Additional work by the Haldar group has focused on the use of dextran-based hydrogels for coating surfaces. Initial work in this area reported the successful use of dextran polyQACs in antimicrobial paint that kills both planktonic MRSA and established MRSA biofilms.<sup>27</sup> During *in vivo* experiments, researchers were able to observe clearance of bacteria from a catheter and surrounding tissue in a dose-dependent response.<sup>28</sup> Later, these dextran polyQACs were expanded into injectable hydrogels for wound healing and sealing. Researchers found that through membrane permeabilization, dextran hydrogels were capable of

preventing infection and bleeding *in vivo*.<sup>29</sup> Further extension of their technology demonstrated that these hydrogels could be further functionalized to form tunable drug release capsules.<sup>30</sup> Most recently, the Haldar group has combined their hydrogel technology with silver nanoparticles to form nontoxic, water-soluble, organo-soluble, antibacterial, and antifungal coatings that can clear MRSA infections from catheters.<sup>31</sup> For further details on the expansive and diverse research in the field of polyQACs, please see the Haldar groups recent review.<sup>12</sup>

### 3.2.2. The Finn Group

The Finn lab at Georgia Tech has made a name for themselves working with polyQACs, by focusing on ones that while retaining potency, can also degrade in aqueous media, as well as those that can be utilized in flexible polyvinyl chloride (PVC) tubing. QACs that can degrade in aqueous media allow for the minimization of active antimicrobial left behind after usage, thereby limiting the potential for resistance development. In 2016, Geng and Finn introduced their modular and fragmentable polyQACs containing a thiabicyclononane core (**Figure 3.2**).

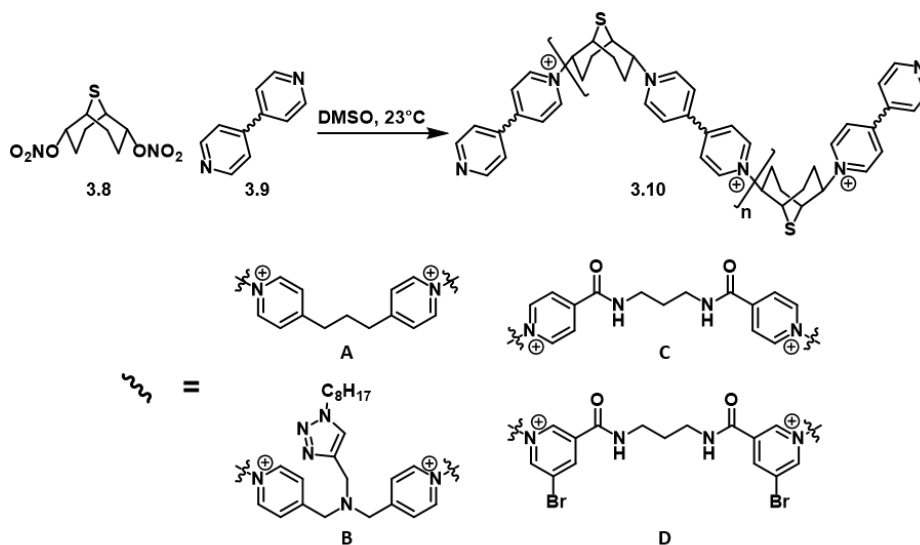


Figure 3.21: Geng et al. polyQACs

These highly functionalized and easily prepared polyQACs had an average of eight to twelve repeating units, with the longest containing twenty, and were easily degraded in aqueous media to give uncharged

components.<sup>32</sup> Though many of their polyQACs had significant activity against Gram-negative and Gram-positive bacteria, their best compound was a 18-mer with the diamide QAC **C** (**Table 3.1**).

Table 3.4: MICs of Geng et al. polyQACs

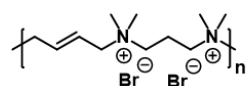
Monomer	n	Minimum Inhibitory Concentration in media (µg/mL)			
		<i>E.coli</i>	<i>B. subtilis</i>	<i>P. aeruginosa</i>	<i>S. aureus</i>
A	20	12.5	3	25	12.5
B	8	6.25	1.5	50	12.5
C	18	1.5	0.4	6	3
D	10	12.5	6.25	25	12.5

Geng and Finn also conducted resistance studies of their polyQACs by growing the bacteria with sub-MIC concentrations of active compound and then testing the MIC again. They found that compared to the known and widely-used QAC, cetylpyridinium chloride (CPC), their polyQACs became resistant at a slower rate.<sup>33</sup>

The Finn lab then turned their sights towards applying their polyQACs to practical situations. PVC tubing has many uses and functions, especially in the medical and food industries where sterility is crucial. If a flexible PVC tubing could be manufactured or treated to be inherently sterile, this would allow for safer medical and food practices. In 2018, Beveridge and colleagues published their work functionalizing flexible PVC tubing with a library of QACs through azide and alkyne handles. Their process works by first converting the PVC chlorines to azides, then utilizing a copper-catalyzed click reaction to append their alkyne-functionalized QACs.<sup>34</sup> Though antimicrobial testing has not been reported yet, stability and flexibility testing of the PVC tubing looks promising.

### 3.2.3. The Tiller Group

In 2015, Strassburg and coworkers at Technische Universität Dortmund, published thoroughly researched work regarding their tetramethyl-1,3-propanediamine polyQACs (PBI) compounds. These polyQACs were found to have activity against Gram-positive and Gram-negative bacteria, as well as significantly low hemotoxicity with HC<sub>50</sub> values above 40,000 µg/mL compared to MICs that were much lower. These PBIs were shown to have minimum bacteriocidal concentrations (MBC) equal to that of their MICs indicating that the polyQACs were capable of killing bacteria very efficiently (**Figure 3.3**).<sup>35</sup>



Bacteria	PBI <sub>n</sub> (μg/mL)	Bacteria Reduction (log(CFU)/mL)	Min. Biocidal Conc. (MBC) (μg/mL)
<i>E. coli</i>	MIC	40	4
	2(MIC)	80	4
	4(MIC)	160	>6
<i>S. aureus</i>	MIC	35	4
	2(MIC)	70	5
	4(MIC)	140	>6
<i>S. mutans</i>	MIC	18	4
	2(MIC)	36	4
	4(MIC)	72	6

**Poly(3,4-en-ionene)**  
**PBI<sub>n</sub>**  
**3.11**

Figure 3.22: General PBI structure and activity against select bacteria

Later, these PBI compounds were converted to self-deactivating polymers by adding backbone ester groups to alleviate resistance development pressure in real-world applications. This series was more potent against Gram-positive bacteria and retained potency against Gram-negative bacteria. For *S. aureus*, a greater distance between carbonyls provided more active polyQACs with little effect from the distance between carbonyl and ammonium groups. In contrast, for *P. aeruginosa*, the greater the distance between carbonyls, the less active the polyQAC. In both cases, this effect is minimal when comparing an X value of 2 or 4, but is readily apparent when X = 8 (**Figure 3.4**).<sup>36</sup>

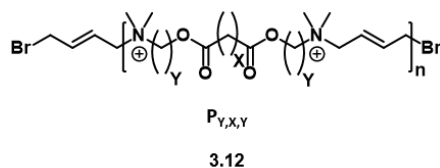


Figure 3.23: General structure of self-deactivating polyQACs

Later, Richter and coworkers investigated the effect of end groups on the antimicrobial activity of poly(ethylene imine)s (PEI). Taking inspiration from prior work on poly(2-methyl-2-oxazoline) telechelic (end active) polymers, the PEIs were synthesized through end-group functionalization with varying lengths of alkyl chains. After full characterization of the polymeric properties, Richter *et al.* investigated the antimicrobial activity. When compared to their oxazoline counterparts, PEI polyQACs had improved activity against *E. coli* (40-160 μg/mL better) and *S. aureus* (20-40 μg/mL better).<sup>36</sup>



Not satisfied with their progress in polyQACs alone, the Tiller group started a new project wherein common antibiotics that are known to have bacterial resistance are combined with polyQACs to form a new chimeric antimicrobial. Schmidt and coworkers combined ciprofloxacin with poly(2-methyl-2-oxazoline) and ethylene diamine, and then studied their activity as well as the rate of resistance occurrence compared to ciprofloxacin alone (**Figure 3.5**).<sup>37</sup> In general, neither of the synthesized chimeras had lower MIC values than ciprofloxacin alone against *S. aureus*, *E. coli*, *K. pneumoniae*, or *P. aeruginosa*. In most cases Me-PMO<sub>x<sub>n</sub></sub>-EDA-eCIP had lower MIC values than Me-PMO<sub>x<sub>n</sub></sub>-EDA-xCIP with the exception of against *S. aureus*. In resistance studies with *S. aureus*, the ciprofloxacin MIC increases drastically to about 800 μM from about 1 μM after 7-8 days of a potentiation assay; however, Me-PMO<sub>27</sub>-EDA-xCIP is ten-times lower resistance development rate. Against *E. coli*, ciprofloxacin's MIC went from 0.10 to 63 μM over ten days. When the same analysis was completed with both chimeras, the MIC of Me-PMO<sub>27</sub>-EDA-xCIP increased to over 400 μM, and the MIC of Me-PMO<sub>39</sub>-EDA-eCIP increased only from 4.6 μM to 34 μM.

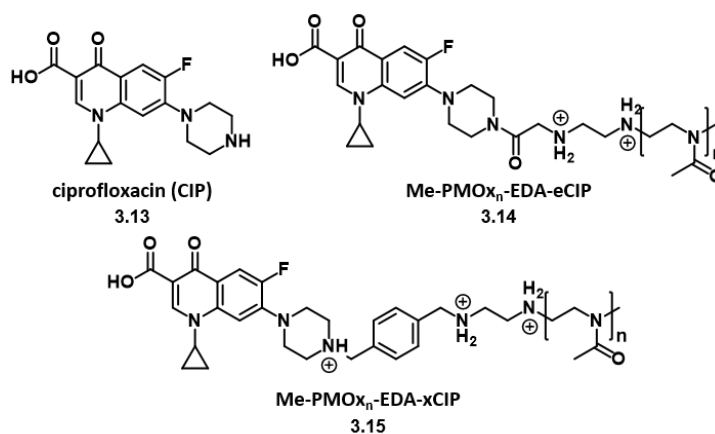


Figure 3.24: General structures for ciprofloxacin-polyQAC chimeras

The opposing preferences for the chimeras was proposed to be an effect of differences in cleavage mechanisms. In Gram-positive *S. aureus*, it was thought that when the eCIP linker is cleaved the ciprofloxacin piece would be similar to the native drug and therefore be susceptible to resistance mechanisms, whereas cleavage of the xCIP linker may be just different enough to prevent the bacteria from

recognizing ciprofloxacin. In Gram-negative *E. coli*, it was theorized that the hydrolysis rate may be slower preventing triggering of resistance.

### 3.3 QACs as small molecules

#### 3.3.1. Commercial QACs

Small molecule QACs have been incorporated into cleaning and disinfecting agents since the early 1900s. They made their first appearance in the US when BAC was approved by the Environmental Protection Agency (EPA) in 1947.<sup>38</sup> Since then, QACs have been incorporated into all kinds of consumer products and more variations of QAC have been discovered. Shelton and coworkers identified a series of new QAC structures including quaternary amines,<sup>39</sup> ester functionalities,<sup>40</sup> as well as the well-known cetylpyridinium chloride (CPC) and cetyltrimethylammonium bromide (CTAB)<sup>41</sup> all published in 1946. Later, in 1962 the EPA registered didecyldimethylammonium chloride (DDAC) as a new biocide (**Figure 3.6**).<sup>42</sup> Based on the EPA registrations, QACs were approved for usage in water processing systems, institutional and commercial equipment, medicinal equipment, agricultural equipment, residential uses, and food handling and storage.<sup>38,42</sup> Their usage continues to grow and spread and has since included the addition of benzethonium chloride (BEC) which is commonly found in topical disinfectants.

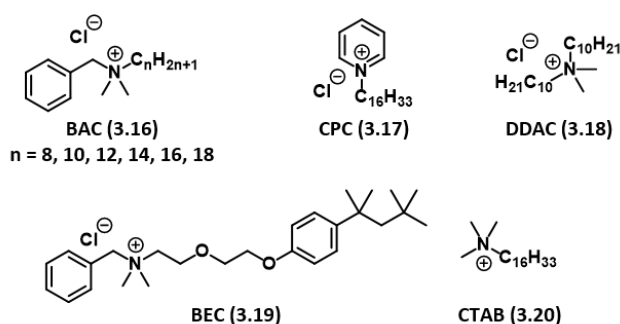


Figure 3.25: Common commercial QACs

#### 3.3.2. Aminosterols as QACs

Aminosterols are small molecules with broad range biological activity. They are so named due to their steroid core and pendant amine groups which under physiological conditions make them QACs. The focus of these investigations, squalamine, was isolated from a dogfish shark in 1993 and demonstrated potent antibiotic activity against Gram-positive and Gram-negative bacteria that seemed dependent on amine

substitution and location for activity.<sup>43</sup> Further investigations proposed that due to squalamine's ability to perturb cell membranes and its inherent ability to evade efflux pumps, it may be a good chemosensitizer for other antibiotics. When squalamine is used in conjunction with known antibiotics, it was shown to sensitize the bacteria in most cases, as can be seen in (**Table 3.2**). Remarkably, when tested against efflux pump overproducing strains, squalamine retains its ability to chemosensitize.<sup>44</sup>

Table 3.5: Squalamine as a chemosensitizer of common antibiotics. Squalamine dosed at 1/5 MIC per bacteria strain. (Squalamine MICs were: AG100 2 mg/L; AG100Atet 2 mg/L; PAO1 16 mg/L; PA124 16 mg/L; ATCC13048 8 mg/L; CM-64 8 mg/L.)

Bacteria/strains	MIC (mg/L)					
	Squalamine	chloramphenicol	ciprofloxacin	tetracycline	cefepime	erythromycin
<i>E. coli</i> AG100	-	8	0.25	2	0.5	512
	+	0.5	0.03	0.125	0.06	256
	-	16	1	64	1	256
	+	2	0.03	8	0.12	256
<i>P. aeruginosa</i> PAO1	-	512	16	16	8	512
	+	16	<1	4	1	256
	-	256	32	32	4	1024
	+	64	16	8	2	256
<i>K. pneumoniae</i> KP63 (porin-)	-	256	16	8	8	256
	+	64	<1	1	2	64
	-	32	32	>128	64	256
	+	<1	<1	8	<1	64
<i>E. aerogenes</i> ATCC13048	-	4	0.5	2	0.25	512
	+	0.25	0.015	0.25	0.03	128
	-	256	0.5/1	16	0.25	512
	+	16	0.03	1	0.06	256
CM-64 (ATCC derivative, overproducing AcrAB)	-	256	0.5/1	16	0.25	512
	+	16	0.03	1	0.06	256

To elucidate the mechanism of action further, the Brunel lab began by synthesizing analogs of squalamine, the most significant of which was claramine A1 (**Figure 3.7**). Claramine A1 has comparable MICs to squalamine against Gram-positive and Gram-negative bacteria. Both compounds, as well as known antibiotic polymyxin B and an inactive analog claramine A19, were tested in a series of assays focused on membrane integrity in order to determine the exact mechanism of action. The first experiment conducted used bioluminescence to detect the presence of ATP leaking from Gram-positive and Gram-negative cells treated with claramine A1. Gram-positive *S. aureus* was greatly affected by claramine A1, showing permeabilization after just two minutes of treatment; however, Gram-negative *E. aerogenes* EA289 showed almost no ATP leakage. Due to the differences in outer membrane structure between these

two bacteria this is not necessarily unexpected, but given the MIC of claramine A1 against EA289 further investigation was warranted.<sup>45</sup>

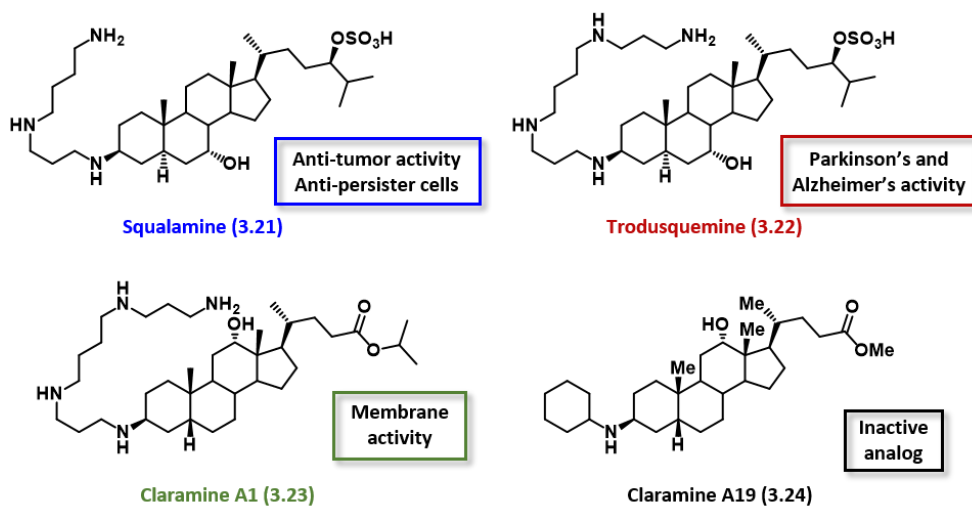


Figure 3.26: Aminosterol structures and biological activities

To focus on the effect of claramine A1 against Gram-negative EA289, a nitrocefin assay was employed. In this assay nitrocefin is hydrolyzed by  $\beta$ -lactamases located in the periplasm causing a color change from yellow to red. Though this effect was observed and it was concluded that claramine A1 does indeed permeabilize the outer membrane, researchers wanted to understand if this was an energy dependent or independent permeabilization which could be measured through a DiSC<sub>3</sub>(5) assay, which is a probe that is sensitive to the membrane potential. In this assay, when a compound affects the membrane potential, specifically the proton gradient, an increase in fluorescence is observed due to the DiSC<sub>3</sub>(5) dye being released. An increase in fluorescence was seen for both the Gram-negative and Gram-positive treated bacteria indicating to researchers that since efflux pumps often use proton gradients to export drugs and dyes, further experimentation was needed to potentially link claramine A1 activity to efflux pumps, specifically AcrAB-TolC.

In the efflux pump inhibition assay, researchers found claramine A1 treatment inhibited > 90% of the dye from being released. This hints that claramine A1 may be an efflux pump inhibitor and therefore

could be used with other known antibiotics, especially those that have lost potency due to efflux pump resistance mechanisms. Combination treatment with doxycycline and claramine A1 led to MICs of 0.5  $\mu\text{g}/\text{mL}$  against EA289 and 2  $\mu\text{g}/\text{mL}$  against PAO1 in comparison to doxycycline alone: 40  $\mu\text{g}/\text{mL}$  against EA289 and 16  $\mu\text{g}/\text{mL}$  against PAO1.<sup>45</sup> Recent reports have even demonstrated that squalamine has potent activity against persister cells and viable but non-culturable cells (VBNCs) of *A. baumannii*.<sup>46</sup>

Other aminosterols have been investigated over the years and have shown significant activity against biological polymers such as amyloid- $\beta$  and  $\alpha$ -synuclein. Specifically, trodusquemine (**Figure 3.6**) has been shown to promote amyloid- $\beta$  aggregation, but inhibit binding to cell membranes, effectively limiting the toxicity of the aggregates.<sup>47,48</sup> Parkinson's, with its similar disease state of plaque formation, was also found to be arrested due to squalamine and trodusquemine both inhibiting  $\alpha$ -synuclein aggregates *in vitro*.<sup>49</sup>

### 3.3.3. Repurposing Known Antibiotics

One school of thought in fighting the battle against antibiotic resistance development is to repurpose known antibiotics through combining multiple modes of action providing an advantage against bacteria. Even if the bacteria has a resistance mechanism to thwart one part of the antibiotic, they may not have both. Alternatively, the energetic cost of bacteria to acquire, evolve, and synthesize two different modifications to defeat the antibiotics is much higher, therefore slowing the observation of resistance. In the following section, efforts to add another mode of action to polymyxin B and vancomycin will be discussed.

#### 3.3.2.1 Vancomycin Analogs by the Boger Lab

One group of pioneers investigating the repurposing of known antibiotics is the Boger lab. Their work with vancomycin analogs has provided the field with methods of combatting known resistance mechanisms and potent potential therapies. Vancomycin, and others of its class, inhibit bacterial growth by interrupting cell wall synthesis by binding the D-Ala-D-Ala end of a peptide, thereby halting further lengthening and effectively inhibiting peptidoglycan crosslinking (**Figure 3.8**). As was discovered by the Walsh lab, in resistant bacteria bearing the *vanA* and *vanB* resistance genes, the second alanine is mutated to a D-lactate.

This mutation has little effect on cell wall synthesis, but it does decrease vancomycin binding by 1000-fold, rendering it useless.<sup>50</sup>

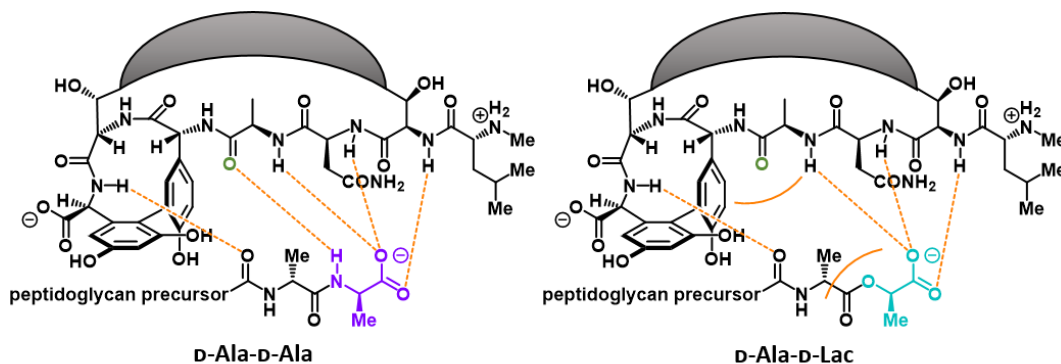


Figure 3.27: Aminosterol structures and biological activities

Further investigation into this binding pocket revealed that a loss of hydrogen bonding and an increase in lone-pair repulsion between the carbonyl of vancomycin and the ester of the lactate were the primary culprits for inactivation of vancomycin.<sup>50,51</sup> With this in mind, the Boger lab was able to design and synthesize a vancomycin analog that replaces the carbonyl (**Figure 3.9, Z**) with a nitrogen forming a temporary QAC structure and regaining potency.<sup>52,53</sup> Overcoming this resistance mechanism by changing one atom of the original structure is truly astounding and has spurred more research in this area.

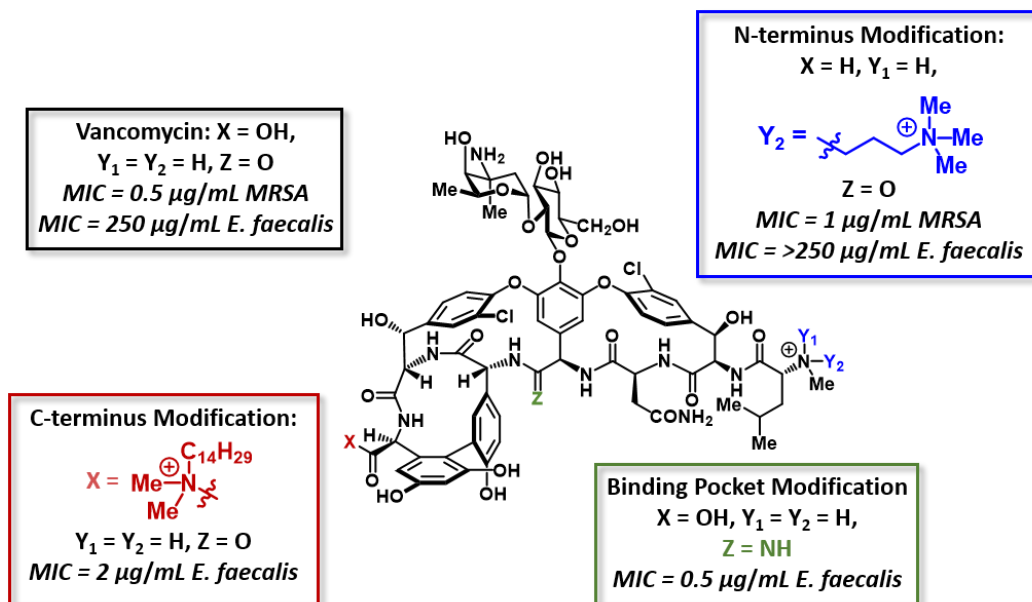


Figure 3.28: Overview of Boger lab QAC-vancomycin analogs and their activity against VanA *E. faecalis*

The next modification that the Boger lab considered was appending a quaternary ammonium moiety to allow for better cell membrane permeability of vancomycin. There are two positions that are amenable to addition of a quaternary ammonium, the C-terminus and the N-terminus (**Figure 3.9, X and Y** respectively). Initial investigations began with the C-terminus of vancomycin and were successful in generating analogs with QAC functionality. In fact, the MIC of vancomycin against VanA *E. faecalis* and VanA *E. faecium* with no modification is 250 µg/mL, but with the quaternized nitrogen they observed an MIC of 2 µg/mL. Researchers showed that the quaternary ammonium moiety increases cell membrane permeability, allowing vancomycin to now have potency against Gram-negative bacteria.<sup>54</sup> The synergistic relationship developed by appending a quaternary ammonium encouraged researchers to investigate functionalization at the N-terminus of vancomycin. While these analogs remained potent against Gram-positive pathogens like MRSA, they were ineffective against *E. faecalis*, demonstrating that both structure and location of the quaternary ammonium is crucial to vancomycin's ability to permeabilize cell membranes.<sup>55</sup>

#### 3.3.2.2. Polymyxin B Analogs with the Pires Lab

Recent work completed in collaboration with the Pires lab has included biological investigation of polymyxin B analogs containing a quaternary ammonium functionality. Polymyxin B, a cyclic decapeptide with a alkyl chain tail at the N-terminus, and many of its family members were originally isolated from *Bacillus polymyxa* (**Figure 3.10**).<sup>56</sup> Polymyxin B was originally used ubiquitously for its potent membrane activity against Gram-negative bacteria, but use was later limited due to its proclivity to cause nephrotoxicity (kidney toxicity). However, when faced with the alarming emergence of multidrug resistant (MDR) PA, AB, and *K. pneumoniae* (KP), physicians elected to prescribe polymyxin in a desperate attempt to save their patients.<sup>57</sup>

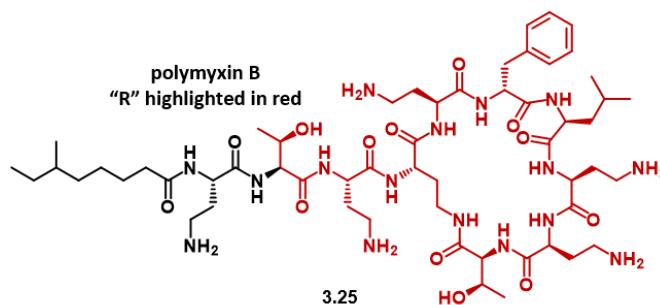


Figure 3.29: Polymyxin B structure highlighting the conserved cyclic peptide core for Pires lab analogs

In physiological conditions, polymyxin B has many positively charged nitrogens allowing for electrostatic interactions with the negatively charged phospholipids of Gram-negative cell membranes. Unfortunately, antibiotic resistance in the form of cell membrane lipid modifications has increased.<sup>58</sup> In 2016, researchers reported that polymyxin resistance could be transferred through the MCR-1 plasmid allowing for ease of transfer and escalation of polymyxin and colistin resistance.<sup>59</sup> Given their mechanism of action and structure, the Pires lab decided to make several permanent QAC analogs in an attempt to increase their potency and perhaps even combat some bacterial resistance.

Talented scientists from the Pires lab synthesized fourteen analogs containing the polymyxin core with varied alkyl chain lengths, type of quaternary nitrogen, and number of quaternary centers (**Figure 3.11**). Alkyl chain lengths on the fatty acid projection were either seven (**3.26, 3.28**) or fourteen (**3.27, 3.29**) carbons, and one example of eight carbons (**3.35**) where the seven carbon chain mimics the native structure of polymyxin B with and without the pendant DAB (diaminobutryl) moiety. Additionally, an analog was synthesized that incorporated three, seven-membered carbon chains without the pendant DAB (**3.38**). Another series of analogs tested the type of lipophilic projection by switching the alkyl chain to a biaryl group (**3.30, 3.31**) and a pyridinium-benzene (**3.32**) structure. Finally, analogs were designed to test specificity for location of the fatty acid chain by switching the alkyl chain to the amine of the pendant DAB (**3.34, 3.37**). In the case of compound **3.36**, the DAB group was switched to a lysine with eight carbon chain, and in an attempt to test the utility of a multiQAC, every DAB residue of polymyxin B was modified to a trimethyl ammonium to yield a pentaQAC (**3.39**).



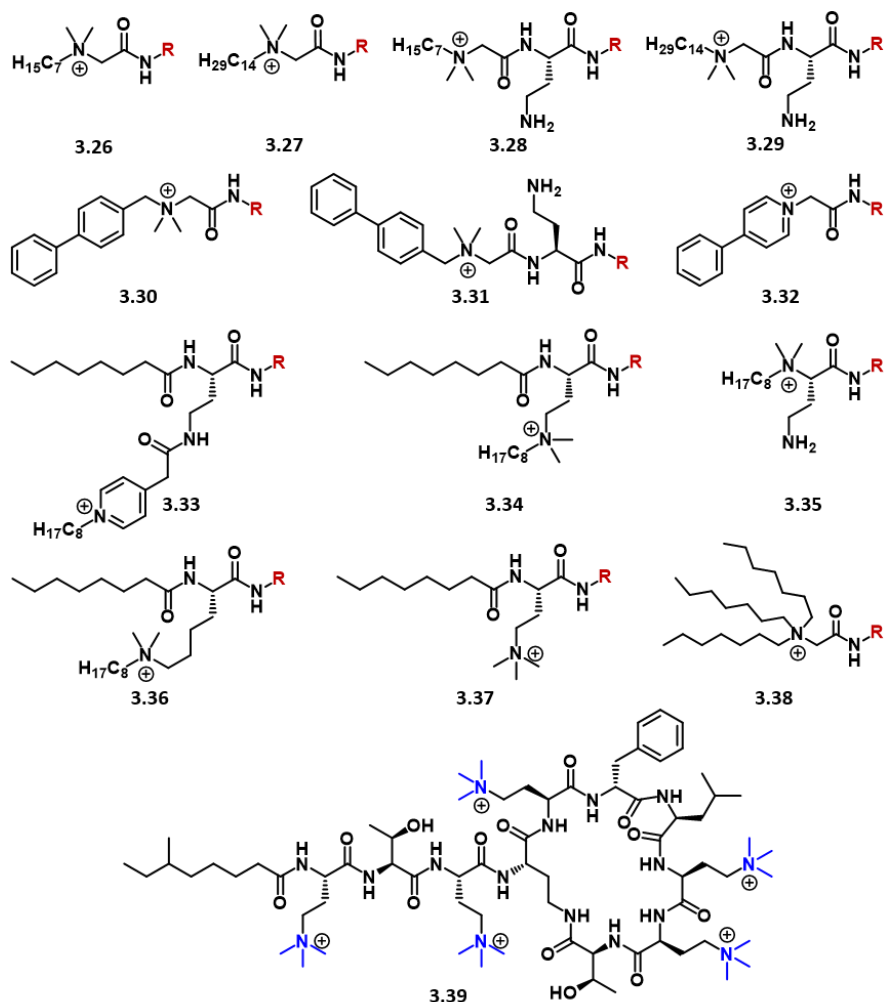


Figure 3.30: Polymyxin B-QAC analogs synthesized by Pires lab

Once the synthesis was completed, biological investigation was continued in the Wuest lab. Five strains of bacteria were chosen for analysis including four Gram-negative strains and one Gram-positive strain. Of the Gram-negative bacteria, two were common strains of PA: PAO1 and the more virulent PA14. The other two Gram-negative strains were a common strain of AB and a clinically isolated strain of AB that carries clinically observed colistin resistance. The final strain was CA-MRSA, which would allow researchers to determine if addition of the quaternary center expanded polymyxin's activity to Gram-positive bacteria.

Biological investigation commenced with MIC assays completed with both colistin and polymyxin B as positive controls. From these studies, some interesting trends began to emerge (**Table 3.3**). Compounds **3.30** – **3.33**, **3.36**, and **3.39** had no, or very poor MICs against all of the bacteria tested. Analogs **3.30** – **3.33** contained an aryl or pyridinium group in place of the typical fatty acid chain of polymyxin B, hinting that chain flexibility or other electronic considerations may inhibit interactions with the phospholipid bilayer. Compound **3.39** is the only compound to have an altered peptide core in that every DAB residue was converted to a trimethyl ammonium species. Its lack of potency suggests that in the case of polymyxin B, increasing positive charge of the cyclic peptide prohibits the molecule from interacting with the hydrophobic portion of cell membranes therefore abolishing activity. When comparing compound **3.36** to the other analogs, one can see that it is closest in structure to analog **3.34**. Each of these analogs contain a quaternary center at the former primary amine position composed of two methyl groups and an eight carbon chain. The only difference is that **3.36** has a pendant lysine residue and **3.34** has the normal DAB residue. The loss of activity when modifying the DAB to a lysine hints that this pendant group may provide a specific spatial interaction with the membrane that is disrupted by extending the chain by two carbons.

Table 3.6: MICs of Polymyxin B-QAC Analogs (*E. coli* data collected by Pires lab)

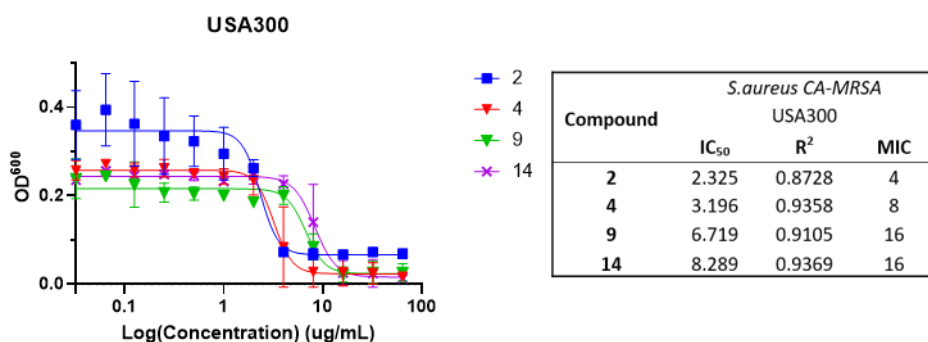
Compound	Minimum Inhibitory Concentration (µg/mL)					
	<i>A. baumannii</i>	<i>A. baumannii</i>	<i>P. aeruginosa</i>	<i>P. aeruginosa</i>	<i>S. aureus</i>	<i>E. coli</i>
	ATCC19606	DoD17943	PAO1	PA14	USA300	ATCC 25922
<b>3.26</b>	>63	>63	8	8	>63	1
<b>3.27</b>	>63	>63	4	4	4	8
<b>3.28</b>	16	>63	2	2	>63	4
<b>3.29</b>	8	>63	4	8	8	16
<b>3.3</b>	>63	>63	>63	63	>63	32
<b>3.31</b>	>63	>63	>63	>63	>63	25
<b>3.32</b>	>63	>63	>63	>63	>63	32
<b>3.33</b>	>63	>63	>63	>63	>63	32
<b>3.34</b>	>63	>63	>63	>63	16	8
<b>3.35</b>	8	>63	2	1	>63	2
<b>3.36</b>	>63	>63	32	63	>63	16
<b>3.39</b>	>63	>63	>63	>63	>63	32
<b>3.37</b>	16	>63	4	2	>63	4
<b>3.38</b>	>63	>63	16	8	16	32
polymyxin B	16	>63	4	2	>63	1
<b>12(3)2(3)12</b>	250	250	4	4	2	NT

Analogs **3.28**, **3.29**, **3.35**, and **3.37** had generally comparable or better activity than polymyxin B against both strains of PA, the commercial strain of AB (ATCC19606), and *E. coli* (EC). Interestingly, all four of these analogs contain the pendant DAB moiety, but **3.28**, **3.29**, and **3.35** have the QAC moiety in place of the polymyxin's fatty acid chain with alkyl chains of seven, eight or fourteen carbons which leaves the DAB primary amine free. In contrast, analog **3.37** has a trimethyl quaternary ammonium functionality on the DAB amine with the rest of the molecule matching that of polymyxin B. All four of these analogs have only one alkyl chain projection, even though they vary in position on the molecule, and the pendant DAB indicating that perhaps these characteristics allow for optimal interactions with cell membranes. Previous research has indicated that longer chain lengths of sixteen carbons interact best with lipid A, a common component of Gram-negative outer membranes.<sup>9</sup>

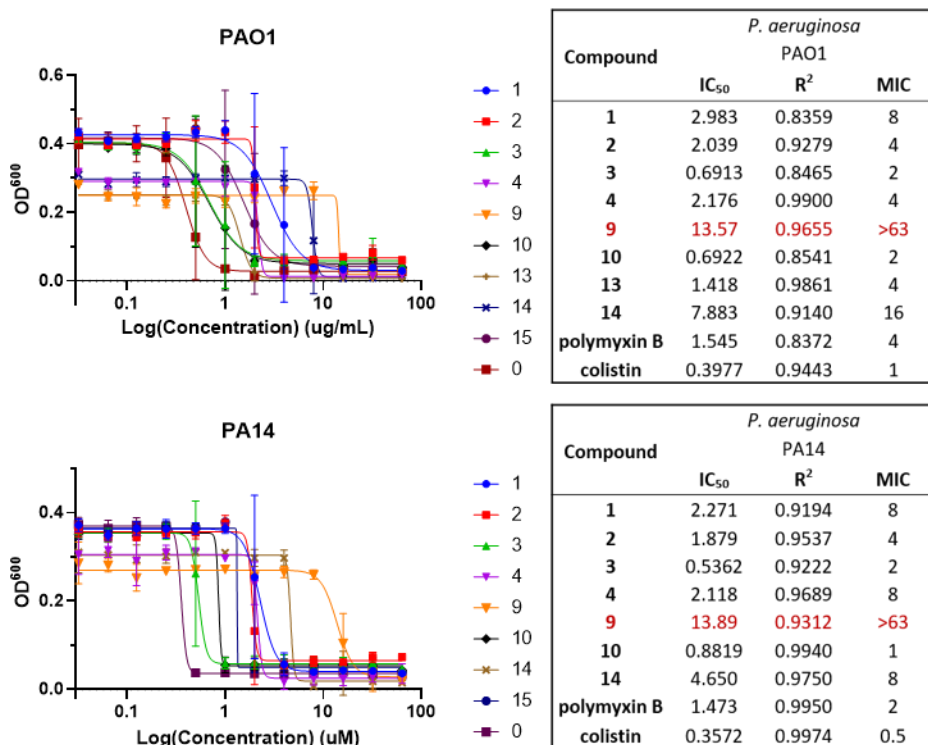
In line with typical polymyxin B and colistin activity, most of the analogs were not active against Gram-positive bacteria with the exception of **3.27**, **3.29**, **3.34**, and **3.38**. Both compounds **3.27** and **3.38** have truncated side chains and no DAB residue; however, **3.27** has an alkyl chain of fourteen carbons while **3.38** has three seven carbon alkyl chains. Compounds **3.29** and **3.34** both have a pendant DAB residue, but **3.29** has an alkyl chain of fourteen carbons whereas **3.34** has the native alkyl chain from polymyxin B and an additional eight carbon alkyl chain from the ammonium on the pendant DAB. From this data, it may be that if the side chain of polymyxin B is truncated or missing the DAB residue, then the molecule can retain potency by compensating with a longer alkyl or bulkier alkyl chain. Overall, the best molecule from this short study is compound **3.29**, which has broad spectrum activity against Gram-negative and Gram-positive bacteria.

Alarmingly, none of the polymyxin analogs, nor polymyxin B or colistin themselves, were active against the clinical strain of AB (MRSN17493). In an attempt to gain more information about the potency of the polymyxin B analogs, IC<sub>50</sub> values were determined. This allows the researchers to ascertain if the analogs are inhibiting at least 50% of the growth. This measurement is calculated based on average optical density of each well, completed in triplicate, whereas MICs are visually determined by wells with no

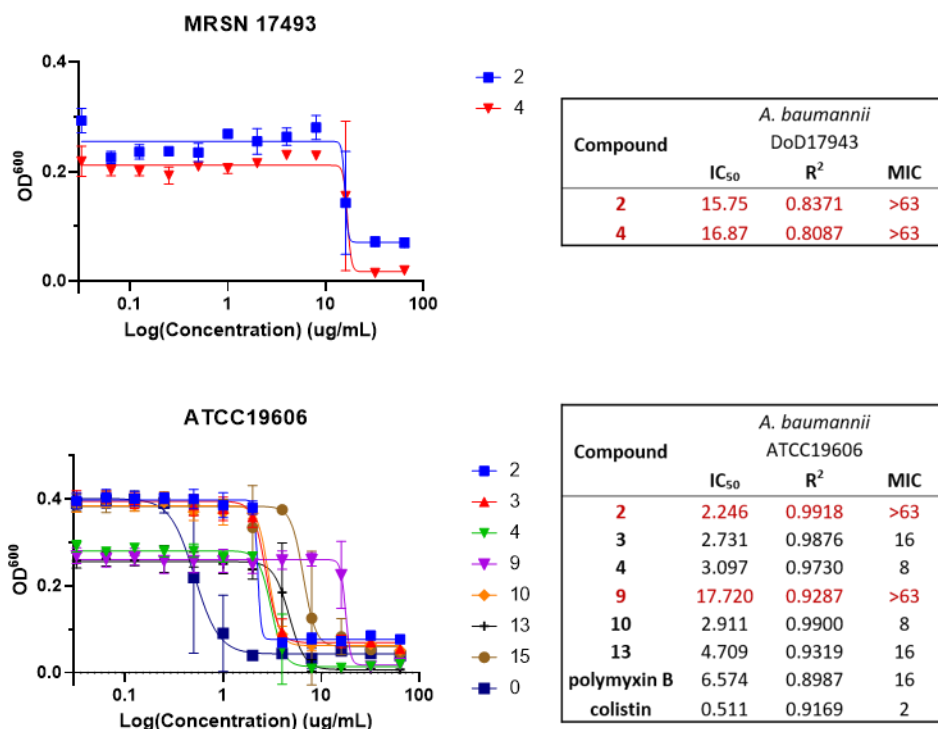
bacterial growth at all. While MICs or complete killing is preferred, we were curious to see if any of the analogs were able to inhibit the growth of AB strain MRSN17493. The IC<sub>50</sub> graphs for each bacterium are provided for those compounds that gave an IC<sub>50</sub> curve with an R<sup>2</sup> value greater than 0.8 (**Graphs 3.1 - 3.3**).



Graph 3.2: IC<sub>50</sub> data of polymyxin B analogs against CA-MRSA



Graph 3.3: IC<sub>50</sub> data of polymyxin B analogs against *P. aeruginosa*



Graph 3.4: IC<sub>50</sub> data of polymyxin B analogs against *A. baumannii*

From the IC<sub>50</sub> data, three compounds stand out as having an inhibitory activity without an observable MIC: **3.27**, **3.29**, and **3.34**. Most significantly, it can be seen that both analogs **3.27** and **3.29** exhibited IC<sub>50</sub>s against AB DoD17493 at 15.75 µg/mL and 16.87 µg/mL respectively (**Graph 3.3**). While this provides hope that researchers will be able to inhibit DoD17493, these concentrations are much higher than desirable, especially given their ability to lyse 20% of blood cells occurs at 32 µg/mL. This parameter indicates a very small therapeutic window for dosing, resulting in the need for further investigations.

### 3.3.2. Minbiole-Wuest Labs: Collaborative QAC Development

Over the last 6 years, the Minbiole and Wuest labs have developed a fruitful partnership investigating the field of quaternary ammonium compound (QAC) disinfectants. Minbiole lab members use their chemical skills to synthesize amphiphilic small molecules which are then investigated for biological activity by the Wuest lab. The following sections will cover some of the most important advancements over the years followed by a focus on several series of antiseptics investigated by myself and fellow lab members.

### 3.3.3.1. TMEDA Inspired QACs: the start of a beautiful thing

The first two publications from Minbiole and Wuest set the stage for future investigations by allowing confirmation of trends in alkyl chain length and number of quaternary centers. These two publications informed their future studies and allowed researchers to explore creatively. Learning from other established groups in the field,<sup>60,61</sup> Minbiole and Wuest began their QAC journey by synthesizing thirty-five asymmetric and symmetric bisQACs with a core structure based on *N,N,N',N'*-tetramethylethylenediamine (TMEDA) (**Figure 3.12**).<sup>62</sup> The Minbiole lab's synthesis of these compounds highlights their synthetic prowess to make asymmetric variants heretofore untouched by the field. Synthesis of TMEDA bisQACs with various alkyl chain lengths from eight to eighteen proceeded in modest to good yields, allowing rapid development of their library, which was later passed to the Wuest lab for biological investigation against four bacteria: *S. aureus* (SH1000), *E. faecalis* (OG1RF), *E. coli* (MC4100), and *P. aeruginosa* (PAO1). In general, researchers were able to determine that an alkyl chain length of twelve carbons, or a total of twenty to twenty-four alkyl sidechain carbons, provided optimal activity against both Gram-positive and Gram-negative strains of bacteria. It was also determined that asymmetry assisted in solubility, and in some cases improved potency in an MIC assay, provided that they followed the twenty to twenty-four sidechain carbon rule, with the exception of the monoQACs only having activity against Gram-positive bacteria.

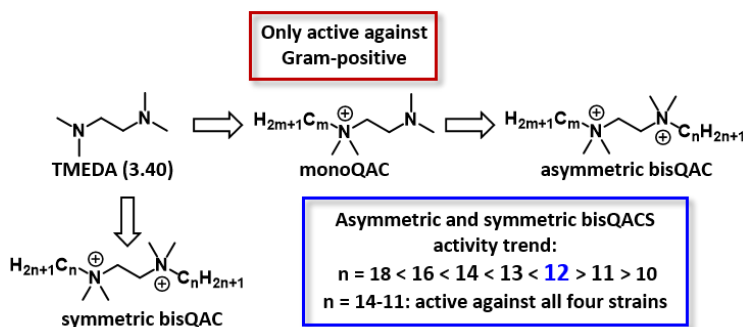


Figure 3.31: General structure and design of TMEDA-based QACs

### 3.3.3. Bis-, Tris-, and TetraQACs

Next, the Minbiole and Wuest groups turned their attention to synthesizing a series of multiQACs that would assess the effect of additional cationic centers and charge separation. The Minbiole lab synthesized

a group of both symmetric and asymmetric QACs ranging from bis- to tetraQACs with alkyl chain lengths ranging from ten to sixteen carbons.<sup>63</sup> They also included carbons with structures other than alkyl chains like benzyl and allyl functionalities (**Figure 3.13**). Biological testing proceeded with the same four strains of bacteria as were previously established. When comparing charge separation, there was little difference in potency observed. There was also little change in the activity based on number of quaternary centers between bis-, tris- and tetraQACs. MonoQACs were again demonstrated to be the least active compounds in the series and chain lengths of twelve sidechain carbons performed optimally. Having established themselves in the field and learned guiding principles for their future investigations, Minbiole and Wuest continued to investigate the creative limits of these cationic biocide compounds.

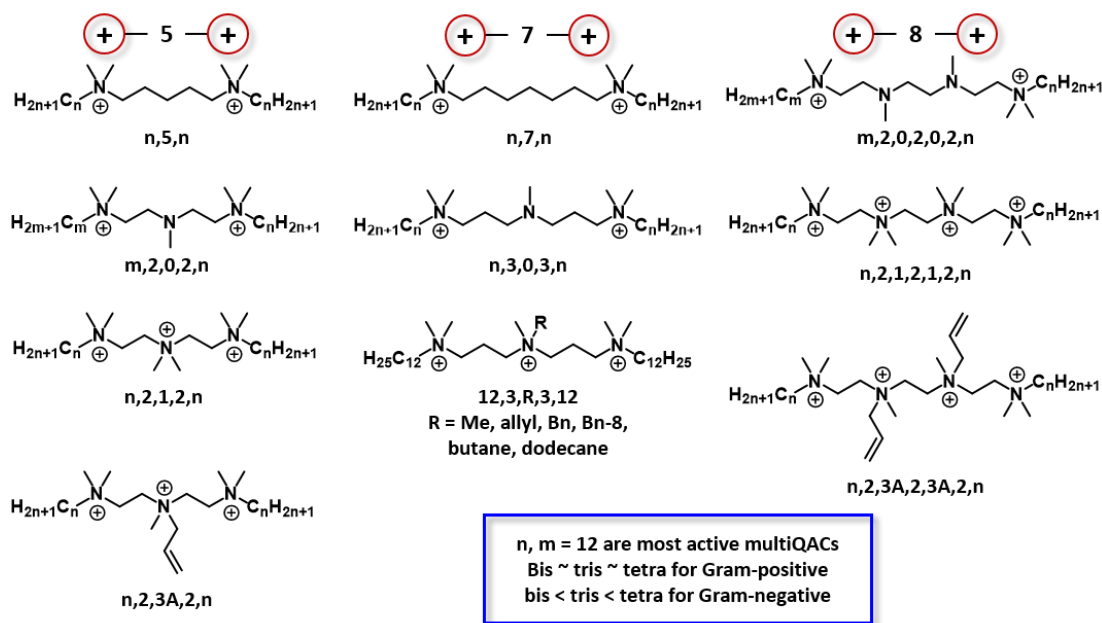


Figure 3.32: General structure and design of bis-, tris-, and tetraQACs

### 3.3.3.3. Hybrid QACs

Two of the most commonly used antiseptics, BAC and CPC, have proven their effectiveness and durability over approximately 90 years of use.<sup>64</sup> Unfortunately, their usefulness is beginning to decline due to resistance development to MRSA and their poor performance inhibiting the growth of Gram-negative bacteria. Though still used in common household disinfectants and oral hygiene products,<sup>1,65</sup> the need to

develop new compounds to supplement or take their place is becoming imperative. With this goal in mind, the Minbiole and Wuest labs designed a series of compounds that would combine the active motifs of BAC and CPC into a new, hybrid form of bisQAC disinfectant (**Figure 3.13**).

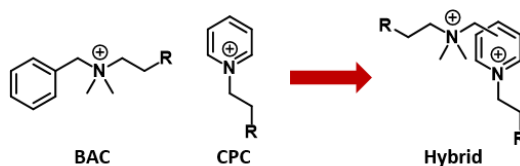
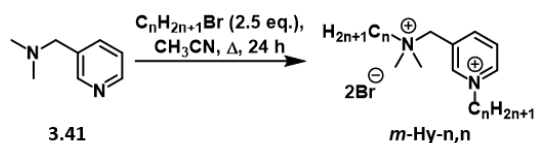


Figure 3.13: Conceptual design of hybrid QACs

By adding the pyridinium component of CPC to the benzyl ammonium component of BAC, 28 bis-QACs were synthesized and tested for bacterial inhibition activity.<sup>66</sup> Original designs aimed to have *ortho*-, *para*-, and *meta*- substitutions, relative to the nitrogen of the pyridine ring, to further compare importance of the chain projection to pyridinium moiety. Due to steric constraints of the available starting materials, alkylation of either the benzyl amine nitrogen or the pyridine nitrogen of 2-dimethylaminomethyl pyridine, 4-dimethylaminomethyl pyridine, or 4-(2-diethylaminoethyl) pyridine were all unsuccessful. Fortunately, alkylation at both nitrogens of 3-dimethylaminomethyl pyridine (**3.41**) was successful yielding eight bisQACs of varied chain lengths with the naming convention *m*-Hy-*n*,*n* where “*m*” is for *meta*-substitution, “Hy” is for hybrid, and “*n*” denotes the number of carbons on the alkyl chain. This partial series was prepared in moderate yields ranging from 54-89% with *n* = 8, 10, 11, 12, 13, 14, 16, or 18 (**Scheme 3.2**).

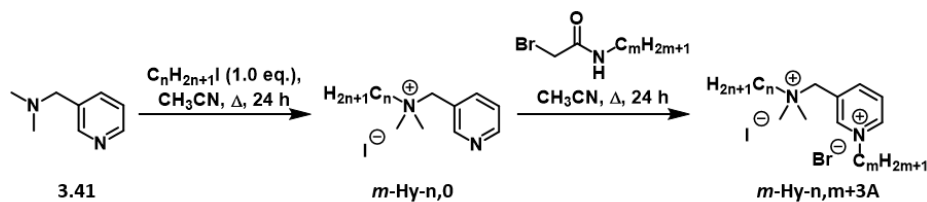


Scheme 3.25: Synthesis of hybrid bisQACs

The library was expanded to contain amide-linked bisQACs to assess the effect of asymmetry<sup>67</sup> and designed instability for favorable environmental degradation.<sup>68</sup> By reacting 3-dimethylaminomethyl pyridine (**3.41**) with a single equivalent of alkyl iodide, alkylation proceeded only at the benzyl amine producing four monoQACs (37-71% yield) bearing the notation *m*-Hy-*n*,0 where *n* = 10, 12, 14, or 16



(Scheme 3.3). These compounds were then further reacted with various amide electrophiles to yield an additional sixteen bisQACs (16-84% yield) and were named *m*-Hy-*n*,*m*+3A (Scheme 3.3). In this series, the “*n*” denotes the number of alkyl chain carbons on the benzylic amine, “A” denotes the presence of an amide functionality, and “*m*” is the number of alkyl chain carbons after the amide nitrogen (*m* = 11, 12, 13, or 15).



Scheme 3.26: Synthesis of amide-containing hybrid bisQACs

In total, twenty-eight compounds were synthesized and analyzed for their biological activity against six strains of bacteria and red blood cell toxicity. Generally, our synthesized compounds had comparable activity and toxicity to CPC and in many cases, better than BAC. Nine of the synthesized bisQACs had single-digit activity against all six of the bacteria evaluated (Table 3.4). The trend emerged that symmetry or asymmetry did not majorly contribute to the activity of the bisQACs, but rather the total number of alkyl carbons (22-25) is a better indicator of performance. For example, when comparing *m*-Hy-12,15A to *m*-Hy-16,11A the only significant difference in activity is against *P. aeruginosa* (8  $\mu$ M and 32  $\mu$ M respectively).

It was also observed that amide-containing QACs performed similarly to their non-amide counterparts as can be seen by comparing *m*-Hy-12,12 and *m*-Hy-12,12A across all bacteria. Additionally, the monoQAC series had significantly diminished activity when comparing *m*-Hy-12,0 and *m*-Hy-12,12, indicating that the placement of the amide while convenient for synthesis, is also beneficial for biological applications. Based on prior studies of amide-containing QACs, the predicted method through which this compound would degrade will allow for a less active monoQAC species; therefore, limiting selective pressure for QAC resistant bacteria.<sup>68</sup> This is beneficial to the field in terms of developing biocides that will

degrade in WWTPs instead of accumulating in our ground water where they promote resistance development

Table 3.7: MICs of hybrid bisQACs

Series	Compound	Minimum Inhibitory Compound ( $\mu\text{M}$ )						Lysis <sup>20</sup> ( $\mu\text{M}$ )
		<i>S. aureus</i>	<i>E. faecalis</i>	<i>E. coli</i>	<i>P. aeruginosa</i>	USA300-0114	ATCC 33591	
	BAC	8	8	32	63	32	16	63
	CPC	0.5	1	8	63	16	1	8
m-Hy-n,0	<i>m-Hy-10,0</i>	32	>250	125	250	32	63	NT
	<i>m-Hy-12,0</i>	63	250	125	250	63	125	NT
	<i>m-Hy-14,0</i>	8	250	32	>250	8	32	63
	<i>m-Hy-16,0</i>	2	125	16	250	2	4	16
Hybrid BisQACs m-Hy-n,n	<i>m-Hy-8,8</i>	63	>250	>250	250	32	250	NT
	<i>m-Hy-10,10</i>	2	32	4	16	1	4	32
	<i>m-Hy-11,11</i>	2	4	2	4	1	2	16
	<i>m-Hy-12,12</i>	2	4	1	4	1	2	8
	<i>m-Hy-13,13</i>	2	32	2	16	2	2	8
	<i>m-Hy-14,14</i>	2	63	4	63	2	4	8
	<i>m-Hy-16,16</i>	2	250	63	250	2	4	16
	<i>m-Hy-18,18</i>	8	>250	125	>250	16	8	63
Asymmetric Hybrid BisQACs m-Hy-n,m+3A	<i>m-Hy-10,11A</i>	2	8	2	8	1	2	32
	<i>m-Hy-10,12A</i>	2	16	4	8	2	4	32
	<i>m-Hy-10,13A</i>	2	4	2	4	2	2	16
	<i>m-Hy-12,11A</i>	2	4	2	4	2	2	16
	<i>m-Hy-12,12A</i>	2	4	2	8	2	2	8
	<i>m-Hy-12,13A</i>	4	4	2	4	2	2	16
	<i>m-Hy-10,15A</i>	2	8	2	8	2	4	16
	<i>m-Hy-14,11A</i>	2	8	2	16	4	2	16
	<i>m-Hy-14,12A</i>	2	16	2	32	2	4	16
	<i>m-Hy-14,13A</i>	4	32	4	63	4	4	8
	<i>m-Hy-16,11A</i>	4	16	4	32	2	4	8
	<i>m-Hy-12,15A</i>	4	8	4	8	4	4	16
	<i>m-Hy-16,12A</i>	4	63	4	63	4	4	16
	<i>m-Hy-14,15A</i>	8	63	8	125	8	8	16
	<i>m-Hy-16,13A</i>	4	63	16	125	8	4	16
	<i>m-Hy-16,15A</i>	16	>250	63	>250	16	16	32

### 3.3.3.4. Cyclic Rigidity QACs

Although much research has been conducted on chain length and number of quaternary centers, little emphasis has been placed on investigating the three-dimensional nature of these compounds. As such, the Minbiole and Wuest labs designed a series of bisQACs that would be able to assess how alkyl chain projection and core rigidity effects the potency of QACs (**Figure 3.14**). By revisiting the diamino functionality previously investigated<sup>67</sup> one could envision connecting the two amines to yield a piperazine core. If the same two amines were connected again to form a fused ring system, a DABCO-derived series of QACs could be formed. These three cores could again be expanded with multiple chain lengths to gain a full scope of activity.

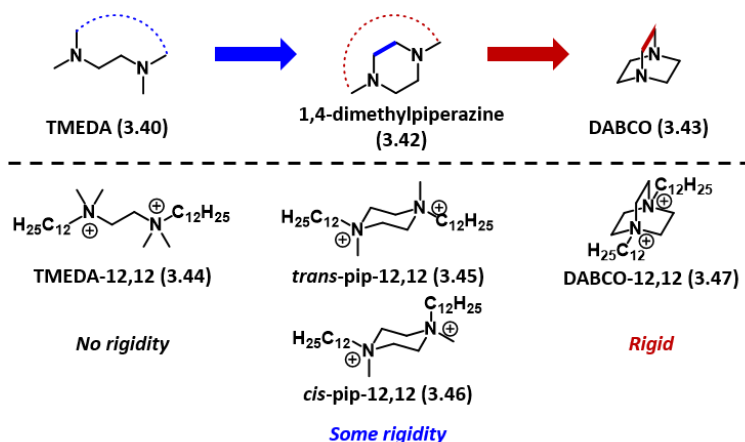
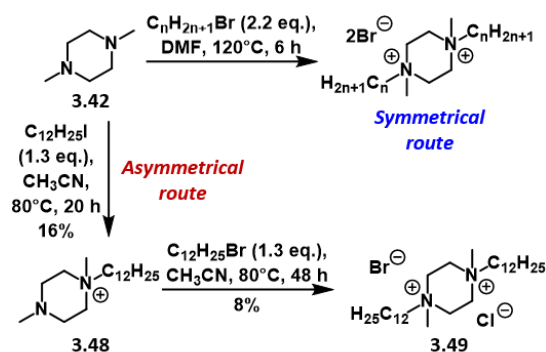


Figure 3.33: Conceptual design of bisQACs for core rigidity investigation

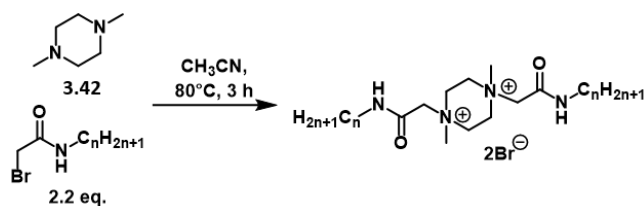
Synthesis of the rigidity QAC series began with a focus on twelve carbon alkyl chains. A small library of eight piperazine analogs were synthesized in moderate to high yields (49-94%) with  $n = 8, 10, 11, 12, 13, 14, 16, \text{ or } 18$  (**Scheme 3.4, top**).



Scheme 3.27: Synthesis of piperazine-based bisQACs

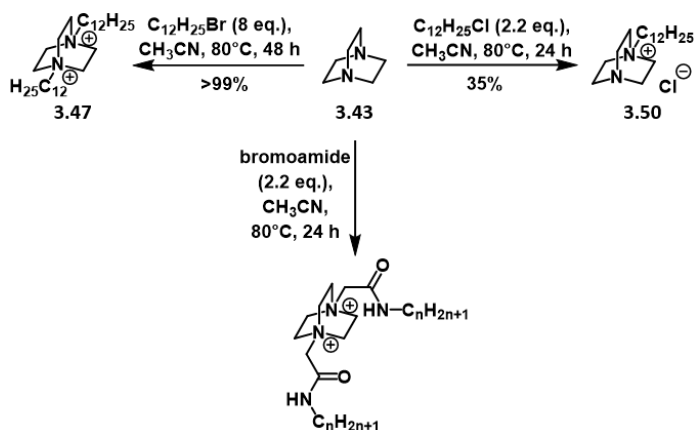
All of these analogs were readily made with heating and an excess of alkyl bromide, but to pursue potential asymmetrical analogs, a mono alkyl addition method was developed by first reacting with alkyl chloride and then with alkyl bromide (**Scheme 3.4, bottom**). Though these asymmetric analogs were not pursued in this work due to poor yields with the initial  $n = 12$  compounds, it has been shown to provide active QAC compounds previously<sup>62</sup> and is beneficial for future studies. The current synthesis of the piperazine analogs had no *cis*-/*trans*- control; however, after recrystallization and X-ray diffraction experiments it was determined that all piperazine compounds favored *trans*-piperazine structures. We theorize that this

preference is due to steric constraints of a six-membered ring system and minimization of axial-1,3 strain of the large alkyl groups. Additionally, amide functionalities were installed in the piperazine series to continue to assess the activity of degradable QACs and to provide a natural bend in the side chain which would promote a less linear chain extension. Six of these amide containing piperazine QACs were formed in good yield (66 - >99%) with  $n = 8, 9, 10, 11, 12,$  or  $14$  (**Scheme 3.5**).



*Scheme 3.28: Synthesis of amide-containing piperazine bisQACs*

Finally, the DABCO series was synthesized with some degree of difficulty. Using standard alkylation conditions and an alkyl chloride electrophile, only mono alkylation occurred to form DABCO-12,0. By switching to an alkyl bromide DABCO-12,12 was prepared in excellent yield (**Scheme 3.6**). Two DABCO-amide compounds with  $n = 9$  or  $10$  were synthesized in good yields (76% and 92% respectively) using an excess of their respective bromoimide.



*Scheme 3.29: Synthesis of DABCO-core bisQACs and amide-containing DABCO bisQACs*

All twenty-one compounds synthesized were carried through to biological assays which confirmed improved activity over commercial compounds like BAC and CPC. This series also supported the trend that chain lengths of 12-13 carbons provide the most active compounds (**Table 3.5**).

Table 3.8: MICs of first-generation rigidity bisQACs

Series	Compound	Minimum Inhibitory Compound ( $\mu\text{M}$ )						Lysis <sup>20</sup> ( $\mu\text{M}$ )
		<i>S. aureus</i>	<i>E. faecalis</i>	<i>E. coli</i>	<i>P. aeruginosa</i>	USA300-0114	ATCC 33591	
	BAC	4	125	63	250	4	16	63
	CPC	1	125	16	125	1	1	16
	TMEDA-12,12	1-2	16	4	16-32	1-2	2	8
Piperazines Pip-n,n	Pip-12,0	63	>250	>250	>250	125	125	>250
	Pip-8,8	>250	>250	>250	>250	250	>250	>250
	Pip-10,10	4	250	32	63	4	8	>250
	Pip-11,11	2	63	16	63	1	2	125
	Pip-12,12	2	8	8	16	1	2	32
	Pip-12,12,Cl,Br	1	8	8	8	1	2	32
	Pip-13,13	4	63	16	63	4	8	63
	Pip-14,14	16	63	32	125	4	32	63
	Pip-16,16	32	250	125	>250	16	63	125
Pip-18,18	63	>250	250	>250	32	125	125	
Piperazines Pip-nA,nA	Pip-11A,11A	2	16	32	16	2	4	125
	Pip-12A,12A	1	4	4	8	1	2	32
	Pip-13A,13A	2	2	2	8	1	1	16
	Pip-14A,14A	8	32	8	63	2	8	32
	Pip-15A,15A	16	250	63	250	16	16	16
	Pip-17A,17A	8	>250	250	>250	8	16	16
DABCO	DABCO-12,0	63	>250	250	>250	125	125	>250
	DABCO-12,12	0.25	4	2	8	2	0.5	8
	DABCO-12A,12A	1	16	8	16	1	2	63
	DABCO-13A,13A	0.5	4	4	8	2	1	16

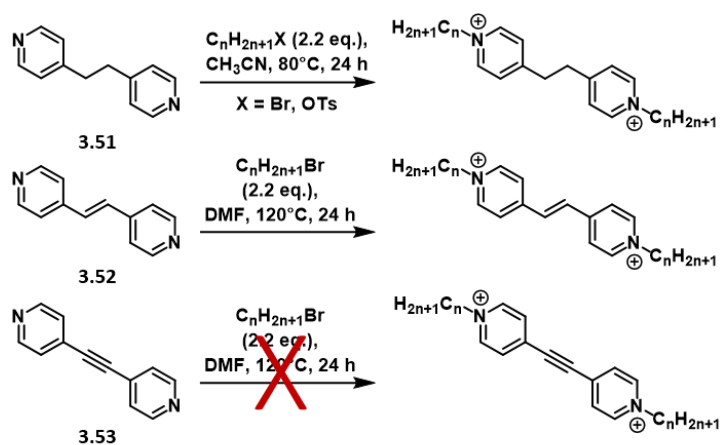
Original hypotheses reasoned that less rigid structures would allow for more fluid interactions with bacterial membranes, leading to higher potency. However, the DABCO series produced the most potent compounds suggesting that more rigid structures promoted more active QACs. This is most obvious when comparing the activities of TMEDA-12,12 with *trans*-pip-12,12 and DABCO-12, 12. Activity was also retained with the addition of an amide functionality. It was also intriguing that the red blood cell lysis analysis showed increased toxicity with increased potency. Overall, the data from this series of QACs suggests that rigid core structures are preferred. Since our conclusion contradicted the original hypothesis, we were spurred to further investigate the relationship between core rigidity and QAC activity.

### 3.3.3.5. Ane, Ene, Yne Rigidity QACs

Based on the unexpected findings reported when investigating our first series of rigid core bisQACs,<sup>69</sup> further studies were completed utilizing a pyridinium motif that has also been shown to have activity and

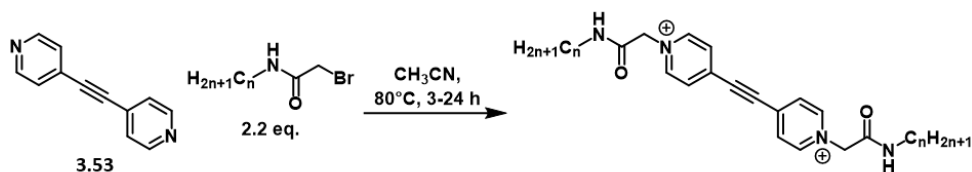
the commercially available CPC.<sup>66,70</sup> We envisioned a dipyridinium scaffold with a two carbon linker *para* to both nitrogens. The linker region could be varied between alkane, alkene, and alkyne functionalities, each providing a different degree of rigidity and therefore, a different projection angle of the alkyl chains that would be bound to both nitrogens.

Synthesis proceeded well in the case of alkane and alkene linked compounds, but were less successful with alkyne linked compounds. Using alkyl bromides, eight alkane linked dipyridinium bisQACs were synthesized in good yield (63->99%) (**Scheme 3.7**). We also synthesized two dipyridinium alkane-linked bisQACs with tosylate counterions to investigate any effect that counterion may have on the system. Synthesis continued smoothly to the alkene-linked bisQACs providing eight more compounds in decent yields (46-86%). Unfortunately, our alkylation conditions were not amenable to the alkyne-linked pyridine starting materials.



*Scheme 3.30: Synthesis of pyridinium based -ane, -ene, -yne core bisQACs.*

However, due to the increased electrophilicity of the bromoamides used, alkyne-linked bisQACs were able to be synthesized (**Scheme 3.8**), as well as alkane- and alkene-linked bisQACs. Six bisQACs of each class were synthesized, all in moderate to excellent yields (alkane: 46-83%, alkene: 79->99%, alkyne: 64-98%).



Scheme 3.31: Synthesis of amide-containing alkyne bisQACs

Altogether, thirty-six dipyridinium QACs were synthesized and carried through to biological analysis against six strains of bacterial. Similar trends were observed in that 11-13 carbon chain links were the most potent compounds in each class of bisQACs tested, and amide containing QACs were slightly less active than their non-amide counterparts though still retained decent potency (**Table 3.6**). In regards to a counterion effect, it was observed that compounds with a tosylate counterion were not as active as those with halide counterions as can be seen when comparing DPA-12,12 (1  $\mu$ M) to DPA-12T,12T (4  $\mu$ M) against CA-MRSA. There was also an increase in toxicity when the tosylate counterion was used. This will be important to continue considering in future work when attempting to design highly potent, but non-toxic disinfectants.

Table 3.9: MICs of the -ane, -ene, -yne core rigidity bisQACs

Series	Compound	Minimum Inhibitory Compound (µM)						Lysis <sup>20</sup> (µM)
		<i>S. aureus</i>	<i>E. faecalis</i>	<i>E. coli</i>	<i>P. aeruginosa</i>	USA300-0114	ATCC 33591	
	BAC	NT	8	32	63	32	16	63
	CPC	1	63	16	125	1	2	8
Alkane, halide salt DPA-n,n	DPA-8,8	32	>250	125	>250	32	63	125
	DPA-10,10	1	32	2	63	2	2	63
	DPA-11,11	1	4	1	4	1	1	63
	DPA-12,12	2	4	1	4	1	1	125
	DPA-13,13	8	16	4	16	4	8	125
	DPA-14,14	4	>250	16	>250	8	4	125
	DPA-16,16	32	>250	>250	>250	8	16	32
	DPA-18,18	63	>250	>250	>250	63	63	125
-OTs	DPA-12T,12T	1	16	2	8	4	2	63
	DPA-14T,14T	8	>250	32	>250	8	8	32
Alkene DPE-n,n	DPE-8,8	16	250	4	125	16	32	125
	DPE-10,10	1	8	1	8	2	2	63
	DPE-11,11	1	2	1	2	2	0.5	63
	DPE-12,12	8	16	8	32	4	4	125
	DPE-13,13	16	>250	16	>250	8	8	125
	DPE-14,14	125	>250	250	>250	63	63	125
	DPE-16,16	>250	>250	>250	>250	>250	>250	125
DPE-18,18	>250	>250	>250	>250	>250	>250	125	
Alkane, amide DPA-nA,nA	DPA-11A,11A	8	125	16	>250	4	8	125
	DPA-12A,12A	2	8	4	16	1	2	32
	DPA-13A,13A	2	8	4	8	2	4	16
	DPA-14A,14A	4	32	8	32	4	4	32
	DPA-15A,15A	16	>250	32	>250	16	16	125
	DPA-17A,17A	63	>250	125	>250	32	63	63
Alkene, amide DPE-nA,nA	DPE-11A,11A	4	32	8	32	2	4	32
	DPE-12A,12A	4	32	16	32	4	4	8
	DPE-13A,13A	16	250	63	250	32	32	63
	DPE-14A,14A	8	>250	32	>250	16	16	63
	DPE-15A,15A	63	>250	125	>250	32	63	63
	DPE-17A,17A	63	>250	>250	>250	32	250	63
Alkyne, amide DPY-nA,nA	DPY-11A,11A	16	63	32	63	16	32	32
	DPY-12A,12A	32	63	32	125	32	32	125
	DPY-13A,13A	32	>250	63	>250	63	32	125
	DPY-14A,14A	63	>250	125	>250	125	125	125
	DPY-15A,15A	125	>250	>250	>250	125	32	63
	DPY-17A,17A	250	>250	>250	>250	125	63	63

In contradiction to the previously reported trend observed in the TMEDA, piperazine, and DABCO series of bisQACs, this series of compounds showed a small negative correlation with increased rigidity. This trend is observed most strongly across all six strains of bacteria when comparing analogous analogs DPA-12A,12A, DPE-12A,12A, and DPY-12A,12A. For example, in the case of CA-MRSA activity, DPA-12A,12A has an MIC of 1 µM, DPE-12A,12A has an MIC of 4 µM, and DPY-12A,12A has an MIC of 32 µM. Overall, the therapeutic indices were well balanced with the exception of the amide series which had rather high levels of toxicity in the red blood cell lysis assay.



Though the biological data from the first-generation rigidity series and the second seems to be contradictory, when analyzed from a different angle a new trend emerges. In the initial rigidity series, positively charged centers were alkyl in nature and in an energy minimized structure held their cationic centers closer than this second series of compounds. For example, the TMEDA, piperazine, and DABCO compound nitrogens are between two and five angstroms apart; however, the second generation of rigidity QACs hold their nitrogens at greater than nine angstroms apart. Perhaps the increase in charge separation counteracts the benefit of increased structural rigidity, and instead of searching for the most rigid bisQAC a balance should be struck between rigidity and charge separation.

### **3.4. QAC Resistance**

Due to their simple structure and generally cheap manufacturing methods, QACs continue to be used non-discriminately, leading to the spread of resistance mechanisms. But what exactly qualifies as resistance and what is the difference between bacterial tolerance and bacterial resistance? Tolerance to QACs, or adaptation, was first discovered in the 1950s and refers to the ability of bacteria to grow in elevated levels of antibiotics without acquiring a permanent genetic change. After removal of the antibiotic stress, the bacteria then becomes susceptible to the antibiotic.<sup>71</sup> On the other hand, resistance is characterized by a permanent genetic change that allows bacteria to survive when in contact to the antibiotics that they have resistance to. The first examples of QAC resistance were found in the 1980s in a mobile genetic element, or plasmid, in *S. aureus*.<sup>72</sup>

In addition to being disinfectants, QACs are also used ubiquitously in products like fabric softeners, antistatic products, hair care products, and even roofing treatments because their amphipathic nature is amenable to surfactants.<sup>73,74</sup> As a result, several research groups, have dedicated time to understanding what happens to QACs once users wash them down the drain. In short, QACs have a tendency to stick around. Worldwide, about 500,000 tons of QACs are used of which, about 75% collects in waste water treatment plants (WWTPs) while the rest is dispersed in the environment.<sup>13</sup> In 2001, Ding and Liao published a study of four rivers and two industrial effluents in Taiwan showing that in the Pu-Tzu river 120

µg/L of linear QAC were detected, and in the Lien-1 company's effluent 300 µg/L of linear QAC were detected.<sup>75</sup> In 2010, the Brownawell group conducted an analysis of QAC contaminants in urban estuary sediments and found an increase of QAC contamination over a span of ten years from 1998 to 2008 from 2820 ng/g to 6750 ng/g in Jamaica Bay, NY near JFK Airport.<sup>76</sup> In 2012, Van de Voorde and co-workers published a study from France of moss-prevention treated roofs demonstrating that  $783 \pm 438$  µg/L of benzylalkonium QAC over four samples was detected in roof run-off due to normal rain fall events five months after the initial treatment.<sup>73</sup> In 2014, the Jiang group from China studied benzylalkonium QACs in WWTPs across the country and found there was a geometric mean concentration of 820 ng/g of BAC-12 making up an average of 69% of the total BAC concentrations detected.<sup>77</sup> Across the world, scientists have confirmed that QACs are not degraded effectively nor are they cleared from the environment after usage. This results in a steady dose of QACs contributing to the accumulation of resistant bacteria, thereby making it even more difficult to sanitize places like hospitals where sterility is often the difference between life and death.<sup>78</sup>

While it has been well established that overuse and over-exposure to QACs is causing bacterial resistance, understanding what methods bacteria use to overcome resistance is still not fully explained. The most commonly reported resistance gene is *qacA*, which is most commonly seen in SA strains, but has also been found in *K. pneumoniae*, *P. aeruginosa*, and *A. baumannii*.<sup>79</sup> The gene *qacA* encodes for a transcriptionally regulated, proton motive efflux pump QacA that confers resistance to both monovalent and divalent lipophilic organic cations. A closely linked gene, *qacB*, shares the same genetic sequence with the exception of seven to nine base pairs and encodes an additional proton-motive efflux pump QacB; however, this efflux pump is generally only able to export monovalent lipophilic organic cations.<sup>80</sup> QacC, encoded by *qacC* has been identified in both Gram-positive and Gram-negative bacteria as a small multidrug resistance (SMR) pump. QacC has been shown to confer resistance to QACs and QAC dyes like ethidium bromide, as well as β-lactam antibiotics.<sup>80</sup> Another type of resistance gene, *qacE*, and its truncated form *qacEΔ1* confer resistance to QACs in both Gram-positive and Gram-negative bacteria with *qacE*

demonstrating greater resistance to the bacteria than *qacEAI*.<sup>80</sup> Finally, *qacJ* was found to have a high degree of similarity to *qacC*, *qacG*, and *qacH*, but has an even greater ability to cause resistance to BAC, one of the most popular disinfectants.<sup>81-83</sup>

With all of this evidence for the presence and function of *qac* resistance genes, it was expected that researchers would be able to study these interactions using small molecule QACs synthesized specifically for that purpose. Jennings and coworkers completed several assays in which dye-QACs were utilized to study the trends in reactivity discovered throughout their collaborative exploration with the Minbiole lab. Unfortunately, experimentation led to more questions and less answers.

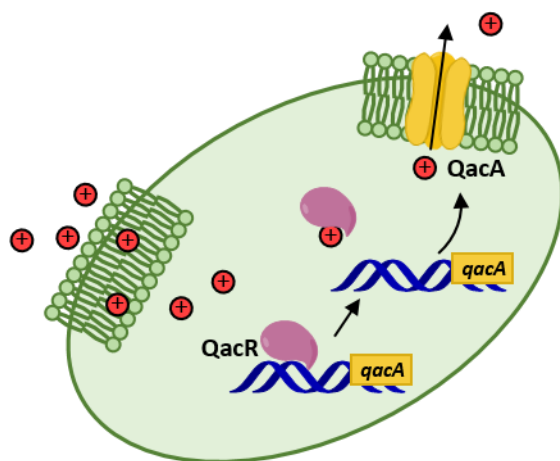


Figure 3.34: Depiction of the *QacR-QacA* resistance mechanism

To study efflux pump mediated QAC resistance, Jennings and colleagues searched for information regarding the active site of the transcriptional regulator QacR of efflux pump, QacA. When QacR is bound by a QAC, transcription of the general efflux pump QacA is turned on, permitting evacuation of the undesired QAC from the cell (**Figure 3.15**). Recent findings indicated that commonly used dyes like malachite green and crystal violet could fit the binding site of QacR,<sup>84</sup> and might provide a scaffold upon which the Minbiole and Wuest labs could build a new library (**Figure 3.16**).<sup>85</sup> The biological activity of this series surprisingly followed typical QAC trends with the exception of their performance against bacteria that tend to have several efflux pump systems; CA-MRSA, *E. coli*, and *P. aeruginosa*. Against

these strains, monoQAC compounds tended to have 125-fold higher MICs than their multiQAC counterparts suggesting that monoQAC dye-mimic compounds may be bound by QacR, but further experimentation would be necessary before making any conclusions. Instead, Jennings proposed three possible causes for resistance of dye QACs. The first was that increased positive charge minimized the ability of a multiQAC from entering the cell, and was therefore unable to enter the cell to turn on any efflux pump, but rather effectively lysed the cell without preamble. The second possible cause of resistance was that the monoQAC dyes were, in fact, binding to QacR and turning on transcription of efflux pump, QacA. The third and final potential cause was that multiQACs could not be effluxed by QacA due to their overall charge and instead, accumulated within the cell until they eventually caused cell death.

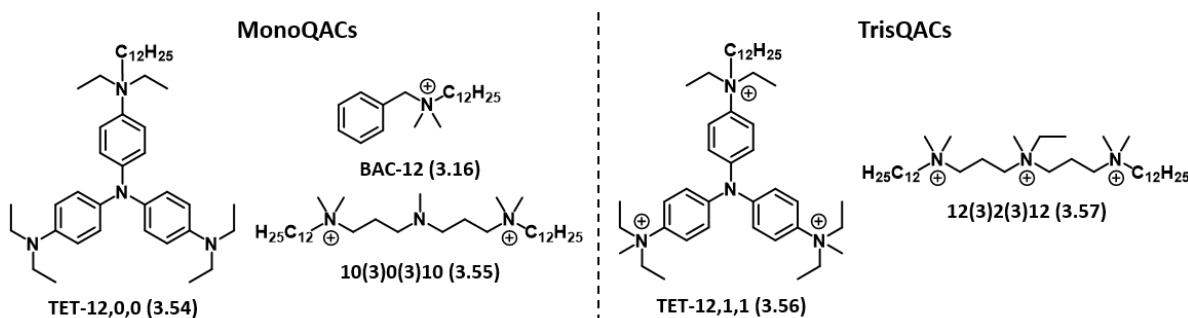


Figure 3.35: Mono- and Tris-dye QACs used for QacR binding experiments

If QACs were being prevented from entering bacterial cells and thereby causing resistance, then a propidium iodide stain kinetic experiment could be used. Propidium iodide is not cell permeable and therefore cannot enter a cell unless the membrane is damaged in some capacity. Once propidium iodide enters a cell, it gives a red fluorescent read-out when it intercalates into DNA. In this manner, Jennings was able to treat bacteria with QAC and propidium iodide and kinetically track cell lysis.<sup>86</sup> At the conclusion of these experiments it was found that there was little difference in cell lysis between strains of bacteria that had efflux pumps and those that did not, with the exception of CA-MRSA. When the propidium iodide experiment was performed on CA-MRSA, the relative fluorescence values were much higher for all compounds when compared to the other strains of bacteria. This result is consistent with the knowledge

that CA-MRSA strains are known to have different enzymatic content in their membranes with an increased number of penicillin-binding proteins, but what these penicillin-binding proteins are specifically doing is still unknown. Overall, researchers were unable to make any firm conclusions about QAC resistance at this time.

Next, Jennings turned to a potentiation assay and MIC assays of *S. aureus* (SA) strains with genetic differences in *qac* genes. During the potentiation assay, Jennings exposed CA-MRSA to sub-MIC concentrations of BAC-12, which is known to bind QacR. At the conclusion of the assay, the colonies growing at concentrations above the MIC were isolated and tested for change in MIC with the selected compounds in these studies. The theory was such that if QacR/A was already activated, then elevated MICs would be seen for QAC compounds; however, researchers were disappointed to see no increases in MIC. At this point, Jennings was able to acquire four new strains of bacteria with known differences in *qac*. One strain had no *qac*, another had both *qacA* and *qacR*, and the remaining two strains had either *qacA* or *qacR*. When tested in an MIC assay against the compound set, there were only modest changes in MICs (**Table 3.7**).<sup>86</sup> In strains carrying *qacA*, monoQACs had a higher MIC, but multiQACs did not. This suggests that the QacA efflux pump has the ability to differentiate between monoQACs and multiQACs, and expels monoQACs preferentially.

Table 3.10: MICs of select QACs against *qac* gene containing SA strains

Compound	Minimum Inhibitory Compound (μM)					
	MSSA <i>S. aureus</i>	CA-MRSA USA300	SK982 <i>no qac</i>	SK5872 <i>qacA/qacR</i>	SK5873 <i>qacA</i>	SK5791 <i>qacR</i>
BAC	8	32	4	8	16	2
10(3)0(3)10	1	2	1	2	2	1
12(3)2(3)12	0.5	0.5	1	0.5	0.5	1
TET-12,0,0	2	125	2	8	8	4
TET-12,1,1	1	4	1	1	1	1

Since the propidium iodide assay about getting QACs into the cell was inconclusive, but the strains with QacA seem to have a preference for monoQACs over multiQACs, Jennings decided to perform an efflux pump inhibition study in an attempt to gain clarity.<sup>86</sup> QacA is a proton-motive efflux pump, but also

likely not the only efflux pump produced by bacteria when subjected to QACs. Therefore, two different efflux pump inhibitors were chosen; reserpine and carbonyl cyanide 3-chlorophenylhydrazone (CCCP). Reserpine is known to be a generalized efflux pump inhibitor, whereas CCCP is specific to proton-motive efflux pumps. When efflux pumps were inhibited, there was no observed difference in MIC with the exception for BAC-12 which had a fourfold lower MIC against CA-MRSA. All of these experiments combined make for a complex and winding story that hints that efflux pumps are important for monoQAC resistance, but seem to have little effect on multiQACs. Also, researchers are directed towards studying membrane composition and looking to other proteins that may be having an effect on QAC resistance development.

### **3.5. QAC activity against clinically isolated bacteria**

*The following experimentation was led by K.R.M. with the invaluable assistance of R.A.A. and Savannah J. Post.*

Over the last several years, efforts have focused primarily on understanding the structure-activity relationship (SAR) of QACs with bacteria, but little research has focused on the bacteria themselves. We have used the same six strains in much of our experimentation to date, all of which are commercial strains. However, the question remains: how do the Minbiole-Wuest QACs behave against clinical bacteria? From these experiments, we hoped to gain better understanding of how effective QACs are in practical use. For example, if a patient presents with a resistant bacterial infection, we know that matching the correct antibiotic can be challenging, if not impossible depending on the resistance, but what about cleaning that room after the patient has left the hospital? What types of cleaning products are used, and are they effective against these resistant bacteria? These questions are imperative to understanding the magnitude of the problems facing the medical field, and also to our research as we try to develop disinfectants that are safe and effective against clinically relevant bacteria.

In order to answer these questions, we first contacted Dr. Patrick T. McGann at Walter Reed Medical Center and asked for strains of clinically isolated bacteria of both *A. baumannii* and *P. aeruginosa*. We were grateful to receive approximately 100 strains of each type of bacteria, each with antibiotic

resistance information, as well as a list of resistance genes for each strain. From this multitude, we began the daunting task of processing the resistance data to select for a more manageable sample size of bacteria to test. Since we were primarily concerned with disinfectant effectiveness against resistant bacteria, we began to sort the bacteria based on a Resistance Score. Resistance Scores were calculated by adding up the number of antibiotics that each strain was resistant to ranging from 0-16. From there, the sample size was analyzed to eliminate genetic repeats, and ensure that each year, sample origin, and geographic location was represented.

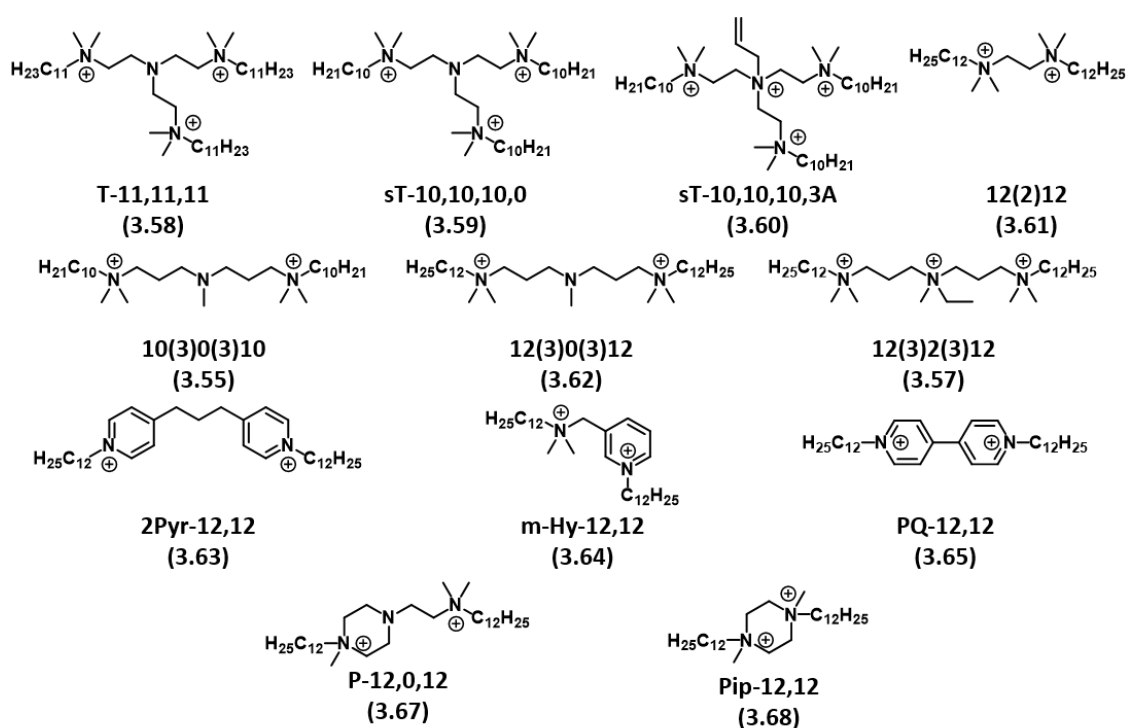


Figure 3.36: Best in class QACs for testing against clinically isolated bacteria

When evaluating which QACs to include in the following studies, we looked for those that performed well against commercial strains and tried to vary them across different classes of QACs. Included in our final twelve compounds whereas super-T multQACs,<sup>87</sup> TMEDA-derived multQACs,<sup>62,63</sup> piperazine-core QACs,<sup>66,88</sup> and pyridine-core QACs.<sup>70,89,90</sup> We also made sure to include four common commercial QACs for a total list of sixteen compounds (**Figure 3.17**). In order to compare the efficacy of

our compounds against clinical bacteria, a table of MICs against commercial bacteria is provided (**Table 3.9**). Overall, the compounds chosen for these experiments are equipotent or more potent when compared to commercial QACs. In most cases, the synthesized QACs have MICs three-fold better for PA compared to commercial QACs.

Table 3.11: Biological activity of best in class QACs against commercial strains

Compound	Minimum Inhibitory Compound (µM)			
	<i>S. aureus</i>	<i>E. faecalis</i>	<i>E. coli</i>	<i>P. aeruginosa</i>
T-11,11,11	0.5	1	1	2
sT-10,10,10,0	0.5	0.5	1	2
sT-10,10,10,3A	0.5	0.5	0.5	1
12(2)12	1	1	2	4
10(3)0(3)10	1	2	4	8
12(3)2(3)12	0.5	0.5	1	2
12(3)0(3)12	1	2	1	4
P-12,0,12	0.5	NT	1	2
Pip-12,12	2	8	8	16
2Pyr-12,12	0.5	0.5	1	4
m-Hy-12,12	2	4	1	4
PQ-12,12	2	2	2	16
BAC	8	8	32	63
BEC	NT	NT	NT	NT
CPC	0.5	1	8	63
DDAC	1	1	2	16

### 3.5.1. Acinetobacter baumannii

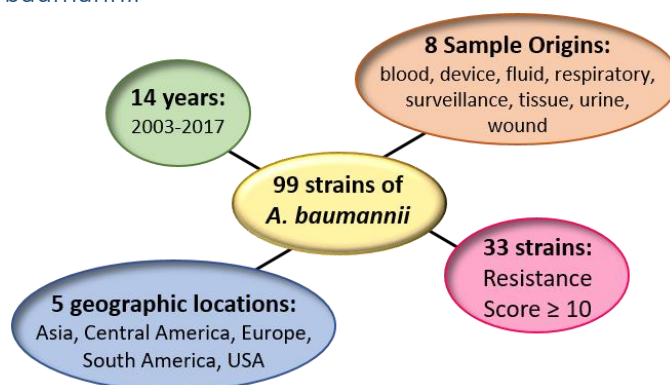


Figure 3.37: General scope of the *A. baumannii* panel from Walter Reed Medical Center

The AB population selected for these assays has a diverse background pictured (**Figure 3.18**). Of the 99 strains, we selected 34 strains to test, one of which was resistant to every antibiotic evaluated including the last resort drug, colistin (MRSN 17493), and one of which only had a resistance score of 8, but was the only



bacteria isolated from the year 2003. Once our bacteria were selected, we performed an MIC assay to get a baseline for which bacteria were susceptible to QACs and which were resistant. From the AB strains, we were able to determine that DDAC (**3.18**), 2Pyr-11,11 (**3.63**), and m-Hy-12,12 (**3.64**) were the most globally active compounds while 10(3)0(3)10 (**3.55**) and 12(3)2(3)12 (**3.57**) were the least active against all strains. Overall, the MICs were much higher than what is normally observed against laboratory strains, confirming our theory that while our data is valuable, testing against clinical strains may provide a more accurate picture of QAC performance in the clinic.

From the MIC data, we also looked at which strains were easiest and hardest to kill. We were hoping that from this data we would be able to extrapolate a correlation between resistance gene and performance against QAC. We defined bacteria that were “easy” to kill as those where at least half of the compounds tested gave an MIC  $\leq 8 \mu\text{M}$ . Of these bacteria we identified six strains: MRSN 334, 7067, 11695, 14427, 29908, and 337038 (**Table 3.9**). We next searched for the bacteria that were “hard” to kill as those that had no more than one MIC  $\leq 8 \mu\text{M}$ . Of these, we identified four strains: MRSN 1174, 32866, 32915, and 480622 (**Table 3.10**). We were especially surprised to discover that our most resistant strain of AB, MRSN 17493, was not included in our list of hardest to kill bacteria. In fact, we were thrilled to find that m-Hy-12,12 and DDAC had an MIC of  $8 \mu\text{M}$  against MRSN 17493. This is the first time that we have observed MICs against this strain.

*Table 3.12: MICs of Best in Class QACs against easiest to kill clinical AB strains*

Compound	Minimum Inhibitory Concentration ( $\mu\text{M}$ ) of Clinical AB Strains					
	334	7067	11695	14427	29908	337038
sT-10,10,10,3A	8	>250	>250	16	8	8
sT-10,10,10,0	8	4	4	63	8	8
T-11,11,11	8	63	125	8	4	8
12(2)12	4	2	4	4	125	4
10(3)0(3)10	125	32	63	125	63	63
12(3)2(3)12	125	125	125	63	125	125
12(3)0(3)012	8	4	4	8	8	8
P-12,0,12	4	2	4	4	4	4
Pip-12,12	16	8	8	16	16	8
m-Hy-12,12	8	4	4	4	8	8
2Pyr-11,11	16	4	4	8	4	8
PQ-12,12	>250	8	4	8	16	8
BAC	32	32	32	32	63	63
BEC	125	32	32	32	63	63
CPC	32	16	32	32	125	32
DDAC	8	4	8	8	8	8

Table 3.13: MICs of Best in class QACs against hardest to kill clinical AB strains

Compound	Minimum Inhibitory Concentration ( $\mu\text{M}$ ) of Clinical AB Strains			
	1174	32866	32915	480622
sT-10,10,10,3A	>250	>250	>250	>250
sT-10,10,10,0	>250	>250	>250	250
T-11,11,11	125	250	63	125
12(2)12	125	250	125	63
10(3)0(3)10	125	>250	>250	>250
12(3)2(3)12	125	125	125	125
12(3)0(3)012	125	125	125	125
P-12,0,12	125	125	125	125
Pip-12,12	>250	>250	>250	>250
m-Hy-12,12	32	250	250	250
2Pyr-11,11	16	>250	>250	250
PQ-12,12	>250	>250	>250	>250
BAC	32	>250	32	>250
BEC	32	>250	32	>250
CPC	32	125	32	125
DDAC	8	8	8	8

From this dataset, we were able to ascertain that the commercial monoQAC, DDAC, was most effective at killing AB clinical strains. This result is confusing due to the repeated evidence that bisQACs tend to be the best performers against the lab strains of bacteria. In order to confirm if this effect is a result of AB susceptibility in general or unique to the selected clinical strains, we will perform MIC assays with the same compounds on lab strains of AB.

Once the preliminary MIC data was collected, we next analyzed our best and worst strains for genetic similarities. We were hoping to discover a correlation between resistance genes and QAC resistance. At this time, there is no correlation between any specific genes or combinations of genes and QAC resistance. We do know that trimethoprim and fosfomycin resistance genes are not correlated to bacteria being resistant to QACs as our four worst bacteria had no resistance genes for either of these antibiotics. In fact, our “easy” to kill bacteria had an average Resistance Score of 11 with an average of 10 resistance genes, whereas the “hard” to kill bacteria had an average Resistance Score of 11 and an average of 8.5 resistance genes. This data clearly represents the complex nature of the question we are asking.

### 3.5.2. Pseudomonas aeruginosa

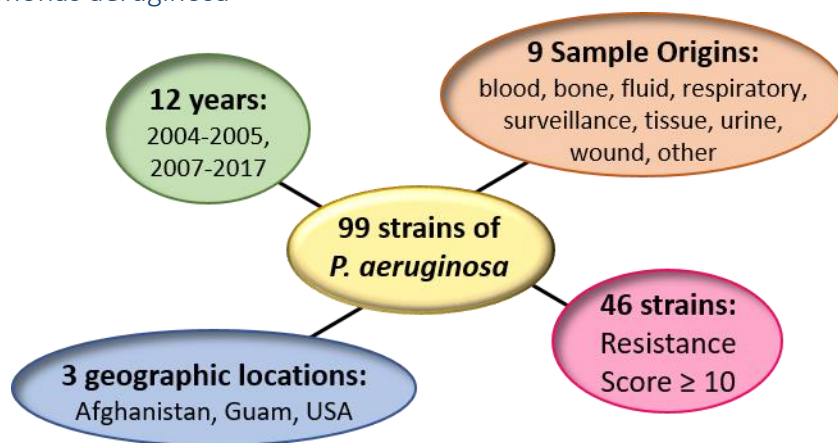


Figure 38: General scope of the *P. aeruginosa* panel from Walter Reed Medical Center

Of the 99 strains of PA, 27 were selected for testing in the same manner that the AB strains. Initial MIC assays with these strains showed that overall, our QAC selection were less effective at killing these bacteria compared to the AB strains. This was surprising given that PA lab strains are commonly used as a benchmark for QAC activity within our lab. The most potent QACs broadly against these bacteria were 12(3)0(3)12 (**3.62**), Pip-12,12 (**3.68**), and PQ-12,12 (**3.65**). Intriguingly, the worst performing QACs were the subset that is commercially available. This is in opposition to the trend seen in AB strains.

Due to the QACs overall poor performance, we were forced to loosen our constraints on what we defined as an “easy” or hard to “kill” bacteria. In the case of the PA strains we determined “hard” to kill bacteria as those that no MIC  $\leq 8 \mu\text{M}$ . Seven strains were identified by this parameter: MRSN 1938, 6678, 6695, 8915, 9873, 11536, and 409937 (**Table 3.12**). The “easy” to kill strains were defined as those that had at least five compounds with an MIC  $\leq 8 \mu\text{M}$ . This time, only four strains were identified: MRSN 5508, 6220, 8914, and 390231 (**Table 3.11**).

Table 3.14: MICs of Best in Class QACs against easiest to kill clinical PA strains

Compound	Minimum Inhibitory Concentration ( $\mu\text{M}$ ) of Clinical PA Strains			
	5508	6220	8914	390231
sT-10,10,10,3A	8	16	>250	63
sT-10,10,10,0	8	16	32	250
T-11,11,11	16	16	32	63
12(2)12	16	8	8	32
10(3)0(3)10	63	125	125	>250
12(3)2(3)12	4	8	8	125
12(3)0(3)012	8	4	8	4
P-12,0,12	8	4	8	4
Pip-12,12	>250	8	8	8
m-Hy-12,12	32	8	8	250
2Pyr-11,11	16	8	8	4
PQ-12,12	>250	8	>250	4
BAC	>250	250	>250	250
BEC	>250	125	>250	250
CPC	125	125	125	125
DDAC	63	32	63	125

Table 3.15: MICs of Best in Class QACs against hardest to kill clinical PA strains

Compound	Minimum Inhibitory Concentration ( $\mu\text{M}$ ) of Clinical PA Strains						
	1938	6678	6695	8915	9873	11536	409937
sT-10,10,10,3A	16	>250	>250	>250	>250	16	16
sT-10,10,10,0	250	>250	250	250	250	32	125
T-11,11,11	32	250	32	63	63	32	32
12(2)12	16	250	32	32	250	32	16
10(3)0(3)10	250	250	125	>250	125	125	250
12(3)2(3)12	63	250	125	125	125	16	32
12(3)0(3)012	63	250	63	63	63	16	16
P-12,0,12	63	250	63	63	125	16	32
Pip-12,12	16	>250	16	>250	>250	16	16
m-Hy-12,12	125	250	>250	125	32	32	125
2Pyr-11,11	16	>250	32	16	>250	16	32
PQ-12,12	16	16	32	>250	>250	32	>250
BAC	>250	>250	>250	250	>250	250	125
BEC	>250	>250	>250	>250	>250	250	125
CPC	125	250	125	125	250	250	125
DDAC	250	125	63	63	250	125	32

At this juncture we turned again to the resistance genes present in both the “easy” to kill and “hard” to kill bacteria to examine any correlations. Unfortunately, we were unable to determine any correlations. Additionally, the average Resistance Score for the “easy” to kill bacteria was 13, while the “hard” to kill bacteria had an average Resistance Score of 12. Since many of the resistance genes known to be present in each strain happen to be efflux pumps, we have arrived at the conclusion that QAC resistance is not solely due to genetic resistance mechanisms and may have more to do with membrane composition.

### 3.5.3. Future Experimentation

#### 3.5.3.1. Resistance or Tolerance

Much to our interest during the MIC assay, we observed what looks to be potential heteroresistance to QAC biocide. When collecting MIC data, we look for the well that contains the lowest concentration of QAC that after 72 hours, shows no visual evidence of growth. We wait 72 hours instead of the typical 24 hours to ensure that the MIC data we collect is more likely to demonstrate a bacteriocidal effect, meaning that the bacteria is not able to mutate or metabolically overcome the presence of the QAC biocide. However, this is not a conclusive test of bacteriocidal activity. We also purposefully do not select single colonies to perform our typical MIC assays. This allows us to test the activity of our compounds against a range of potential genetic strains as they are free to mutate while growing. Normally this is a sign of strength that our biocides are active against a diverse community of bacteria as opposed to only being able to kill one

component of the community. This is essentially like saying our biocide can kill all brunettes, not just brunettes who are five feet-four inches tall and have green eyes.

While testing our clinical strains, instead of observing distinct MICs like those seem in the top row of **Figure 3.20**, we instead saw clear wells with a small colony growing in the bottom of the U-bottom wells (**Figure 3.20**, second row). Preliminary results suggest that these small colonies that grow above the MIC are the result of distinctly different colonies emerging over the course of the 72-hour assay, especially since none of these small colonies were observed at the 24-hour mark. However, we intend to confirm these results in future bacteriocidal assays, membrane studies, and resistance assays.

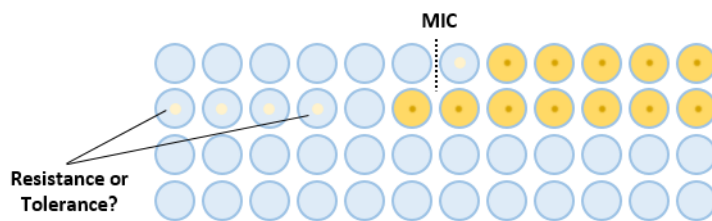


*Figure 3.39: An example of observed MICs in QAC assays*

First, we intend to confirm that any growth at high concentrations is a result of treatment with compound and not as a result of a genetically diverse population. To do this, we will repeat the MIC assays for a subset of bacteria, but we will grow them up from single colonies. If we still see bacterial growth at high concentrations of compound, then we will be able to say with more certainty that the growth is due to bacterial behavior when treated with QAC, not genetic diversity. Next, we will perform assays to confirm that the QACs are bacteriocidal (killing) as opposed to bacteriostatic (non-growing). To perform this analysis, we would begin with an MIC assay, followed by removing aliquots above and below the MIC and testing for viable cell growth.<sup>91</sup>

In addition to these assays, we would like to attempt a resistance assay to determine the ability of the bacteria to mutate and therefore overcome the QAC mechanism of action. This assay would be conducted by making agar plates with QAC in them at various concentrations; 4xMIC, 2xMIC, and MIC.

If the bacteria of choice can grow at elevated concentrations of compounds it is likely that it has developed a genetic mutation that confers resistance. Once this is confirmed through isolation of the colony and an additional MIC assay, we would then send the bacteria to be sequenced. In this manner, we can compare to the normal strain to see if any genetic mutations have occurred. Furthermore, we could use transcriptomic methods to determine if any specific efflux pumps or other resistance mechanisms are upregulated.

### 3.5.3.2. Membrane Contribution to QAC Potency

Additionally, since genetics does not seem to be the key reason for QAC resistance as has been theorized in the past, we propose more attention be paid to the structural differences in membranes between strains of bacteria. Our first assay will investigate the ability of our compounds to destabilize the membrane through the use of DPH<sup>92</sup> or other fluorescent reporters.<sup>93</sup> DPH is a fluorescent compound which intercalates into membranes and its fluorescent polarization can be used to collect data about the fluidity of a membrane as it is treated with a compound. As the membrane becomes more fluid, it is more likely that proteins and other cellular components can leak out of the cell, or membrane bound proteins can change shape or location. Perhaps some QACs are more likely to affect membrane fluidity. Perhaps some strains of bacteria are better able to counteract increased membrane fluidity. In either case, we will be able to collect valuable data about what effect the QACs have on membrane fluidity.

Additionally, we can perform a general analysis of the membrane-bound proteins. Proteins that are bound to the membrane and contain the amino acid phenylalanine tend to be fluorescent naturally. By first collecting a baseline of what the fluorescent spectrum of each bacteria looks like with no compound treatment and then dosing in QAC, we will be able to see if there is an effect on the membrane-bound proteins. Though this method does not tell us specific proteins that are effected, it can tell us if there is a conformational change of the membrane proteins or if additional proteins are added or taken away from the membrane, which could affect membrane fluidity.

It may also be valuable to conduct additional efflux-pump inhibitor experiments and cell permeability assays. Though we have had conflicting evidence from these experiments in the past, they were only conducted on the lab strains of bacteria.<sup>86</sup> In order to confirm that the QACs are acting on clinical bacteria similarly, we propose that these experiments be repeated to be thorough in our characterization of QAC mechanism of resistance, especially since this is still widely contested.

### 3.6 Conclusions

While QACs make up a significant portion of our biocides and surfactants in a variety of applications, the scientific community as a whole still has much to learn about their mechanisms of resistance. In a world where resistance to deadly bacteria like PA, AB, EC, and SA continues to pose a threat to human health, the scientific community at large needs to dedicate more time to understanding how these bacteria are resistant to our most reliable form of sterilization. It is also evident from our initial findings with QACs against clinically isolated bacteria that the scientific community needs to find ways to make their biological assays more relevant to real world situations. Lab strains of bacteria are decent benchmarks and useful for many microbiology studies, but they tend to be inherently more susceptible to biocides and therefore are less valuable for assessing how QACs will perform in a hospital setting where people's lives depend on their effectiveness.

### 3.7 References

- (1) Walker, E. B.; Paulson, D. *Quaternary Ammonium Compounds*; Marcel Dekker: New York, 1983; Vol. 23. [https://doi.org/10.1016/S0301-4770\(08\)60921-5](https://doi.org/10.1016/S0301-4770(08)60921-5).
- (2) Jacobs, W. A. No Title. *J. Exp. Med.* **1916**, *23*, 577–599.
- (3) Jacobs, W. A. No Title. *J. Exp. Med.* **1916**, *23*, 569–576.
- (4) Jacobs, W. A. No Title. *J. Exp. Med.* **1916**, *23*, 563–568.
- (5) Ortiz, S.; Lopez, V.; Martinez-Suarez, J. V. No Title. *Food Microbiol.* **2014**, *39*, 81–88.
- (6) Cummings, J. L.; Hawker, D. W.; Nugent, K. W.; Chapman, H. F. J. No Title. *J. Environ. Sci. Heal. A* **2008**, *43*, 113–117.
- (7) Rieger, M. M.; Rhein, L. D. *In Surfactants in Cosmetics*; Marcel Dekker: New York, 1997.
- (8) Alkhalifa, S.; Jennings, M.; Granata, D.; Klein, M.; Wuest, W. M.; Minbiole, K.; Carnevale, V. The Analysis of the Destabilization of Bacterial Membranes by Quaternary Ammonium Compounds: A Combined Experimental and Computational Study. *ChemBioChem* **2020**,



accepted. <https://doi.org/10.1002/cbic.201900698>.

- (9) AHLSTRÖM, B.; THOMPSON, R. A.; EDEBO, L. The Effect of Hydrocarbon Chain Length, PH, and Temperature on the Binding and Bactericidal Effect of Amphiphilic Betaine Esters on Salmonella Typhimurium. *APMIS* **1999**, *107*, 318–324. <https://doi.org/10.1111/j.1699-0463.1999.tb01560.x>.
- (10) Zubris, D.; Minbiole, K.; Wuest, W. Polymeric Quaternary Ammonium Compounds: Versatile Antimicrobial Materials. *Curr. Top. Med. Chem.* **2016**, *17* (3), 305–318. <https://doi.org/10.2174/1568026616666160829155805>.
- (11) Morrison, K. R.; Allen, R. A.; Minbiole, K. P. C.; Wuest, W. M. More QACs, More Questions: Recent Advances in Structure Activity Relationships and Hurdles in Understanding Resistance Mechanisms. *Tetrahedron Letters*. 2019. <https://doi.org/10.1016/j.tetlet.2019.07.026>.
- (12) Konai, M. M.; Bhattacharjee, B.; Ghosh, S.; Haldar, J. Recent Progress in Polymer Research to Tackle Infections and Antimicrobial Resistance. *Biomacromolecules* **2018**, *19* (6), 1888–1917. <https://doi.org/10.1021/acs.biomac.8b00458>.
- (13) Tezel, U.; Pavlostathis, S. G. Role of Quaternary Ammonium Compounds on Antimicrobial Resistance in the Environment. In *Antimicrobial Resistance in the Environment*; Keen, Montforts, Eds.; John Wiley and Sons Inc: New York, 2011; pp 349–387.
- (14) Kougia, E.; Tselepi, M.; Vasilopoulos, G.; Lainioti, G. C.; Koromilas, N. D.; Druvari, D.; Bokias, G.; Vantarakis, A.; Kallitsis, J. K.; McPhee, D. J. Evaluation of Antimicrobial Efficiency of New Polymers Comprised by Covalently Attached and/or Electrostatically Bound Bacteriostatic Species, Based on Quaternary Ammonium Compounds. *Molecules* **2015**, *20* (12), 21313–21327. <https://doi.org/10.3390/molecules201219768>.
- (15) Charnley, M.; Textor, M.; Acikgoz, C. Designed Polymer Structures with Antifouling-Antimicrobial Properties. *React. Funct. Polym.* **2011**, *71* (3), 329–334. <https://doi.org/10.1016/j.reactfunctpolym.2010.10.013>.
- (16) Schaer, T. P.; Stewart, S.; Hsu, B. B.; Klivanov, A. M. Hydrophobic Polycationic Coatings That Inhibit Biofilms and Support Bone Healing during Infection. *Biomaterials* **2012**, *33* (5), 1245–1254. <https://doi.org/10.1016/j.biomaterials.2011.10.038>.
- (17) Beyth, N.; Yudovin-Farber, I.; Perez-Davidi, M.; Domb, A. J.; Weiss, E. I. Polyethyleneimine Nanoparticles Incorporated into Resin Composite Cause Cell Death and Trigger Biofilm Stress in Vivo. *Proc. Natl. Acad. Sci. U. S. A.* **2010**, *107* (51), 22038–22043. <https://doi.org/10.1073/pnas.1010341107>.
- (18) Uppu, D. S. S. M.; Samaddar, S.; Ghosh, C.; Paramanandham, K.; Shome, B. R.; Haldar, J. Amide Side Chain Amphiphilic Polymers Disrupt Surface Established Bacterial Biofilms and Protect Mice from Chronic Acinetobacter Baumannii Infection. *Biomaterials* **2016**, *74*, 131–143.
- (19) Dijkshoorn, L.; Nemeč, A.; Seifert, H. An Increasing Threat in Hospitals : Multidrug-Resistant Acinetobacter Baumannii. *Nat. Rev. Microbiol.* **2007**, *5*, 939–951. <https://doi.org/10.1038/nrmicro1789>.
- (20) Towner, K. J. Acinetobacter : An Old Friend , but a New Enemy. *J. Hosp. Infect.* **2009**, *73*, 355–363. <https://doi.org/10.1038/nrmicro1789>.
- (21) Uppu, D. S. S. M.; Bhowmik, M.; Samaddar, S.; Haldar, J. Cyclization and Unsaturation Rather than Isomerisation of Side Chains Govern the Selective Antibacterial Activity of Cationic-

- Amphiphilic. *ChemComm* **2016**, *52*, 4644–4647. <https://doi.org/10.1039/c5cc09930g>.
- (22) Hoque, J.; Konai, M. M.; Sequeira, S. S.; Samaddar, S.; Haldar, J. Antibacterial and Antibiofilm Activity of Cationic Small Molecules with Spatial Positioning of Hydrophobicity: An in Vitro and in Vivo Evaluation. *J. Med. Chem.* **2016**, *59* (23), 10750–10762. <https://doi.org/10.1021/acs.jmedchem.6b01435>.
- (23) Uppu, D. S. S. M.; Konai, M. M.; Baul, U.; Singh, P.; Siersma, T. K.; Samaddar, S.; Vemparala, S.; Hamoen, L. W.; Narayana, C.; Haldar, J. Isosteric Substitution in Cationic-Amphiphilic Polymers Reveals an Important Role for Hydrogen Bonding in Bacterial Membrane Interactions. *Chem. Sci.* **2016**, *7*, 4613–4623. <https://doi.org/10.1039/c6sc00615a>.
- (24) Uppu, D. S. S. M.; Samaddar, S.; Hoque, J.; Konai, M. M.; Krishnamoorthy, P.; Shome, B. R.; Haldar, J. Side Chain Degradable Cationic – Amphiphilic Polymers with Tunable Hydrophobicity Show in Vivo Activity. *Biomacromolecules* **2016**, *17*, 3094–3102. <https://doi.org/10.1021/acs.biomac.6b01057>.
- (25) Uppu, D. S. S. M.; Konai, M. M.; Sarkar, P.; Samaddar, S.; Fensterseifer, I. C. M.; Farias-Junior, C.; Krishnamoorthy, P.; Shome, B. R.; Franco, O. L.; Haldar, J. Membrane-Active Macromolecules Kill Antibiotic-Tolerant Bacteria and Potentiate Antibiotics towards Gram-Negative Bacteria. *PLoS One* **2017**, *12* (8), 1–30. <https://doi.org/10.1371/journal.pone.0183263>.
- (26) Uppu, D. S. S. M.; Haldar, J. Lipopolysaccharide Neutralization by Cationic-Amphiphilic Polymers through Pseudoaggregate Formation. *Biomacromolecules* **2016**, *17*, 862–873. <https://doi.org/10.1021/acs.biomac.5b01567>.
- (27) Hoque, J.; Haldar, J. Direct Synthesis of Dextran-Based Antibacterial Hydrogels for Extended Release of Biocides and Eradication of Topical Biofilms. *ACS Appl. Mater. Interfaces* **2017**, *9* (19), 15975–15985. <https://doi.org/10.1021/acsami.7b03208>.
- (28) Hoque, J.; Akkapeddi, P.; Ghosh, C.; Uppu, D. S. S. M.; Haldar, J. A Biodegradable Polycationic Paint That Kills Bacteria in Vitro and in Vivo. *ACS Appl. Mater. Interfaces* **2016**, *8* (43), 29298–29309. <https://doi.org/10.1021/acsami.6b09804>.
- (29) Hoque, J.; Prakash, R. G.; Paramanandham, K.; Shome, B. R.; Haldar, J. Biocompatible Injectable Hydrogel with Potent Wound Healing and Antibacterial Properties. *Mol. Pharm.* **2017**, *14* (4), 1218–1230. <https://doi.org/10.1021/acs.molpharmaceut.6b01104>.
- (30) Hoque, J.; Bhattacharjee, B.; Prakash, R. G.; Paramanandham, K.; Haldar, J. Dual Function Injectable Hydrogel for Controlled Release of Antibiotic and Local Antibacterial Therapy. *Biomacromolecules* **2018**, *19* (2), 267–278. <https://doi.org/10.1021/acs.biomac.7b00979>.
- (31) Hoque, J.; Yadav, V.; Prakash, R. G.; Sanyal, K.; Haldar, J. Dual-Function Polymer-Silver Nanocomposites for Rapid Killing of Microbes and Inhibiting Biofilms. *ACS Biomater. Sci. Eng.* **2019**, *5* (1), 81–91. <https://doi.org/10.1021/acsbiomaterials.8b00239>.
- (32) Geng, Z.; Finn, M. G. Fragmentable Polycationic Materials Based on Anchimeric Assistance. *Chem. Mater.* **2016**, *28* (1), 146–152. <https://doi.org/10.1021/acs.chemmater.5b03445>.
- (33) Geng, Z.; Finn, M. G. Thiabicyclononane-Based Antimicrobial Polycations. *J. Am. Chem. Soc.* **2017**, *139* (43), 15401–15406. <https://doi.org/10.1021/jacs.7b07596>.
- (34) Beveridge, J. M.; Chenot, H. M.; Crich, A.; Jacob, A.; Finn, M. G. Covalent Functionalization of Flexible Polyvinyl Chloride Tubing. *Langmuir* **2018**, *34* (35), 10407–10412. <https://doi.org/10.1021/acs.langmuir.7b03115>.

- (35) Strassburg, A.; Kracke, F.; Weners, J.; Jemeljanova, A.; Kuepper, J.; Petersen, H.; Tiller, J. C. Nontoxic, Hydrophilic Cationic Polymers - Identified as Class of Antimicrobial Polymers. *Macromol. Biosci.* **2015**, *15* (12), 1710–1723. <https://doi.org/10.1002/mabi.201500207>.
- (36) Richter, L.; Hijazi, M.; Arfeen, F.; Krumm, C.; Tiller, J. C. Telechelic , Antimicrobial Hydrophilic Polycations with Two Modes of Action. *Macromol. Biosci.* **2018**, *18*, 1700389. <https://doi.org/10.1002/mabi.201700389>.
- (37) Schmidt, M.; Romanovska, A.; Wolf, Y.; Nguyen, T. D.; Krupp, A.; Tumbrink, H. L.; Lategahn, J.; Volmer, J.; Rauh, D.; Luetz, S.; et al. Insights into the Kinetics of the Resistance Formation of Bacteria against Ciprofloxacin Poly(2-Methyl-2-Oxazoline) Conjugates. *Bioconjugate Chem.* **2018**, *29* (8), 2671–2678. <https://doi.org/10.1021/acs.bioconjchem.8b00361>.
- (38) US-EPA. Reregistration Eligibility Decision for Alkyl Dimethyl Benzyl Ammonium Chloride (ADBAC). *Fed. Regist.* **2006**, EPA739-R-06–009.
- (39) Shelton, B. R. S.; Campen, M. G. Van; Tilford, C. H.; Lang, H. C.; Nisonger, L.; Bandelin, F. J.; Rubenkoenig, H. L.; Campen, V. Non-Acylated Quaternary Ammonium Salts Quaternary Ammonium Salts as Germicides . I . Non-Acylated Quaternary Ammonium Salts Derived from Aliphatic Amines I. *J. Am. Chem. Soc.* **1946**, *68* (5), 753–755.
- (40) Shelton, R. S.; Van Campen, M. G.; Tilford, C. H.; Lang, H. C.; Nisonger, L.; Bandelin, F. J.; Rubenkoenig, H. L. Quaternary Ammonium Salts as Germicides . II. Acetoxy and Carboethoxy Derivatives of Aliphatic Quaternary Ammonium Salts. *J. Am. Chem. Soc.* **1946**, *68* (1), 755–757.
- (41) Shelton, B. R. S.; Campen, M. G. Van; Tilford, C. H.; Lang, H. C.; Nisonger, L.; Bandelin, F. J.; Rubenkoenig, H. L.; Campen, V. Quaternary Ammonium Salts as Germicides . III . Quaternary Ammonium Salts Derived from Cyclic Amines. *J. Am. Chem. Soc.* **1946**, *68* (5), 757–759. <https://doi.org/10.1021/ja01209a014>.
- (42) US-EPA. Reregistration Eligibility Decision for Aliphatic Alkyl Quaternaries (DDAC). *Fed. Regist.* **2006**, EPA739-R-06-008.
- (43) Moore, K. S.; Wehrlit, S.; Rodert, H.; Rogers, M.; Forrest, J. N.; Mccrimmon, D.; Zasloff, M. Squalamine : An Aminosterol Antibiotic from the Shark. *Proc. Natl. Acad. Sci.* **1993**, *90* (February), 1354–1358.
- (44) Lavigne, J.-P.; Brunel, J.-M.; Chevalier, J.; Pages, J.-M. Squalamine, an Original Chemosensitizer to Combat Antibiotic- Resistant Gram-Negative Bacteria. *J. Antimicrob Chemother* **2010**, *65* (4), 799–801. <https://doi.org/10.1093/jac/dkq031>.
- (45) Blanchet, M.; Borselli, D.; Rodallec, A.; Peiretti, F.; Vidal, N.; Bolla, J. M.; Digiorgio, C.; Morrison, K. R.; Wuest, W. M.; Brunel, J. M. Claramines: A New Class Of Broad-Spectrum Antimicrobial Agents With Bimodal Activity. *ChemMedChem* **2018**. <https://doi.org/10.1002/cmde.201800073>.
- (46) Nicol, M.; Amine Ben Mlouka, M.; Berthe, T.; Di Martino, P.; Jouenne, T.; Brunel, J.; Dé, E. Anti-Persister Activity of Squalamine against *Acinetobacter Baumannii*. *Int. J. Antimicrob.* **2019**, *53*, 337–342.
- (47) Luo, J.; Yu, C.-H.; Borstnar, R.; Kamerelin, S. C. L.; Graslund, A.; Abrahams, J. P.; Warmlander, S. K. T. S. Cellular Polyamines Promote Amyloid-Beta (A  $\beta$ ) Peptide Fibrillation and Modulate the Aggregation Pathways. *ACS Chem. Neurosci.* **2013**, *4*, 454–462.
- (48) Limbocker, R.; Chia, S.; Ruggeri, F. S.; Perni, M.; Cascella, R.; Heller, G. T.; Meisl, G.; Mannini,

- B.; Habchi, J.; Michaels, T. C. T.; et al. Trodusquemine Enhances AB42 Aggregation but Suppresses Its Toxicity by Displacing Oligomers from Cell Membranes. *Nat. Commun.* **2019**, *10* (225), 1–13.
- (49) Perni, M.; Flagmeier, P.; Limbocker, R.; Cascella, R.; Aprile, F. A.; Galvagnion, C.; Heller, G. T.; Meisl, G.; Chen, S. W.; Kumita, J. R.; et al. Multistep Inhibition of  $\alpha$  - Synuclein Aggregation and Toxicity in Vitro and in Vivo by Trodusquemine. *ACS Chem. Biol.* **2018**, *13*, 2308–2319. <https://doi.org/10.1021/acscchembio.8b00466>.
- (50) Bugg, T. D. H.; Wright, G. D.; Walsh, C. T.; Dutka-Malen, S.; Arthur, M.; Courvalin, P. Molecular Basis for Vancomycin Resistance in *Enterococcus Faecium* BM4147: Biosynthesis of a Depsipeptide Peptidoglycan Precursor by Vancomycin Resistance Proteins VanH and VanA. *Biochemistry* **1991**, *30* (43), 10408–10415. <https://doi.org/10.1021/bi00107a007>.
- (51) Healy, V. L.; Lessard, I. A. D.; Roper, D. I.; Knox, J. R.; Walsh, C. T. Vancomycin Resistance in Enterococci: Reprogramming of the D-Ala-D-Ala Ligases in Bacterial Peptidoglycan Biosynthesis. *Chem. Biol.* **2000**, *7* (5), 109–119. [https://doi.org/10.1016/S1074-5521\(00\)00116-2](https://doi.org/10.1016/S1074-5521(00)00116-2).
- (52) Okano, A.; Nakayama, A.; Wu, K.; Lindsey, E. A.; Schammel, A. W.; Feng, Y.; Collins, K. C.; Boger, D. L. Total Syntheses and Initial Evaluation of [ $\Psi$ [C(=S)NH]Tpg4]Vancomycin, [ $\Psi$ [=NH)NH]Tpg4]Vancomycin, [ $\Psi$ [CH<sub>2</sub>NH]Tpg4]Vancomycin, and Their (4-Chlorobiphenyl)Methyl Derivatives: Synergistic Binding Pocket and Peripheral Modifications for the Glycopeptide Antibio. *J. Am. Chem. Soc.* **2015**, *137* (10), 3693–3704. <https://doi.org/10.1021/jacs.5b01008>.
- (53) Xie, J.; Okano, A.; Pierce, J. G.; James, R. C.; Stamm, S.; Crane, C. M.; Boger, D. L. Total Synthesis of [ $\psi$ [C(=S)NH]Tpg 4]Vancomycin Aglycon, [ $\psi$ [C(=NH)NH]Tpg 4]Vancomycin Aglycon, and Related Key Compounds: Reengineering Vancomycin for Dual D-Ala-D-Ala and D-Ala-D-Lac Binding. *J. Am. Chem. Soc.* **2012**, *134* (2), 1284–1297. <https://doi.org/10.1021/ja209937s>.
- (54) Okano, A.; Isley, N. A.; Boger, D. L. Peripheral Modifications of [ $\Psi$ [CH<sub>2</sub>NH]Tpg4]Vancomycin with Added Synergistic Mechanisms of Action Provide Durable and Potent Antibiotics. *Proc. Natl. Acad. Sci. U. S. A.* **2017**, *114* (26), E5052–E5061. <https://doi.org/10.1073/pnas.1704125114>.
- (55) Wu, Z. C.; Isley, N. A.; Boger, D. L. N-Terminus Alkylation of Vancomycin: Ligand Binding Affinity, Antimicrobial Activity, and Site-Specific Nature of Quaternary Trimethylammonium Salt Modification. *ACS Infect. Dis.* **2018**, *4* (10), 1468–1474. <https://doi.org/10.1021/acsinfecdis.8b00152>.
- (56) Benedict, R. G.; Langlykke, A. F. Antibiotic Activity of *Bacillus Polymyxa*. *J. Bacteriol.* **1947**, *54*, 24–25.
- (57) Velkov, T.; Roberts, K. D.; Thompson, P. E.; Li, J. Polymyxins: A New Hope in Combating Gram-Negative Superbugs? *Futur. Med. Chem.* **2016**, *8* (10), 1017–1025.
- (58) Tran, A. X.; Lester, Melissa, E.; Stead, C. M.; Raetz, C. R. H.; Maskell, D. J.; McGrath, S. C.; Cotter, R. J.; Trent, M. S. Resistance to the Antimicrobial Peptide Polymyxin Requires Myristoylation of *Escherichia Coli* and *Salmonella Typhimurium* Lipid A. *J. biol. Chem.* **2005**, *280*, 28186–28194.
- (59) Liu, Y.-Y.; Wang, Y.; Walsh, T. R.; Yi, L.-X.; Zhang, R.; Spencer, J.; Doi, Y.; Tian, G.; Dong, B.; Huang, X.; et al. Emergence of Plasmid-Mediated Colistin Resistance Mechanism MCR-1 in Animals and Human Beings in China: A Microbiological and Molecular Biological Study. *Lancet*

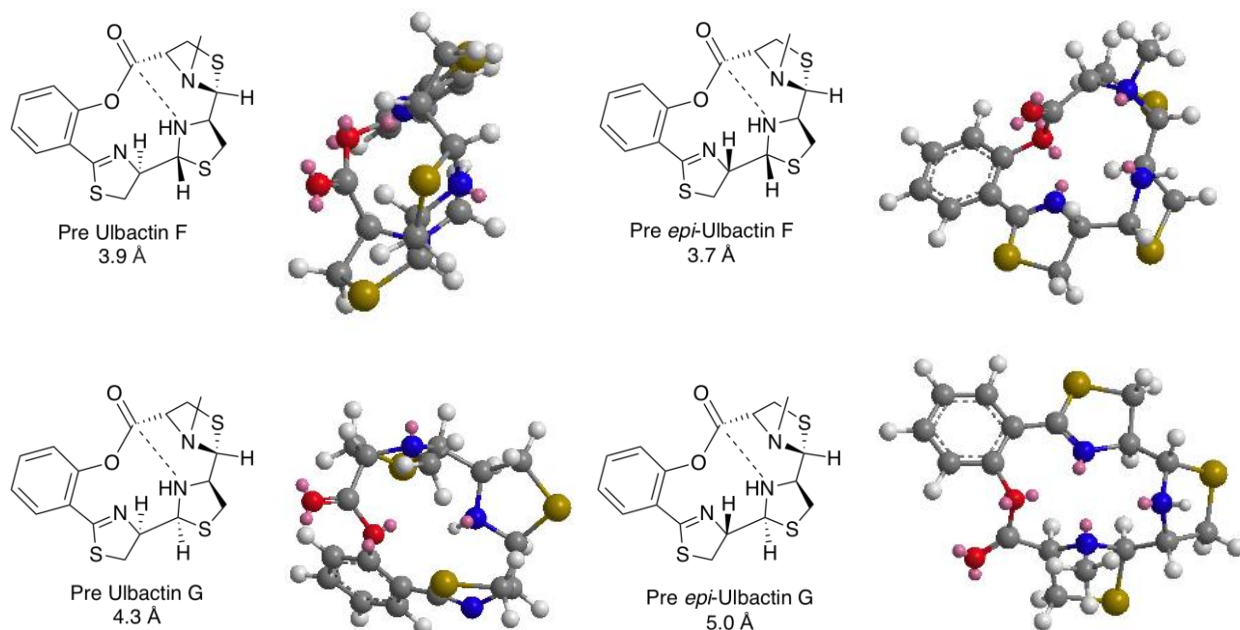
- Infect. Dis.* **2016**, *16*, 161–168.
- (60) Böttcher, T.; Kolodkin-Gal, I.; Kolter, R.; Losick, R.; Clardy, J. Synthesis and Activity of Biomimetic Biofilm Disruptors. *J. Am. Chem. Soc.* **2013**, *135* (8), 2927–2930. <https://doi.org/10.1021/ja3120955>.
- (61) Kolodkin-Gal, I.; Cao, S.; Chai, L.; Böttcher, T.; Kolter, R.; Clardy, J.; Losick, R. A Self-Produced Trigger for Biofilm Disassembly That Targets Exopolysaccharide. *Cell* **2012**, *149* (3), 684–692. <https://doi.org/10.1016/j.cell.2012.02.055>.
- (62) Black, J. W.; Jennings, M. C.; Azarewicz, J.; Paniak, T. J.; Grenier, M. C.; Wuest, W. M.; Minbiole, K. P. C. TMEDA-Derived Biscationic Amphiphiles: An Economical Preparation of Potent Antibacterial Agents Dedicated to Professor Amos B. Smith, III, in Celebration of His 40 Years of Mentoring Scientists. *Bioorganic Med. Chem. Lett.* **2014**. <https://doi.org/10.1016/j.bmcl.2013.11.070>.
- (63) Paniak, T. J.; Jennings, M. C.; Shanahan, P. C.; Joyce, M. D.; Santiago, C. N.; Wuest, W. M.; Minbiole, K. P. C. The Antimicrobial Activity of Mono-, Bis-, Tris-, and Tetracationic Amphiphiles Derived from Simple Polyamine Platforms. *Bioorganic Med. Chem. Lett.* **2014**. <https://doi.org/10.1016/j.bmcl.2014.10.018>.
- (64) Domagk, G. A New Class of Disinfectant. *Dtsch. Med. Wochenschr* **1935**, *61*, 829–832.
- (65) Jennings, M. C.; Minbiole, K. P. C.; Wuest, W. M. Quaternary Ammonium Compounds: An Antimicrobial Mainstay and Platform for Innovation to Address Bacterial Resistance. *ACS Infect. Dis.* **2016**, *1* (7), 288–303. <https://doi.org/10.1021/acsinfecdis.5b00047>.
- (66) Schallenhammer, S. A.; Duggan, S. M.; Morrison, K. R.; Bentley, B. S.; Wuest, W. M.; Minbiole, K. P. C. Hybrid BisQACs: Potent Biscationic Quaternary Ammonium Compounds Merging the Structures of Two Commercial Antiseptics. *ChemMedChem* **2017**. <https://doi.org/10.1002/cmdc.201700597>.
- (67) Black, J. W.; Jennings, M. C.; Azarewicz, J.; Paniak, T. J.; Grenier, M. C.; Wuest, W. M.; Minbiole, K. P. C. TMEDA-Derived Biscationic Amphiphiles: An Economical Preparation of Potent Antibacterial Agents. *Bioorg. Med. Chem. Lett.* **2014**. <https://doi.org/10.1016/j.bmcl.2013.11.070>.
- (68) Allen, R. A.; Jennings, M. C.; Mitchell, M. A.; Al-Khalifa, S. E.; Wuest, W. M.; Minbiole, K. P. C. Ester- and Amide-Containing MultiQACs: Exploring Multicationic Soft Antimicrobial Agents. *Bioorganic Med. Chem. Lett.* **2017**. <https://doi.org/10.1016/j.bmcl.2017.03.077>.
- (69) Kontos, R. C.; Schallenhammer, S. A.; Bentley, B. S.; Morrison, K. R.; Feliciano, J. A.; Tasca, J. A.; Kaplan, A. R.; Bezpalko, M. W.; Kassel, W. S.; Wuest, W. M.; et al. An Investigation into Rigidity–Activity Relationships in BisQAC Amphiphilic Antiseptics. *ChemMedChem* **2019**. <https://doi.org/10.1002/cmdc.201800622>.
- (70) Al-Khalifa, S. E.; Jennings, M. C.; Wuest, W. M.; Minbiole, K. P. C. The Development of Next-Generation Pyridinium-Based MultiQAC Antiseptics. *ChemMedChem* **2017**. <https://doi.org/10.1002/cmdc.201600546>.
- (71) Meyer, B.; Cookson, B. Does Microbial Resistance or Adaptation to Biocides Create a Hazard in Infection Prevention and Control? *J. Hosp. Infect.* **2010**, *76*, 200–205.
- (72) Tennent, J. M.; Lyon, B. R.; Gillespie, M. T.; May, J. W.; Skurray, R. A. Cloning and Expression of Staphylococcus Aureus Plasmid-Mediated Quaternary Ammonium Resistance in Escherichia

- Coli. Antimicrob. Agents Chemother.* **1985**, *27*, 79–83. <https://doi.org/10.1128/AAC.27.1.79>.
- (73) Voorde, A. Van De; Lorgeoux, C.; Gromaire, M.; Chebbo, G. Analysis of Quaternary Ammonium Compounds in Urban Stormwater Samples. *Environ. Pollut.* **2012**, *164*, 150–157. <https://doi.org/10.1016/j.envpol.2012.01.037>.
- (74) Tsai, P.; Ding, W. Determination of Alkyltrimethylammonium Surfactants in Hair Conditioners and Fabric Softeners by Gas Chromatography – Mass Spectrometry with Electron-Impact and Chemical Ionization. *J. Chromatogr. A* **2004**, *1027*, 103–108. <https://doi.org/10.1016/j.chroma.2003.10.047>.
- (75) Ding, W.; Liao, Y. Determination of Alkylbenzyltrimethylammonium Chlorides in River Water and Sewage Effluent by Solid-Phase Extraction and Gas Chromatography / Mass Spectrometry. *Anal. Chem.* **2001**, *73*, 36–40.
- (76) Lara-Martin, P. A.; Li, X.; Bopp, R. F.; Brownawell, B. J. Occurrence of Alkyltrimethylammonium Compounds in Urban Estuarine Sediments : Behentrimonium As a New Emerging Contaminant. *Environ. Sci. Technol.* **2010**, *44*, 7569–7575.
- (77) Ruan, T.; Song, S.; Wang, T.; Liu, R.; Lin, Y.; Jiang, G. Identification and Composition of Emerging Quaternary Ammonium Compounds in Municipal Sewage Sludge in China. *Environ. Sci. Technol.* **2014**, *48*, 4289–4297. <https://doi.org/10.1021/es4050314>.
- (78) Zhang, C.; Cui, F.; Zeng, G.; Jiang, M.; Yang, Z.; Yu, Z.; Zhu, M.; Shen, L. Quaternary Ammonium Compounds ( QACs ): A Review on Occurrence , Fate and Toxicity in the Environment. *Sci. Total Environ.* **2015**, *518–519*, 352–362.
- (79) Vijayakumar, R.; Sandle, T.; Al-Aboody, M. S.; AlFonaisan, M. K.; Alturaiki, W.; Mickymaray, S.; Premanathan, M.; Alsagaby, S. A. Distribution of Biocide Resistant Genes and Biocides Susceptibility in Multidrug-Resistant *Klebsiella Pneumoniae*, *Pseudomonas Aeruginosa* and *Acinetobacter Baumannii* — A First Report from the Kingdom of Saudi Arabia. *J. Infect. Public Heal.* **2018**, *11* (6), 812–816. <https://doi.org/10.1016/j.jiph.2018.05.011>.
- (80) Paulsen, I. T.; Brown, M. H.; Littlejohn, T. G.; Mitchell, B. A.; Skurray, R. A. Multidrug Resistance Proteins QacA and QacB from *Staphylococcus Aureus* : Membrane Topology and Identification of Residues Involved in Substrate Specificity. *Proc. Natl. Acad. Sci.* **2006**, *93*, 3630–3635.
- (81) Bjorland, J.; Steinum, T.; Sunde, M.; Waage, S.; Heir, E. Novel Plasmid-Borne Gene QacJ Mediates Resistance to Quaternary Ammonium Compounds in Equine *Staphylococcus Aureus* , *Staphylococcus Simulans* , and *Staphylococcus Intermedius*. *Antimicrob. Agents Chemother.* **2003**, *47* (10), 3046–3052. <https://doi.org/10.1128/AAC.47.10.3046>.
- (82) Heir, E.; Sundheim, G.; Holck, A. L. The *Staphylococcus QacH* Gene Product : A New Member of the SMR Family Encoding Multidrug Resistance. *FEMS Microbiol. Lett.* **1998**, *163*, 49–56.
- (83) Heir, E.; Sundheim, G.; Holck, A. L. The QacG Gene on Plasmid PST94 Confers Resistance to Quaternary Ammonium Compounds in *Staphylococci* Isolated from the Food Industry. *J. Appl. Microbiol.* **1999**, *86*, 378–388.
- (84) Wilhelm, M. J.; Sheffield, J. B.; Sharifian Gh., M.; Wu, Y.; Spahr, C.; Gonella, G.; Xu, B.; Dai, H. L. Gram’s Stain Does Not Cross the Bacterial Cytoplasmic Membrane. *ACS Chem. Biol.* **2015**, *10* (7), 1711–1717. <https://doi.org/10.1021/acscchembio.5b00042>.
- (85) Forman, M. E.; Fletcher, M. H.; Jennings, M. C.; Duggan, S. M.; Minbiole, K. P. C.; Wuest, W.

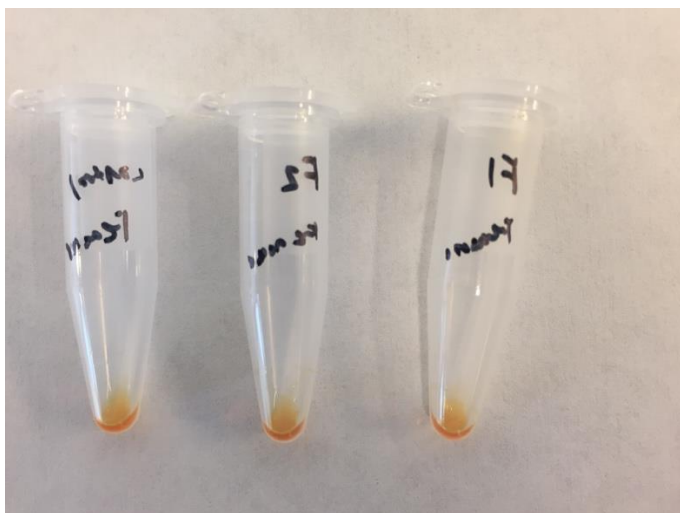
- M. Structure-Resistance Relationships: Interrogating Antiseptic Resistance in Bacteria with Multicationic Quaternary Ammonium Dyes. *ChemMedChem* **2016**.  
<https://doi.org/10.1002/cmdc.201600095>.
- (86) Jennings, M. C.; Forman, M. E.; Duggan, S. M.; Minbirole, K. P. C.; Wuest, W. M. Efflux Pumps Might Not Be the Major Drivers of QAC Resistance in Methicillin-Resistant *Staphylococcus Aureus*. *ChemBioChem* **2017**. <https://doi.org/10.1002/cbic.201700233>.
- (87) Forman, M. E.; Jennings, M. C.; Wuest, W. M.; Minbirole, K. P. C. Building a Better Quaternary Ammonium Compound (QAC): Branched Tetracationic Antiseptic Amphiphiles. *ChemMedChem* **2016**. <https://doi.org/10.1002/cmdc.201600176>.
- (88) Mitchell, M. A.; Iannetta, A. A.; Jennings, M. C.; Fletcher, M. H.; Wuest, W. M.; Minbirole, K. P. C. Scaffold-Hopping of Multicationic Amphiphiles Yields Three New Classes of Antimicrobials. *ChemBioChem* **2015**. <https://doi.org/10.1002/cbic.201500381>.
- (89) Ator, L. E.; Jennings, M. C.; McGettigan, A. R.; Paul, J. J.; Wuest, W. M.; Minbirole, K. P. C. Beyond Paraquats: Dialkyl 3,3'- and 3,4'-Bipyridinium Amphiphiles as Antibacterial Agents. *Bioorg. Med. Chem. Lett.* **2014**, *24*, 3706–3709. <https://doi.org/10.1016/j.bmcl.2014.07.024>.
- (90) Grenier, M. C.; Davis, R. W.; Wilson-Henjum, K. L.; Ladow, J. E.; Black, J. W.; Caran, K. L.; Seifert, K.; Minbirole, K. P. C. The Antibacterial Activity of 4,4'-Bipyridinium Amphiphiles with Conventional, Bicephalic and Gemini Architectures. *Bioorg. Med. Chem. Lett.* **2012**, *22* (12), 4055–4058. <https://doi.org/10.1016/j.bmcl.2012.04.079>.
- (91) Mah, T.-F. Establishing the Minimal Bactericidal Concentration of an Antimicrobial Agent for Planktonic Cells (MBC-P) and Biofilm Cells (MBC-B). *J. Vis. Exp.* **2014**, No. 83, e50854. <https://doi.org/10.3791/50854>.
- (92) Wu, Y.; Bai, J.; Zhong, K.; Huang, Y.; Qi, H.; Jiang, Y.; Gao, H. Antibacterial Activity and Membrane-Disruptive Mechanism of 3-p-Trans-Coumaroyl-2-Hydroxyquinic Acid, a Novel Phenolic Compound from Pine Needles of *Cedrus Deodara*, against *Staphylococcus Aureus*. *Molecules* **2016**, *21*, 1084. <https://doi.org/10.3390/molecules21081084>.
- (93) Sanchez, S. A.; Triccerri, M. A.; Gratton, E. Laurdan Generalized Polarization Fluctuations Measures Membrane Packing Micro-Heterogeneity in Vivo. *Proc. Natl. Acad. Sci.* **2012**, *109* (19), 7314–7319. <https://doi.org/10.1073/pnas.1118288109>.

## 4. Supporting Information

### 1. Supplementary Figures:

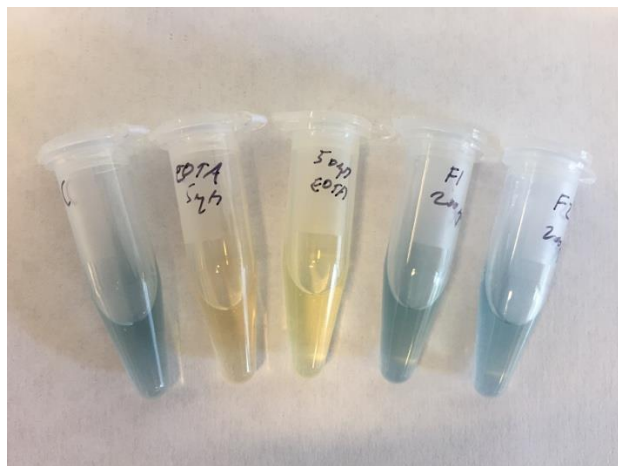


**Supplementary Figure 1:** Energy minimizations of proposed macrocycles leading to various epimers of Ulbactins with relevant atom-to-atom distance highlighted. Structures and calculations are generated in Chem3D. Dashed atom-to-atom distances are reported in Ångströms.

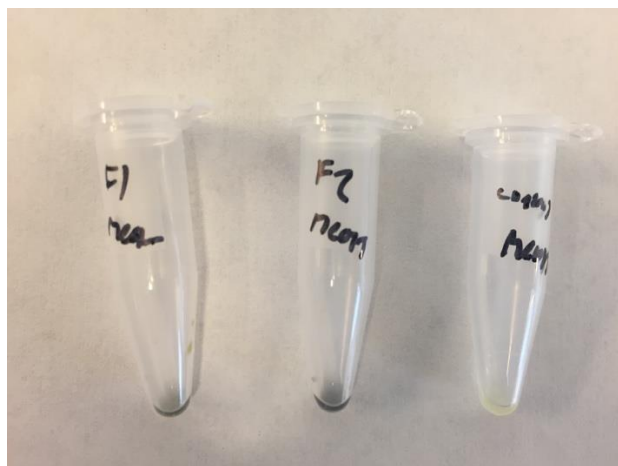




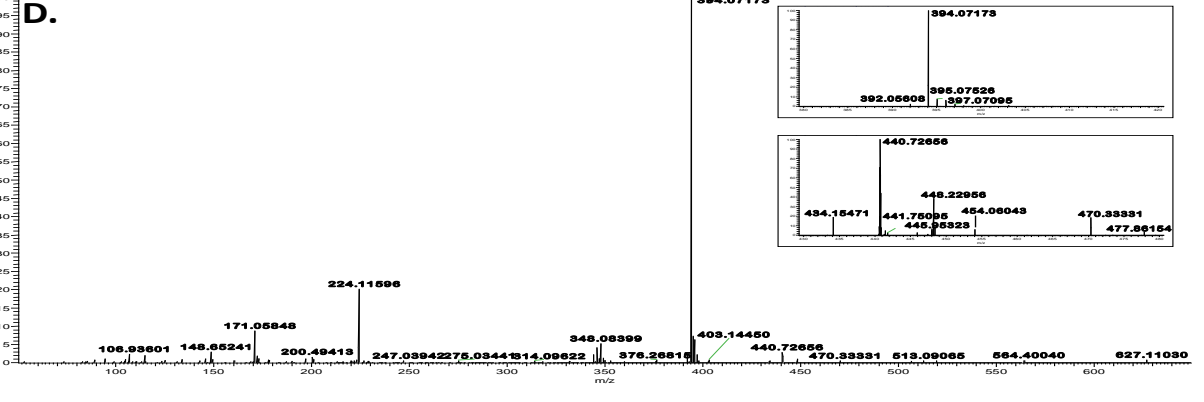
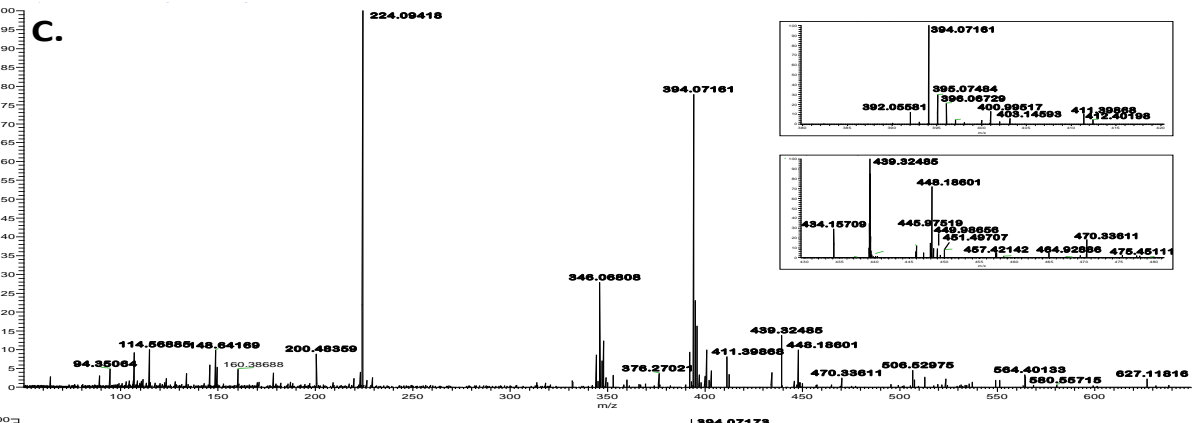
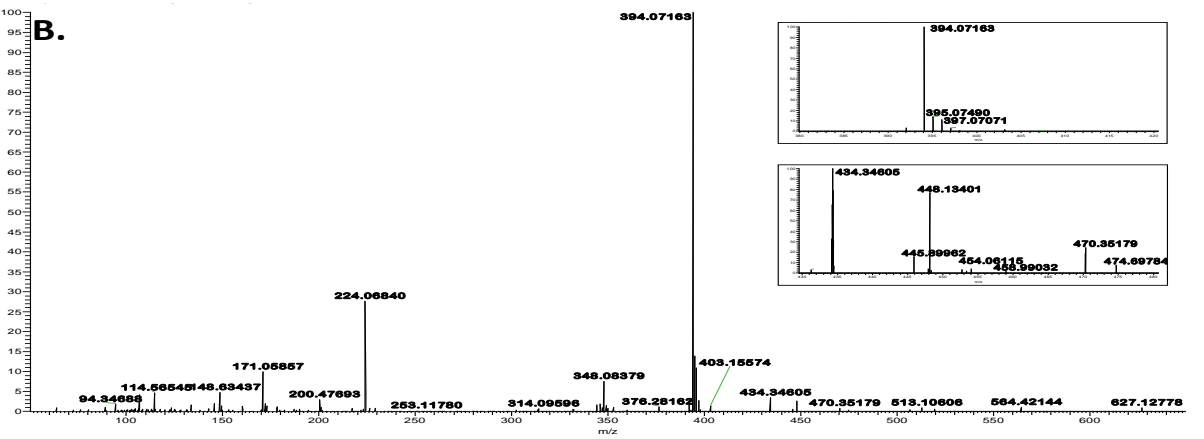
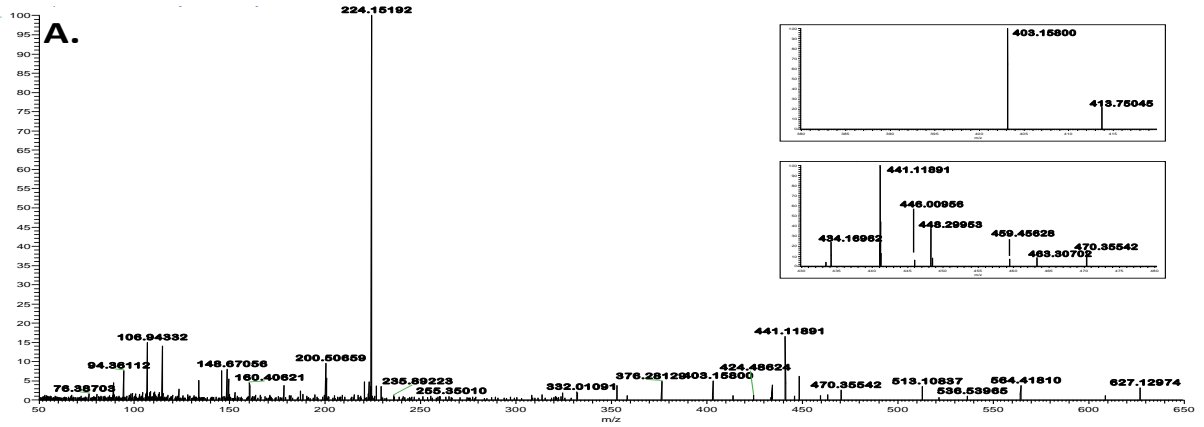
**Supplementary Figure 2:** (Left) Methanol containing 100  $\mu\text{M}$  iron (III) acetylacetonate. (Middle) Methanol containing 100  $\mu\text{M}$  *epi*-ulbactin F and 100  $\mu\text{M}$  iron (III) acetylacetonate. (Right) Methanol containing 100  $\mu\text{M}$  ulbactin F and 100  $\mu\text{M}$  iron (III) acetylacetonate.



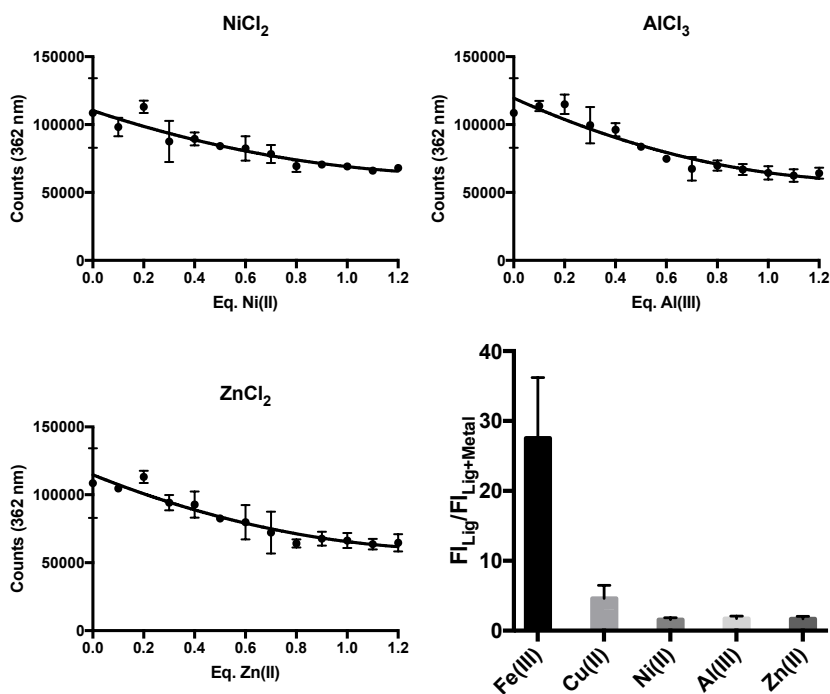
**Supplementary Figure 3:** From left to right: CAS media, CAS media containing 5  $\mu\text{M}$  EDTA, CAS media containing 50  $\mu\text{M}$  EDTA, CAS media containing 200  $\mu\text{M}$  ulbactin F, and CAS media containing 200  $\mu\text{M}$  *epi*-ulbactin F.



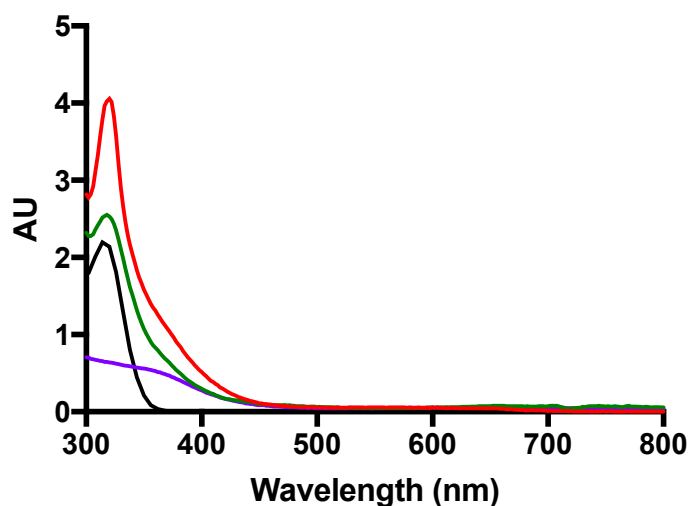
**Supplementary Figure 4:** (Left) Methanol containing 100  $\mu\text{M}$  ulbactin F and 100  $\mu\text{M}$  iron (III) chloride. (Middle) Methanol containing 100  $\mu\text{M}$  *epi*-ulbactin F and 100  $\mu\text{M}$  iron (III) chloride. (Right) Methanol containing 100  $\mu\text{M}$  iron (III) chloride.



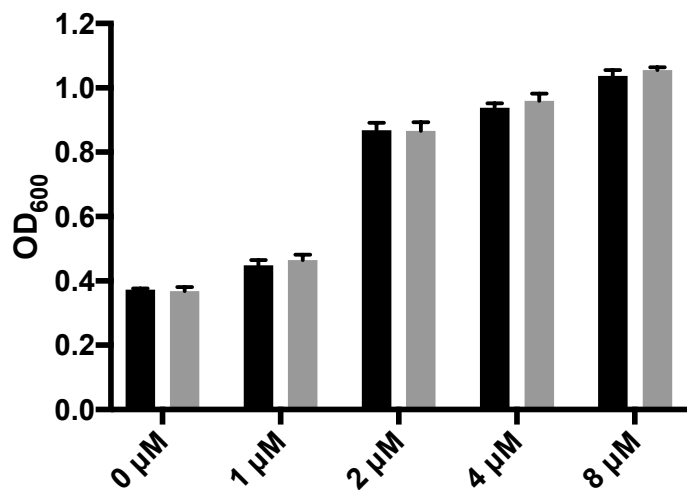
**Supplementary Figure 5:** Mass Chromatograms of ulbactin F samples. (A) Background chromatogram (B) Ulbactin F before treatment with iron (III) chloride (C) Ulbactin F after treatment with iron (III) chloride (D) ulbactin F after treatment with iron (III) chloride and subsequent extraction between ethyl acetate and 5% aqueous sodium citrate. All samples dissolved in methanol.



**Supplementary Figure 6:** Fluorescence titrations of ulbactin F with (Top left) Nickel (II) chloride, (Top right) Aluminum (III) chloride, and (Bottom left) Zinc (II) chloride. Ratio of fluorescence of 400  $\mu\text{M}$  ligand over fluorescence of 400  $\mu\text{M}$  ligand + 400  $\mu\text{M}$  metal (Bottom right). Measurements taken in methanol.



**Supplementary Figure 7:** UV-Vis spectra of 400  $\mu\text{M}$  Fe<sup>3+</sup>-ulbactin F complex (Red), 400  $\mu\text{M}$  Fe<sup>3+</sup>-ulbactin F complex + 500  $\mu\text{M}$  catechol (Green), 400  $\mu\text{M}$  ulbactin F (black), and 100  $\mu\text{M}$  catechol<sub>3</sub>-Fe<sup>3+</sup> complex. All spectra taken in methanol.



**Supplementary Figure 8:** Growth of *Pseudomonas aeruginosa* PAO1 cultures grown in M9 minimal media containing 300 μM 2,2'-dipyridyl and supplemented with Fe<sup>3+</sup>-ulbactin F complex (black bars) or FeCl<sub>3</sub> (grey bars).

## 2. Methods

**General:** NMR spectra were recorded using the following spectrometers: Varian INOVA500, Varian INOVA400, VNMR400, and Bruker Ascend 600. All NMR spectra were recorded under ambient temperature. Chemical shifts are quoted in ppm relative to solvents used ( $^1\text{H}$ :  $\delta = 7.26$  and  $^{13}\text{C}$ :  $\delta = 77.16$  for residual  $\text{CHCl}_3$ ,  $^1\text{H}$ :  $\delta = 3.49, 1.09$  and  $^{13}\text{C}$ :  $\delta = 50.41$  for residual  $\text{CH}_3\text{OH}$ ,  $^1\text{H}$ :  $\delta = 1.56$  for residual  $\text{H}_2\text{O}$ ). The abbreviations used to describe splitting are as follows: s (singlet), d (doublet), t (triplet), q (quartet), m (multiplet), dd (doublet of doublets), dt (doublet of triplets), etc.

Accurate mass spectra were recorded on a Thermo LTQ-FTMS using either APCI or ESI techniques.

Infrared spectra were obtained using a ThermoScientific Nicolet with an attenuated total reflectance (ATR) with a Germanium crystal. Samples were tested neat or in chloroform. Peaks are reported in  $\text{cm}^{-1}$  and described as either weak (w), strong (s), or broad (b).

Specific rotations were obtained with 1 dm path length using a Perkin Elmer Model 341 Polarimeter with a Na/Hal lamp set to 598 nm. Samples were dissolved in either chloroform or water depending on the solubility restrictions of some compounds. In all cases, the polarimeter was zeroed to the solvent first. Measurements were taken over several minutes and then adjusted based on concentration.

Non-aqueous reactions were performed under an atmosphere of argon in flame-dried glassware with HPLC-grade solvents dried by passage through alumina. Amine bases were freshly distilled over  $\text{CaH}_2$  prior to use. Brine refers to a saturated aqueous solution of sodium chloride. Purification via flash chromatography refers to usage of Biotage Isolera One Automated column. Reactions monitored via thin-layer chromatography (TLC) using EMD Millipore® TLC silica gel glass plates with various stains specified in each procedure. Reactions monitored by LCMS were injected into an Agilent Technologies 1220 Infinity HPLC Liquid Chromatograph connected to an Advion Expression Compact Mass Spectrometer. Solvents used were HPLC grade water and acetonitrile each spiked with 0.1% formic acid.

Fluorescence measurements were recorded on a FluoroMax spectrophotometer (Horiba Scientific, Edison, New Jersey) in a quartz fluorescence cuvette with a 1 cm pathlength, an integration range of 285-550 nm and an excitation and emission slit width of 2 nm.

### 3. Biological Assays

For all biological assays bacteria were grown with shaking at 37°C overnight from freezer stocks in 5 mL of Mueller-Hinton media.

**Metal Dependent Growth studies** were conducted using *Pseudomonas aeruginosa* PAO1. A test-tube culture of liquid LB media was inoculated with PAO1 and grown overnight at 37° C, 200 RPM. Overnight culture was diluted 1:100 in fresh media and grown at 37° C, 200 RPM. OD<sub>600</sub> was monitored until exponential growth, approximately 0.2, was reached. Regrown culture was then diluted into M9 minimal media containing 600 µM 2,2'-dipyridyl to achieve a 0.5 McFarland standard inoculum. Stock solutions of either 10 mM Fe<sup>3+</sup>-ulbactin F complex or 10 mM FeCl<sub>3</sub> in methanol were diluted into M9 minimal media to a concentration of 512 µM and added to separate wells of the first column of a sterile 96-well microtiter plate (200 µL per well). All other wells were filled with 100 µL of M9 minimal media and the first column was serially diluted across the plate. Inoculum was added (100 µL per well) to achieve a final volume of 200 µL per well, 300 µM 2,2'-dipyridyl and 256->1 µM iron (III) source. The plate was then grown at 37° C for 24 hours and OD<sub>600</sub> was monitored by plate reader.

**Minimum inhibitory concentration (MIC).** Compounds were serially diluted two-fold from stock solutions to yield twelve test concentrations. Overnight cultures were diluted to ca. 10<sup>6</sup> cfu/mL in MH media and regrown to exponential phase as determined by optical density recorded at 600 nm (OD<sub>600</sub>). All cultures were diluted again to ca. 10<sup>6</sup> cfu/mL in MH media (CLSI Standards)<sup>37</sup> and 100 µL were inoculated into each well of a U-bottom 96-well plate (BD Biosciences, BD 351177) containing 100 µL of compound solution. Plates were incubated statically at 37°C for 24 h upon which time wells were evaluated visually for bacterial growth. The MIC was determined as the lowest concentration of compound resulting in no bacterial growth visible to the naked eye, based on the majority of three independent experiments. Aqueous DMSO controls were conducted as appropriate for each compound.

#### 3.1 Full MIC Data for QACs against clinical isolates

A. *baumannii*

	sT-10,10,10,3A	T-11,11,11	10(3)0(3)10	12(3)2(3)12	12(3)0(3)12	P-12,0,12	sT-10,10,10,0	2Pyr-11,11
MRSN 17493	>250	125	>250	250	250	250	>250	>250
MRSN 1311	>250	63	125	125	8	4	>250	8
MRSN 1174	>250	125	125	125	125	125	>250	16
MRSN 334	8	8	125	125	8	4	8	16
MRSN 959	16	16	63	8	4	4	16	8
MRSN 960	>250	125	125	16	8	8	16	8
MRSN 7521	8	16	125	125	125	4	>250	4
MRSN 4484	>250	63	>250	125	125	125	250	4
MRSN 11703	8	63	125	125	125	4	>250	8
MRSN 11695	>250	125	63	125	4	4	4	4
MRSN 14193	>250	125	>250	125	125	125	>250	4
MRSN 3874	125	125	>250	250	8	4	>250	4
MRSN 11224	250	63	>250	63	125	125	250	8
MRSN 11663	>250	32	125	125	125	63	>250	8
MRSN 14427	16	8	125	63	8	4	63	8
MRSN 15049	>250	125	125	125	125	4	>250	16
MRSN 14237	>250	63	125	125	16	8	16	8
MRSN 918	>250	250	125	250	250	250	>250	8
MRSN 21681	>250	125	>250	125	8	4	>250	4
MRSN 21660	>250	63	125	125	63	125	16	8
MRSN 337038	8	8	63	125	8	4	8	8
MRSN 29908	8	4	63	125	8	4	8	4
MRSN 480561	>250	125	63	125	125	4	>250	8
MRSN 480622	>250	125	>250	125	125	125	>250	250
MRSN 32866	>250	250	>250	125	125	125	>250	>250
MRSN 31196	>250	63	125	16	8	4	8	4
MRSN 32104	>250	125	125	125	125	125	>250	8
MRSN 423159	125	32	250	63	32	4	250	8
MRSN 489669	>250	250	63	250	125	125	>250	4
MRSN 7076	>250	63	32	125	4	2	1	1
MRSN 32915	>250	63	>250	125	125	125	>250	>250
MRSN 19482	>250	8	125	125	125	125	250	250
MRSN 15574	>250	63	63	125	4	4	8	4
MRSN 25547	250	4	63	63	63	4	8	8
MRSN 30000	>250	63	>250	125	125	125	>250	4

	PQ-12,12	m-Hy-12,12	Pip-12,12	12(2)12	BAC	BEC	CPC	DDAC
MRSN 17493	>250	8	>250	250	>250	>250	125	8
MRSN 1311	250	250	>250	125	63	>250	32	8
MRSN 1174	>250	32	>250	125	32	32	32	8
MRSN 334	>250	8	16	4	32	125	32	8
MRSN 959	16	8	16	4	63	63	32	8
MRSN 960	16	8	16	63	63	63	63	8
MRSN 7521	8	16	16	8	32	32	32	8
MRSN 4484	125	250	>250	63	32	>250	32	8
MRSN 11703	63	250	16	125	32	63	32	8
MRSN 11695	4	4	8	4	32	32	32	8
MRSN 14193	>250	8	>250	125	32	32	32	8
MRSN 3874	4	8	16	125	32	32	32	8
MRSN 11224	125	32	>250	63	>250	>250	63	8
MRSN 11663	16	8	>250	63	32	32	32	8
MRSN 14427	8	4	16	4	32	32	32	8
MRSN 15049	250	250	>250	125	63	>250	32	8
MRSN 14237	8	16	32	63	32	63	32	8
MRSN 918	>250	250	>250	250	63	>250	63	8
MRSN 21681	8	8	16	125	63	32	32	8
MRSN 21660	32	250	32	63	32	32	63	8
MRSN 337038	8	8	8	4	63	63	32	8
MRSN 29908	16	8	16	125	63	63	125	8
MRSN 480561	8	8	8	63	32	32	32	8
MRSN 480622	>250	250	>250	63	>250	>250	125	8
MRSN 32866	8	250	>250	250	>250	>250	125	8
MRSN 31196	16	8	16	63	32	32	63	8
MRSN 32104	>250	250	>250	125	32	>250	16	8
MRSN 423159	125	250	>250	63	>250	>250	63	>250
MRSN 489669	>250	8	>250	125	63	63	32	8
MRSN 7076	8	4	8	2	32	32	16	4
MRSN 32915	>250	250	>250	125	32	32	32	8
MRSN 19482	125	8	8	125	32	32	125	8
MRSN 15574	8	4	8	125	63	63	63	8
MRSN 25547	63	8	16	4	32	32	63	8
MRSN 30000	>250	250	16	63	32	32	32	8

*P. aeruginosa*



	sT-10,10,10,3A	T-11,11,11	10(3)0(3)10	12(3)2(3)12	12(3)0(3)12	P-12,0,12	sT-10,10,10,0	2Pyr-11,11
MRSN 4841	>250	32	>250	63	63	63	125	16
MRSN 1739	16	16	125	63	8	125	125	16
MRSN 3705	16	32	125	32	8	16	16	16
MRSN 321	>250	>250	>250	>250	125	>250	>250	8
MRSN 1938	16	32	250	63	63	63	250	16
MRSN 2444	16	32	250	63	8	63	16	8
MRSN 994	>250	32	250	63	8	63	16	16
MRSN 5498	>250	63	>250	125	125	125	>250	>250
MRSN 5508	8	16	63	4	8	8	8	16
MRSN 5524	16	16	125	16	8	8	16	16
MRSN 6220	16	16	125	8	4	4	16	16
MRSN 8130	>250	63	250	16	8	8	125	>250
MRSN 8914	>250	63	125	8	8	8	32	8
MRSN 6695	>250	>250	125	125	63	63	>250	32
MRSN 8136	16	16	125	16	8	16	16	16
MRSN 5539	8	32	250	63	250	250	16	16
MRSN 8912	>250	32	>250	63	8	63	125	16
MRSN 6241	>250	63	125	125	125	250	>250	>250
MRSN 8141	16	16	>250	125	4	8	63	16
MRSN 6678	>250	250	250	250	250	250	>250	>250
MRSN 8915	>250	63	>250	125	63	63	250	16
MRSN 9873	>250	63	125	125	63	125	250	>250
MRSN 409937	16	32	250	32	26	32	125	32
MRSN 23861	16	125	125	16	8	32	16	32
MRSN 12914	16	16	125	8	8	16	16	16
MRSN 11536	16	32	125	16	16	16	32	16
MRSN 390231	63	63	>250	63	4	4	250	4

	PQ-12,12	m-Hy-12,12	Pip-12,12	12(2)12	BAC	BEC	CPC	DDAC
MRSN 4841	4	250	>250	32	>250	>250	250	125
MRSN 1739	8	8	>250	63	>250	>250	250	125
MRSN 3705	8	16	8	8	125	125	250	32
MRSN 321	>250	63	>250	250	>250	>250	125	32
MRSN 1938	16	125	16	16	>250	>250	125	250
MRSN 2444	16	32	8	32	>250	>250	250	125
MRSN 994	8	16	8	125	250	250	125	125
MRSN 5498	>250	16	>250	8	>250	>250	125	125
MRSN 5508	>250	32	>250	16	>250	>250	125	63
MRSN 5524	8	32	8	16	>250	250	250	125
MRSN 6220	8	8	8	8	250	125	125	32
MRSN 8130	>250	250	>250	125	>250	>250	250	250
MRSN 8914	>250	8	8	8	>250	>250	125	63
MRSN 6695	32	>250	16	32	>250	>250	125	63
MRSN 8136	16	32	8	16	>250	125	125	125
MRSN 5539	32	125	16	32	>250	>250	>250	250
MRSN 8912	8	125	8	63	250	125	250	63
MRSN 6241	8	125	8	16	>250	>250	250	63
MRSN 8141	8	32	>250	250	>250	>250	250	>250
MRSN 6678	16	250	>250	250	>250	>250	250	125
MRSN 8915	>250	125	>250	32	250	>250	125	63
MRSN 9873	>250	32	>250	250	>250	>250	250	250
MRSN 409937	>250	125	16	16	250	125	125	32
MRSN 23861	16	32	16	63	>250	>250	250	250
MRSN 12914	16	16	16	16	>250	>250	250	250
MRSN 11536	32	32	16	32	250	250	250	125
MRSN 390231	4	250	8	32	250	250	125	125

#### 4. Metal Chelation Assays

All fluorescence titrations were performed in methanol. Briefly, a 350  $\mu\text{L}$  stock solution of 400  $\mu\text{M}$  ulbactin F was prepared and an emission spectrum was recorded ( $\lambda_{\text{excitation}} = 316 \text{ nm}$ , integration time = 1 second, accumulations = 10). Metal chloride stock solution (10 mM) was added in 1.4  $\mu\text{L}$  portions, the solution was gently mixed, and an emission spectrum was recorded after each addition.

Isolation of  $\text{Fe}^{3+}$ -ulbactin F complex was conducted by treating ulbactin F in methanol with excess iron (III) chloride. Once addition of iron resulted in no further color change, the solution was concentrated by rotary evaporation and excess iron (III) chloride was removed by trituration with diethyl ether. The complex was then dissolved in methanol.

HRMS analysis of ulbactin F samples treated with iron and citrate was conducted by ionizing samples through Atmospheric-Pressure Chemical Ionization (APCI) using Atmospheric Solids Analysis Probe (ASAP) to load each sample. Ulbactin F (1 mg) was dissolved in minimal methanol and an aliquot was taken (**Supplementary Figure 5b**). Sample was then treated with excess iron (III) chloride methanol solution. The sample was concentrated and triturated with ether to remove excess iron. Sample was redissolved in methanol and an aliquot was taken (**Supplementary Figure 5c**). Sample was concentrated, redissolved in ethyl acetate and washed with 5% aqueous sodium citrate. Ethyl acetate was partitioned and concentrated. Sample was redissolved in methanol and an aliquot was taken (**Supplementary Figure 5d**).

CAS liquid media was prepared as described previously [1].

Reference:

[1] Loudon, B. C.; Haarmann, D.; Lynne, A. M. *J. Microbiol. Biol. Educ.* **2011**, *12* (1), 51-53

## 5. Crystal Analysis

Single crystal of  $C_{17}H_{19}N_3O_2S_3$  Ulbactin diastereomer were recrystallized from pentane and dichloromethane as supplied. A suitable crystal was selected and the crystal was mounted on a loop with paratone oil on a XtaLAB Synergy, Duaflex, HyPix diffractometer. The crystal was kept at 100(2) K during data collection. Using Olex2 [1], the structure was solved with the She1XT [2] structure solution program using Intrinsic Phasing and refined with the She1XL [3] refinement package using Least Squares minimization.

[1] Dolomanov, O.V., Bourhis, L.J., Gildea, R.J, Howard, J.A.K. & Puschmann, H. (2009), *J. Appl. Cryst.* 42, 339-341.

[2] Sheldrick, G.M. (2015). *Acta Cryst.* A71, 3-8.

[3] Sheldrick, G.M. (2015). *Acta Cryst.* C71, 3-8.

### Crystal structure determination of [Ulbactin diastereomer]

**Crystal Data** for  $C_{17}H_{19}N_3O_2S_3$  ( $M = 393.53$  g/mol): monoclinic, space group I2 (no. 5),  $a = 11.9054(5)$  Å,  $b = 7.9651(3)$  Å,  $c = 19.2708(9)$  Å,  $\beta = 103.596(4)^\circ$ ,  $V = 1776.20(13)$  Å<sup>3</sup>,  $Z = 4$ ,  $T = 100(2)$  K,  $\mu(\text{MoK}\alpha) = 0.434$  mm<sup>-1</sup>,  $D_{\text{calc}} = 1.472$  g/cm<sup>3</sup>, 13787 reflections measured ( $3.676^\circ \leq 2\theta \leq 58.246^\circ$ ), 4765 unique ( $R_{\text{int}} = 0.0478$ ,  $R_{\text{sigma}} = 0.0487$ ) which were used in all calculations. The final  $R_1$  was 0.0327 ( $I > 2\sigma(I)$ ) and  $wR_2$  was 0.0784 (all data).

### Refinement model description

Number of restraints - 1, number of constraints - unknown.

Details:

#### 1. Fixed Uiso

At 1.2 times of:

All C(H) groups, All C(H,H) groups

At 1.5 times of:

All C(H,H,H) groups, All O(H) groups

#### 2.a Ternary CH refined with riding coordinates:

C13(H13), C8(H8), C6(H6), C3(H3), C5(H5)

#### 2.b Secondary CH2 refined with riding coordinates:

C2(H2A,H2B), C17(H17A,H17B), C10(H10A,H10B)

#### 2.c Aromatic/amide H refined with riding coordinates:

C23(H23), C22(H22), C24(H24), C21(H21)

#### 2.d Idealised Me refined as rotating group:

C12(H12A,H12B,H12C)

#### 2.e Idealised tetrahedral OH refined as rotating group:

O25(H25)

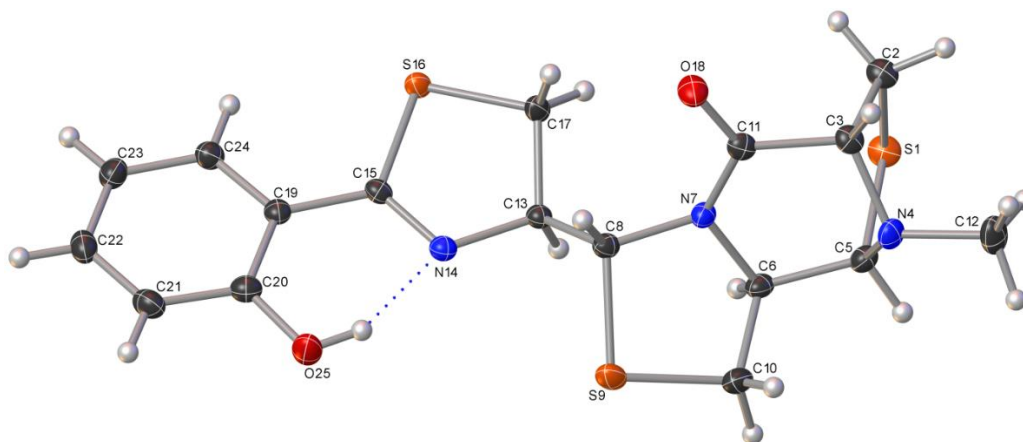


**Table 1 Crystal data and structure refinement for Ulbactin\_diastereomer.**

Identification code	Ulbactin_diastereomer
Empirical formula	$C_{17}H_{19}N_3O_2S_3$
Formula weight	393.53
Temperature/K	100(2)
Crystal system	monoclinic
Space group	I2
$a/\text{\AA}$	11.9054(5)
$b/\text{\AA}$	7.9651(3)
$c/\text{\AA}$	19.2708(9)
$\alpha/^\circ$	90
$\beta/^\circ$	103.596(4)
$\gamma/^\circ$	90
Volume/ $\text{\AA}^3$	1776.20(13)
Z	4
$\rho_{\text{calc}}/\text{g cm}^{-3}$	1.472
$\mu/\text{mm}^{-1}$	0.434
F(000)	824.0
Crystal size/ $\text{mm}^3$	$0.196 \times 0.157 \times 0.028$
Radiation	MoK $\alpha$ ( $\lambda = 0.71073$ )
$2\theta$ range for data collection/ $^\circ$	3.676 to 58.246
Index ranges	$-16 \leq h \leq 15, -10 \leq k \leq 10, -26 \leq l \leq 26$
Reflections collected	13787
Independent reflections	4765 [ $R_{\text{int}} = 0.0478, R_{\text{sigma}} = 0.0487$ ]
Data/restraints/parameters	4765/1/228
Goodness-of-fit on $F^2$	1.006
Final R indexes [ $I \geq 2\sigma(I)$ ]	$R_1 = 0.0327, wR_2 = 0.0769$
Final R indexes [all data]	$R_1 = 0.0361, wR_2 = 0.0784$
Largest diff. peak/hole / $e \text{\AA}^{-3}$	0.30/-0.21
Flack parameter	-0.04(4)

**Table 2 Fractional Atomic Coordinates ( $\times 10^4$ ) and Equivalent Isotropic Displacement Parameters ( $\text{\AA}^2 \times 10^3$ ) for Ulbactin\_diastereomer.  $U_{eq}$  is defined as 1/3 of of the trace of the orthogonalised  $U_{ij}$  tensor.**

Atom	x	y	z	U(eq)
S16	4757.9(5)	3401.1(7)	5928.5(3)	16.07(13)
S1	10099.5(6)	787.4(8)	7337.9(4)	19.58(15)
S9	8526.9(5)	7141.0(7)	6827.3(4)	22.19(16)
O18	8639.4(15)	3153(2)	5319.9(9)	21.4(4)
O25	5168.2(16)	9185(2)	5886.8(11)	24.0(4)
N14	5972.3(18)	6143(2)	6218.2(11)	15.2(4)
N4	11128.0(16)	3202(3)	6747.6(11)	17.9(4)
N7	8840.7(17)	4018(3)	6465.8(11)	14.1(4)
C19	3947(2)	6724(3)	5778.8(13)	14.8(5)
C13	6804(2)	4778(3)	6451.2(13)	13.7(5)
C8	7947(2)	5289(3)	6288.4(14)	15.0(5)
C15	4937(2)	5601(3)	5987.1(13)	14.1(4)
C23	1869(2)	7149(4)	5428.5(14)	21.3(5)
C2	10168(2)	511(3)	6412.7(13)	18.0(5)
C11	9211.9(19)	3211(3)	5937.7(13)	15.8(4)
C22	2047(2)	8849(3)	5341.0(15)	22.1(5)
C6	9530(2)	4185(3)	7202.0(13)	16.4(5)
C17	6310.9(19)	3154(3)	6078.4(14)	17.5(5)
C3	10366(2)	2304(3)	6159.4(13)	15.8(5)
C24	2818(2)	6096(3)	5633.8(14)	18.2(5)
C20	4109(2)	8474(3)	5719.8(13)	18.4(5)
C12	12311(2)	2556(3)	6914.3(17)	25.5(6)
C21	3151(2)	9510(3)	5482.3(14)	22.4(5)
C5	10569(2)	3027(3)	7330.2(13)	17.0(5)
C10	9833(2)	6055(3)	7285.7(16)	23.1(6)

**Table 3 Anisotropic Displacement Parameters ( $\text{\AA}^2 \times 10^3$ ) for Ulbactin\_diastereomer. The Anisotropic displacement factor exponent takes the form:  $-2\pi^2[h^2a^2U_{11}+2hka*b*U_{12}+...]$ .**

Atom	$U_{11}$	$U_{22}$	$U_{33}$	$U_{23}$	$U_{13}$	$U_{12}$
S16	14.2(3)	13.2(3)	20.9(3)	-1.6(2)	4.5(2)	-1.4(2)
S1	24.3(3)	20.0(3)	15.8(3)	3.5(2)	7.5(2)	-1.1(2)
S9	19.2(3)	14.5(3)	32.7(4)	-5.6(3)	5.5(3)	-3.0(2)
O18	23.8(9)	26.8(10)	13.4(8)	-2.3(8)	3.7(7)	5.2(8)
O25	20.3(9)	14.9(8)	34.6(11)	1.1(8)	2.3(8)	-1.2(7)
N14	16.3(9)	15.0(10)	14.5(10)	-1.7(8)	3.9(8)	-0.2(7)

N4	11.5(8)	20.6(10)	21.8(11)	0.2(9)	4.4(8)	-1.8(8)
N7	12.8(9)	16.9(9)	12.6(10)	-1.1(8)	3.0(7)	0.1(7)
C19	16.3(11)	16.4(12)	11.7(11)	-1.5(8)	3.5(9)	0.6(8)
C13	14.8(10)	13.8(10)	12.7(11)	-1.4(9)	3.5(9)	0.1(9)
C8	14.6(10)	15.6(11)	15.3(11)	-2.2(9)	4.7(9)	-1.1(8)
C15	17.2(10)	13.0(10)	13.5(11)	-0.7(9)	6.4(9)	0.7(9)
C23	16.6(11)	24.9(13)	21.1(13)	-2.8(11)	1.8(10)	0.6(10)
C2	23.0(11)	18.5(11)	14.3(12)	1.0(9)	8.3(10)	0.3(10)
C11	16.0(10)	15.6(11)	17.3(11)	0.3(9)	7.0(9)	-2.8(9)
C22	20.6(12)	26.2(13)	18.4(13)	-1.8(10)	2.6(10)	7.1(10)
C6	15.8(11)	19.2(11)	14.1(11)	-4.5(9)	3.3(9)	-1.6(9)
C17	12.4(10)	14.9(11)	25.2(13)	-2.9(10)	4.7(9)	-0.6(9)
C3	17.4(11)	17.7(11)	14.5(11)	0.5(9)	8.0(9)	0.0(9)
C24	18.2(11)	17.0(12)	19.7(13)	-1.2(9)	5.2(10)	-0.3(9)
C20	21.2(11)	17.6(11)	16.5(12)	-1.8(10)	5.0(9)	-2.0(10)
C12	14.2(12)	24.6(14)	38.4(17)	3.7(12)	7.5(11)	1.0(9)
C21	27.4(13)	17.1(12)	21.8(13)	-1.2(10)	3.7(11)	2.9(10)
C5	15.4(11)	19.3(12)	15.3(11)	-1.1(9)	1.5(9)	-1.5(9)
C10	17.9(12)	22.0(13)	27.4(15)	-8.8(11)	1.3(11)	-2.3(10)

**Table 4 Bond Lengths for Ulbactin\_diastereomer.**

Atom	Atom	Length/ Å	Atom	Atom	Length/ Å
S16	C15	1.766(3)	C23	H23	0.9500
S16	C17	1.814(2)	C23	C22	1.387(4)
S1	C2	1.818(3)	C23	C24	1.388(4)
S1	C5	1.871(3)	C2	H2A	0.9900
S9	C8	1.842(2)	C2	H2B	0.9900
S9	C10	1.816(3)	C2	C3	1.545(3)
O18	C11	1.226(3)	C11	C3	1.522(3)
O25	H25	0.8400	C22	H22	0.9500
O25	C20	1.350(3)	C22	C21	1.382(4)
N14	C13	1.468(3)	C6	H6	1.0000
N14	C15	1.283(3)	C6	C5	1.517(3)
N4	C3	1.461(3)	C6	C10	1.532(4)
N4	C12	1.462(3)	C17	H17 A	0.9900
N4	C5	1.440(3)	C17	H17 B	0.9900
N7	C8	1.450(3)	C3	H3	1.0000
N7	C11	1.362(3)	C24	H24	0.9500
N7	C6	1.468(3)	C20	C21	1.395(4)
C19	C15	1.459(3)	C12	H12 A	0.9800
C19	C24	1.400(3)	C12	H12 B	0.9800
C19	C20	1.415(4)	C12	H12 C	0.9800
C13	H13	1.0000	C21	H21	0.9500
C13	C8	1.522(3)	C5	H5	1.0000
C13	C17	1.528(3)	C10	H10 A	0.9900
C8	H8	1.0000	C10	H10 B	0.9900

**Table 5 Bond Angles for Ulbactin\_diastereomer.**

Atom	Atom	Atom	Angle/°	Atom	Atom	Atom	Angle/°
C15	S16	C17	89.67(11)	N7	C6	C5	110.6(2)
C2	S1	C5	91.45(12)	N7	C6	C10	104.7(2)
C10	S9	C8	93.31(11)	C5	C6	H6	109.0
C20	O25	H25	109.5	C5	C6	C10	114.3(2)

C15	N14	C13	112.4(2)	C10	C6	H6	109.0
C3	N4	C12	112.8(2)	S16	C17	H17A	110.9
C5	N4	C3	103.98(18)	S16	C17	H17B	110.9
C5	N4	C12	113.1(2)	C13	C17	S16	104.32(16)
C8	N7	C6	112.14(19)	C13	C17	H17A	110.9
C11	N7	C8	120.2(2)	C13	C17	H17B	110.9
C11	N7	C6	123.97(19)	H17A	C17	H17B	108.9
C24	C19	C15	120.8(2)	N4	C3	C2	108.7(2)
C24	C19	C20	118.6(2)	N4	C3	C11	109.9(2)
C20	C19	C15	120.6(2)	N4	C3	H3	109.6
N14	C13	H13	108.8	C2	C3	H3	109.6
N14	C13	C8	108.05(19)	C11	C3	C2	109.41(19)
N14	C13	C17	109.05(19)	C11	C3	H3	109.6
C8	C13	H13	108.8	C19	C24	H24	119.3
C8	C13	C17	113.12(19)	C23	C24	C19	121.3(2)
C17	C13	H13	108.8	C23	C24	H24	119.3
S9	C8	H8	109.2	O25	C20	C19	122.1(2)
N7	C8	S9	105.59(16)	O25	C20	C21	118.4(2)
N7	C8	C13	114.00(19)	C21	C20	C19	119.5(2)
N7	C8	H8	109.2	N4	C12	H12A	109.5
C13	C8	S9	109.45(16)	N4	C12	H12B	109.5
C13	C8	H8	109.2	N4	C12	H12C	109.5
N14	C15	S16	116.62(19)	H12A	C12	H12B	109.5
N14	C15	C19	122.5(2)	H12A	C12	H12C	109.5
C19	C15	S16	120.86(17)	H12B	C12	H12C	109.5
C22	C23	H23	120.4	C22	C21	C20	120.4(3)
C22	C23	C24	119.2(2)	C22	C21	H21	119.8
C24	C23	H23	120.4	C20	C21	H21	119.8
S1	C2	H2A	110.9	S1	C5	H5	110.2
S1	C2	H2B	110.9	N4	C5	S1	106.98(16)
H2A	C2	H2B	109.0	N4	C5	C6	108.8(2)
C3	C2	S1	104.07(17)	N4	C5	H5	110.2
C3	C2	H2A	110.9	C6	C5	S1	110.30(16)
C3	C2	H2B	110.9	C6	C5	H5	110.2
O18	C11	N7	122.6(2)	S9	C10	H10A	110.8
O18	C11	C3	120.9(2)	S9	C10	H10B	110.8
N7	C11	C3	116.4(2)	C6	C10	S9	104.96(17)
C23	C22	H22	119.6	C6	C10	H10A	110.8
C21	C22	C23	120.9(2)	C6	C10	H10B	110.8
C21	C22	H22	119.6	H10A	C10	H10B	108.8
N7	C6	H6	109.0				

**Table 6 Torsion Angles for Ulbactin\_diastereomer.**

A	B	C	D	Angle/°	A	B	C	D	Angle/°
S1	C2	C3	N4	36.8(2)	C11	N7	C6	C5	-12.7(3)



S1	C2	C3	C11	-83.2(2)	C11	N7	C6	C10	110.9(2)
O18	C11	C3	N4	150.0(2)	C22	C23	C24	C19	2.3(4)
O18	C11	C3	C2	-90.7(3)	C6	N7	C8	S9	30.5(2)
O25	C20	C21	C22	-176.6(2)	C6	N7	C8	C13	-89.7(2)
N14	C13	C8	S9	64.4(2)	C6	N7	C11	O18	-176.7(2)
N14	C13	C8	N7	-177.62(19)	C6	N7	C11	C3	5.9(3)
N14	C13	C17	S16	-29.3(2)	C17	S16	C15	N14	-11.4(2)
N7	C11	C3	N4	-32.5(3)	C17	S16	C15	C19	168.5(2)
N7	C11	C3	C2	86.8(3)	C17	C13	C8	S9	-174.77(16)
N7	C6	C5	S1	-70.0(2)	C17	C13	C8	N7	-56.8(3)
N7	C6	C5	N4	47.1(3)	C3	N4	C5	S1	44.4(2)
N7	C6	C10	S9	40.3(2)	C3	N4	C5	C6	-74.8(2)
C19	C20	C21	C22	3.4(4)	C24	C19	C15	S16	10.0(3)
C13	N14	C15	S16	-5.1(3)	C24	C19	C15	N14	-170.2(2)
C13	N14	C15	C19	175.0(2)	C24	C19	C20	O25	176.5(2)
C8	S9	C10	C6	-21.0(2)	C24	C19	C20	C21	-3.5(4)
C8	N7	C11	O18	-20.2(4)	C24	C23	C22	C21	-2.6(4)
C8	N7	C11	C3	162.4(2)	C20	C19	C15	S16	-170.06(19)
C8	N7	C6	C5	-170.8(2)	C20	C19	C15	N14	9.8(4)
C8	N7	C6	C10	-47.3(3)	C20	C19	C24	C23	0.7(4)
C8	C13	C17	S16	-149.56(17)	C12	N4	C3	C2	69.3(3)
C15	S16	C17	C13	22.39(17)	C12	N4	C3	C11	-171.0(2)
C15	N14	C13	C8	146.5(2)	C12	N4	C5	S1	-78.4(2)
C15	N14	C13	C17	23.2(3)	C12	N4	C5	C6	162.4(2)
C15	C19	C24	C23	-179.4(2)	C5	S1	C2	C3	-8.82(17)
C15	C19	C20	O25	-3.5(4)	C5	N4	C3	C2	-53.6(2)
C15	C19	C20	C21	176.5(2)	C5	N4	C3	C11	66.1(2)
C23	C22	C21	C20	-0.3(4)	C5	C6	C10	S9	161.48(18)
C2	S1	C5	N4	-20.37(17)	C10	S9	C8	N7	-4.03(19)
C2	S1	C5	C6	97.87(18)	C10	S9	C8	C13	119.08(19)
C11	N7	C8	S9	-128.60(19)	C10	C6	C5	S1	172.20(19)
C11	N7	C8	C13	111.2(2)	C10	C6	C5	N4	-70.7(3)

**Table 7 Hydrogen Atom Coordinates ( $\text{\AA}\times 10^4$ ) and Isotropic Displacement Parameters ( $\text{\AA}^2\times 10^3$ ) for Ulbactin\_diastereomer.**

Atom	x	y	z	U(eq)
H25	5674.02	8429.76	5980.72	36
H13	6921.52	4627.29	6978.63	16
H8	7815.13	5576.86	5770.37	18
H23	1107.3	6711.68	5348.97	26
H2A	10814.8	-240.12	6376.49	22
H2B	9437.62	34.46	6126.02	22
H22	1401.83	9569.13	5181.77	26
H6	9038.72	3881.19	7538.82	20
H17A	6580.52	2167.38	6384.75	21
H17B	6541.92	3016.03	5620.56	21
H3	10734.95	2242.97	5744.26	19
H24	2698.05	4925.11	5676.71	22
H12A	12323.6	1429.97	7120.56	38
H12B	12809.09	3304.32	7257.92	38
H12C	12592.79	2502.33	6476.25	38
H21	3257.94	10676.44	5417.43	27
H5	11120.32	3314.26	7792.1	20
H10A	10483.02	6325.27	7065.51	28
H10B	10049.47	6374.86	7796.32	28

## 6. Computational

Computational Details. The presented calculations were carried out using the Gaussian 09 suite of programs.[1] Geometry of all reported structures were optimized without symmetry constraint at the B3LYP level of density functional theory (DFT) [2,3] in conjunction with Lanl2dz basis set and corresponding Hay-Wadt effective core potential (ECP) for Fe.[4,5] Standard 6-31G(d,p) basis sets were used for all remaining atoms. The nature of each stationary point was characterized by the presence of zero imaginary frequencies. The relative enthalpies ( $\Delta H$ ) and Gibbs energies ( $\Delta G$ ) are presented as  $\Delta H/\Delta G$ , and calculated under standard conditions (1 atm and 298.15 K). Cartesian coordinates of all reported structures are given in the Supporting Information.

### References:

- [1] Frisch, M. J.; Trucks, G. W.; Schlegel, H. B.; Scuseria, G. E.; Robb, M. A.; Cheeseman, J. R.; Scalmani, G.; Barone, V.; Mennucci, B.; Petersson, G. A.; Nakatsuji, H.; Caricato, M.; Li, X.; Hratchian, H. P.; Izmaylov, A. F.; Bloino, J.; Zheng, G.; Sonnenberg, J. L.; Hada, M.; Ehara, M.; Toyota, K.; Fukuda, R.; Hasegawa, J.; Ishida, T.; Nakajima, M.; Honda, Y.; Kitao, O.; Nakai, H.; Vreven, T.; Montgomery, J., J. A. ; Peralta, J. E.; Ogliaro, F.; Bearpark, M.; Heyd, J. J.; Brothers, E.; Kudin, K. N.; Staroverov, V. N.; Keith, T.; Kobayashi, R.; Normand, J.; Raghavachari, K.; Rendell, A.; Burant, J. C.; Iyengar, S. S.; Tomasi, J.; Cossi, M.; Rega, N.; Millam, J. M.; Klene, M.; Knox, J. E.; Cross, J. B.; Bakken, V.; Adamo, C.; Jaramillo, J.; Gomperts, R.; Stratmann, R. E.; Yazyev, O.; Austin, A. J.; Cammi, R.; Pomelli, C.; Ochterski, J. W.; Martin, R. L.; Morokuma, K.; Zakrzewski, V. G.; Voth, G. A.; Salvador, P.; Dannenberg, J. J.; Dapprich, S.; Daniels, A. D.; Farkas, O.; Foresman, J. B.; Ortiz, J. V.; Cioslowski, J.; Fox, D. J. Gaussian 09, Revision E.01, Gaussian, Inc., Wallingford CT, 2013.
- [2] Lee, C.; Yang, W.; Parr, R. G., Development of the Colle-Salvetti correlation-energy formula into a functional of the electron density. *Phy. Rev. B* 1988, 37 (2), 785-789.
- [3] Becke, A. D., Density-functional thermochemistry. III. The role of exact exchange. *J. Chem. Phys.* 1993, 98 (7), 5648-5652.
- [4] Hay, P. J.; Wadt, W. R., Ab initio effective core potentials for molecular calculations. Potentials for the transition metal atoms Sc to Hg. *J. Chem. Phys.* 1985, 82 (1), 270-283.
- [5] Hay, P. J.; Wadt, W. R., Ab initio effective core potentials for molecular calculations. Potentials for K to Au including the outermost core orbitals. *J. Chem. Phys.* 1985, 82 (1), 299-310.

Cartesian Coordinates (in Å)

### HCl

H	0.00000000	0.00000000	0.15708900
Cl	0.00000000	0.00000000	1.44291100

### FeCl<sub>3</sub> (Sixtet electronic state)

Fe	-6.58924000	-3.62556400	2.58518100
Cl	-6.07605900	-2.00331300	1.25209100
Cl	-5.45715800	-5.46472000	2.52963900
Cl	-8.22453000	-3.40047200	3.98055600

**Ligand**

C	-3.08776600	-2.76263800	3.09316000
C	-2.33589500	-0.86748400	4.13466400
N	-1.89955000	-2.18129600	3.65854300
S	-3.88796600	-1.43045000	1.98999900
C	-3.04888000	-0.11595000	2.96692800
H	-2.32371100	0.40826200	2.33961600
H	-3.77319200	0.60854600	3.34420500
H	-2.85892900	-3.62516100	2.46425900
H	-1.48930800	-0.29086700	4.51308600
C	-3.28948600	-1.04897100	5.31891800
O	-3.30420700	-0.25018300	6.24906300
C	-4.04041200	-3.17817000	4.21916700
N	-4.14220400	-2.12551600	5.24573800
C	-4.83075000	-2.56718000	6.45179400
S	-4.49393900	-4.40390100	6.57122700
C	-3.58917900	-4.44253300	4.97039900
H	-2.51094400	-4.42173700	5.14514400
H	-3.86342400	-5.35140800	4.42980400
H	-5.03556500	-3.34571400	3.80067900
C	-6.34272000	-2.25698000	6.47801000
C	-6.60161000	-0.73484200	6.66979200
N	-7.02637400	-2.71641400	5.27963600
S	-8.11643000	-0.35677900	5.70193100
H	-6.77342500	-0.48678200	7.71821500
C	-7.92030900	-1.90843800	4.82132500
C	-8.74791100	-2.23895300	3.66415700
C	-9.69560600	-1.33459000	3.14818400
C	-8.59550300	-3.50771300	3.03506000
C	-10.47919000	-1.65783100	2.05099500
H	-9.80588200	-0.36196100	3.61909700
C	-9.39383600	-3.82401200	1.92374300
O	-7.71282400	-4.42523100	3.46093100
C	-10.32070000	-2.91097800	1.44108600
H	-11.20347200	-0.94670300	1.66791700
H	-9.26014400	-4.79694400	1.46279700
H	-10.92860400	-3.17376600	0.57975800
H	-7.27091800	-4.05153200	4.27440700
H	-5.77067500	-0.13173000	6.30021400
H	-4.36490000	-2.06381800	7.30112600
H	-6.76288000	-2.80749200	7.33308100
C	-0.73906500	-2.14620600	2.76775900
H	0.09778000	-1.67829900	3.29315600
H	-0.45042900	-3.17094400	2.51821700

H	-0.92303600	-1.60077800	1.83000900
---	-------------	-------------	------------

**Complex (Sextet Electronic State)**

C	-1.76507900	-2.57086100	3.62683500
C	-2.61145900	-0.46836500	3.92170100
N	-1.50001600	-1.33849200	4.32454600
S	-2.13919000	-2.12544300	1.82889600
C	-2.75223300	-0.47716000	2.36909500
H	-2.13713400	0.30767900	1.92266900
H	-3.78885600	-0.34259500	2.05589900
H	-0.89529500	-3.23168600	3.63171800
H	-2.45717500	0.54705200	4.29244400
C	-3.85418400	-0.97916900	4.65114400
O	-4.63439800	-0.20787800	5.19826500
C	-2.95122100	-3.29950100	4.28459600
N	-4.01279600	-2.34997300	4.73166500
C	-4.79061400	-2.80938000	5.90069800
S	-4.13988900	-4.47986200	6.33717200
C	-2.54634700	-4.09449600	5.52987800
H	-1.90164800	-3.50503300	6.18859100
H	-2.05338000	-5.03295800	5.26710200
H	-3.38813300	-3.98769700	3.55931400
C	-6.35459200	-2.82681200	5.84020300
C	-6.90603400	-1.71775300	6.75413600
N	-7.01019300	-2.67985500	4.51994100
S	-8.62061400	-1.45833400	6.18876700
H	-6.90743500	-2.02332500	7.80163800
C	-8.18303600	-2.09472800	4.59270300
C	-9.17858500	-1.99869500	3.53126100
C	-10.19885800	-1.02436500	3.60643300
C	-9.21396800	-2.94494700	2.45861300
C	-11.22311000	-0.97893900	2.67595700
H	-10.16139000	-0.28222100	4.39730300
C	-10.28504500	-2.90262100	1.54018200
O	-8.29119700	-3.87965200	2.32377800
C	-11.26688800	-1.93251900	1.64492800
H	-11.98458500	-0.20937600	2.74409300
H	-10.29374900	-3.64236000	0.74722400
H	-12.07289100	-1.90565600	0.91729300
Fe	-6.50446100	-3.49255100	2.69134100
H	-6.33789600	-0.79606100	6.61837400
H	-4.54149400	-2.12605700	6.71863100
H	-6.68750200	-3.80211000	6.22222600
Cl	-5.97470700	-1.82279400	1.31182200
Cl	-5.34141300	-5.37353400	2.57655900
C	-0.17230100	-0.76670300	4.09518500
H	-0.08595900	0.16610200	4.65890700
H	0.58449300	-1.46044000	4.47222100
H	0.03981400	-0.56662000	3.03457100

**Fe(acac)<sub>3</sub> (Sextet electronic state)**

O	-6.69847400	-3.57454600	4.55100200
C	-7.77428800	-3.46043000	5.22471900
C	-9.06009100	-3.35637800	4.66859800
O	-8.40289600	-3.44375700	2.38846200
C	-9.30449700	-3.35926600	3.28525200
H	-9.90549600	-3.27179000	5.33998900
Fe	-6.39861900	-3.61574500	2.55458700
O	-6.23339700	-3.49669600	0.54780400
O	-6.07369800	-1.62423000	2.56547000
C	-6.03590800	-2.48971400	-0.20811900
C	-5.87844200	-0.81274600	1.60221100
C	-5.85512200	-1.17219600	0.24435000
H	-5.68651500	-0.39492200	-0.49048500
O	-6.56134300	-5.62233100	2.41681500
O	-4.43293600	-3.93211700	2.87051900
C	-5.68027500	-6.53450300	2.54210900
C	-3.77333300	-5.01881400	2.96443100
C	-4.32165000	-6.30325900	2.81480000
H	-3.66300500	-7.15775100	2.90735000
C	-7.60088200	-3.44344800	6.72802000
H	-8.54983100	-3.34997600	7.25997600
H	-7.09808100	-4.36345800	7.04374400
H	-6.94692200	-2.60975200	7.00402600
C	-10.72426100	-3.25517300	2.77176000
H	-10.94778200	-4.13236000	2.15575700
H	-11.45835500	-3.18218800	3.57674400
H	-10.81013500	-2.37737400	2.12290400
C	-5.66235200	0.63062900	2.00242500
H	-5.50463100	1.28643100	1.14374400
H	-6.53003800	0.98118100	2.57086800
H	-4.79603500	0.69204600	2.66920700
C	-5.99949800	-2.78821700	-1.69123400
H	-6.94752800	-3.24903500	-1.98741000
H	-5.82670500	-1.89576600	-2.29615300
H	-5.21046500	-3.52019000	-1.89269500
C	-2.29663100	-4.85941900	3.25428600
H	-1.77586400	-5.81653400	3.32449900
H	-1.83737500	-4.25476400	2.46533400
H	-2.17295100	-4.30927800	4.19282000
C	-6.18397700	-7.95189900	2.37608800
H	-5.39356000	-8.69591400	2.49407900
H	-6.97329900	-8.14274000	3.11057200
H	-6.63628500	-8.05766700	1.38458600

**L-Fe(acac)<sub>2</sub> (Sextet Electronic State)**

C	-3.28480200	0.36201200	3.60717600
---	-------------	------------	------------

C	-2.90064500	0.40154000	5.86654300
N	-2.25757100	0.64822000	4.57386800
S	-4.86268300	1.24620400	4.20189600
C	-4.23987800	1.20227200	5.93284300
H	-4.06962100	2.22004700	6.29244900
H	-4.96118300	0.71048100	6.58855500
H	-3.03390700	0.75362700	2.61947700
H	-2.23675900	0.67901500	6.68787000
C	-3.16357700	-1.09808000	6.01799100
O	-3.07378600	-1.65384700	7.10774800
C	-3.50468700	-1.15377200	3.52635800
N	-3.53478800	-1.75464300	4.87070400
C	-3.49043600	-3.20633100	4.84234200
S	-2.45789500	-3.63580500	3.35261200
C	-2.39835400	-1.89795100	2.75673300
H	-1.41875200	-1.46393600	2.97045400
H	-2.59713100	-1.88714000	1.68323800
H	-4.46293600	-1.35304900	3.04023100
C	-4.87470600	-3.91162200	4.88692000
C	-5.46722200	-3.84089800	6.31782000
N	-5.85413700	-3.35517400	3.94221100
S	-6.67998400	-2.47461300	6.27931800
H	-5.98608100	-4.76504400	6.58325700
C	-6.74671800	-2.57941300	4.49088100
C	-7.76012200	-1.80203200	3.79048900
C	-8.62846000	-0.95520800	4.51449700
C	-7.86707400	-1.83138700	2.36317400
C	-9.55422100	-0.14321900	3.88327600
H	-8.56916900	-0.93743300	5.59828700
C	-8.81069900	-0.97866700	1.73729000
O	-7.12987400	-2.60689800	1.61074600
C	-9.63683500	-0.15604400	2.48036200
H	-10.20597200	0.49742100	4.46818400
H	-8.86600500	-1.01371800	0.65428700
H	-10.35844000	0.48006400	1.97454000
Fe	-6.34372100	-4.30009000	1.96564700
H	-4.70797900	-3.60998600	7.06652000
H	-2.94455400	-3.53345400	5.72898900
H	-4.70313500	-4.95536100	4.61031100
C	-1.63692900	1.96702200	4.44978100
H	-0.88664000	2.08189600	5.23677500
H	-1.12607800	2.03129900	3.48489100
H	-2.35502000	2.79839100	4.51576100
O	-7.02146200	-5.29924500	0.30980300
O	-4.70297400	-3.92096500	0.88084000
C	-6.40405000	-5.61254800	-0.75709000
C	-4.31661000	-4.39518200	-0.23995400
C	-5.08455900	-5.23146500	-1.06216800
H	-4.65745300	-5.56043100	-2.00132900
O	-8.09692000	-4.95792200	2.82162700

O	-5.53952600	-6.02364000	2.70607400
C	-8.42721400	-6.15366900	3.09593900
C	-6.14727300	-7.11586500	2.98028200
C	-7.53213100	-7.24154300	3.15533500
H	-7.93025500	-8.21819700	3.40166200
C	-5.25687400	-8.33025500	3.13839500
H	-4.50393500	-8.13371100	3.90904300
H	-5.81533700	-9.23073100	3.40213000
H	-4.71518900	-8.50304500	2.20240200
C	-9.89563200	-6.37753900	3.38872100
H	-10.48018900	-6.10259300	2.50444300
H	-10.11916300	-7.41094200	3.66191100
H	-10.20834300	-5.71140900	4.19918000
C	-7.19212400	-6.44313700	-1.74827000
H	-6.60603000	-6.71826700	-2.62759000
H	-7.55299900	-7.35025800	-1.25301600
H	-8.07449400	-5.87809200	-2.06693200
C	-2.92982600	-3.98121600	-0.68222700
H	-2.20623900	-4.27521900	0.08483900
H	-2.64508800	-4.42681900	-1.63743900
H	-2.88778800	-2.89024200	-0.77244600

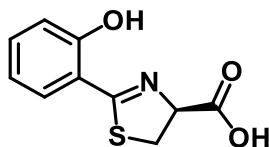
**H-ACAC, (protonated acac)**

O	-0.02909600	0.24719500	0.00038800
C	0.54101800	1.44244600	0.00080400
C	-0.20067600	2.59971600	0.00040000
C	-1.64110800	2.53095000	-0.00050900
O	-2.24578400	1.43381800	-0.00090700
H	0.29975500	3.56012700	0.00075000
H	-1.02689500	0.42950400	-0.00024300
C	-2.43725100	3.81818900	-0.00122300
H	-2.18993100	4.42179800	0.87928200
H	-2.19157700	4.41951200	-0.88377500
H	-3.50390700	3.59072900	-0.00005700
C	2.03812800	1.40415600	0.00175700
H	2.39382600	0.85892900	0.88256900
H	2.39494200	0.85879500	-0.87851900
H	2.46707400	2.40745800	0.00196500



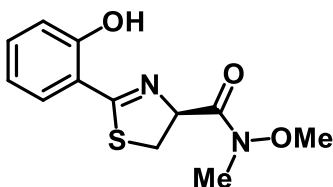
## 7. Synthesis

### 7.1 Experimental Procedures



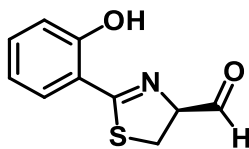
**(S)-2-(2-hydroxyphenyl)-4,5-dihydrothiazole-4-carboxylic acid (2.14)** Synthesized as described previously by Mislin<sup>9</sup>. Briefly, commercially available 2-hydroxy-benzonitrile (2.44 g, 20.5 mmol) was dissolved in methanol (15 mL). D-cysteine hydrochloride monohydrate (3.0 g, 17.1 mmol) was added to the solution and stirred to dissolve. Phosphate buffer (0.1 M, pH 6.4, 15 mL) was added and the pH of the reaction mixture was adjusted to 6.4 by addition of solid  $K_2CO_3$  and solid citric acid. The reaction was stirred at 60 °C overnight. The reaction mixture was then concentrated and the crude material was dissolved in 100 mL water. The aqueous solution was brought to pH 2 by addition of solid citric acid. The aqueous solution was extracted with dichloromethane (3 x 100 mL). The combined organic layers were washed with brine, dried over anhydrous sodium sulfate, filtered, and concentrated to a yellow solid (3.22 g, 14.54 mmol, 85% yield).

**<sup>1</sup>H NMR:** (600 MHz,  $(CD_3)_2CO$ ) (Rotamers)  $\delta$  7.47 (dd,  $J = 7.8, 1.6$  Hz, 1H), 7.43 (ddd,  $J = 8.5, 7.3, 1.6$  Hz, 1H), 6.98 (dd,  $J = 8.3, 0.8$  Hz, 1H), 6.95 (ddd,  $J = 7.8, 7.4, 1.1$  Hz, 1H), 5.54 (dd,  $J = 9.4, 7.8$  Hz, 1H), 3.77 (qd,  $J = 11.3, 8.6$  Hz, 2H).

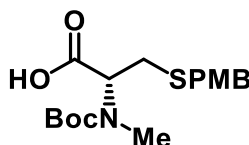


**(S)-2-(2-hydroxyphenyl)-N-methoxy-N-methyl-4,5-dihydrothiazole-4-carboxamide (2.34)** Synthesized as described previously by Mislin<sup>9</sup>. To a base-washed, flamed dried reaction flask charged with argon, phenol-thiazoline acid (1.73 g, 7.8 mmol) was added and dissolved in DMF (40 mL). Then, EDC (5.94 g, 31 mmol), HOBt (4.18 g, 31 mmol), N,N-dimethyl hydroxylamine hydrochloride (1.51 g, 15.5 mmol) were added. Dry trimethylamine was added dropwise by syringe until the reaction mixture was basic (pH 9) by pH paper (soak indicator in DMF solution and then spray with water). The reaction mixture was stirred overnight at room temperature. The reaction was then diluted with 5 volumes of water. The aqueous mixture was brought to pH 2 by addition of 1 M HCl and extracted with ethyl acetate (3 x 100 mL). The combined organic layers were washed with brine, dried over anhydrous sodium sulfate, filtered, and concentrated. The crude material was purified by silica gel chromatography (10% to 100% EtOAc in hexanes) to give a white solid (1.16 g, 4.34 mmol, 56% yield).

**<sup>1</sup>H NMR:** (400 MHz, CDCl<sub>3</sub>) δ 12.33 (s, 1H), 7.43 (dd, *J* = 7.8, 1.6 Hz, 1H), 7.36 (ddd, *J* = 8.8, 7.4, 1.6 Hz, 1H), 6.98 (dd, 1H), 6.88 (ddd, *J* = 8.4, 7.6, 1.1 Hz, 1H), 5.70 (t, *J* = 9.0 Hz, 1H), 3.83 (s, 3H), 3.78 (dd, *J* = 16.2, 16.0 Hz, 1H), 3.48 (dd, *J* = 10.9, 9.3 Hz, 1H), 3.29 (s, 3H)



**(S)-2-(2-hydroxyphenyl)-4,5-dihydrothiazole-4-carbaldehyde (2.16)** Synthesized as described previously by Mislin<sup>9</sup>. Briefly, Weinreb amide **2.34** (172 mg, 0.644 mmol) was added to a flame-dried, base-washed flask under argon and dissolved in dry THF (13 mL). The reaction mixture was brought to -40 °C in a bath of dry ice and acetone. Lithium aluminum hydride (27 mg, 0.71 mmol) was put under argon and suspended in 0.71 mL dry THF (1 M solution). The suspension was cooled in the bath and added dropwise by syringe down the side of the reaction flask into the reaction mixture. The reaction was stirred at between -50 and -30 °C and monitored by TLC. After 2 hours, the reaction was quenched by addition of 8 mL saturated NH<sub>4</sub>Cl and 3 mL 10% NaHSO<sub>4</sub> (alternating additions of 1-2 mL each). The reaction was allowed to warm to room temperature while stirring vigorously until two phases formed. The phases were separated, and the aqueous layer was extracted with EtOAc (3 x 25 mL). The combined organic layers were washed with brine, dried over anhydrous sodium sulfate, filtered, and concentrated. The crude aldehyde was unstable and thus quickly carried on to the synthesis of **2.23** and **2.41** without further purification.



**N-(tert-butoxycarbonyl)-S-w(4-methoxybenzyl)-N-methyl-L-cysteine (2.36)** Commercially available N-Boc-S-PMB-L-Cysteine (**2.35**) (5 g, 14.6 mmol) was added to a flame-dried, base-washed flask under argon and dissolved in dry THF (40 mL). Methyl iodide (2.73 mL, 43.8 mmol) was added by syringe and the reaction mixture was brought to 0 °C. Sodium hydride (60% dispersion in oil, 1.76 g, 43.8 mmol) was weighed and transferred to a capped vial. Small portions of sodium hydride were added as solid under argon. Bubbling was given time to subside before next addition. The reaction was allowed to come to room temperature and stirred overnight. Then, the reaction was quenched by dropwise addition of isopropanol (2 mL) and water (2 mL) and then concentrated by rotary evaporation to approximately 1/5 initial volume. The mixture was then diluted with 100 mL water. The aqueous mixture was extracted with diethyl ether (3 x 50 mL) to remove oil from sodium hydride. The aqueous mixture was then acidified to pH 2 by addition of 1 M HCl. The acidic aqueous mixture was extracted with ethyl acetate (3 x 50 mL). Combined organic layers were washed with acidic (pH 2) brine, dried over Na<sub>2</sub>SO<sub>4</sub>, filtered, and concentrated. The crude material was purified by two rounds of silica gel chromatography (gradient of ethyl acetate in hexanes, 0.5% acetic acid) to give a white solid (3.9 g, 11.1 mmol, 76% yield).

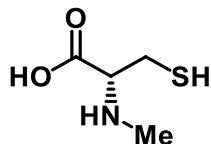
**<sup>1</sup>H NMR** (600 MHz, CDCl<sub>3</sub>) (Rotamers) δ 7.22 (d, *J* = 7.8 Hz, 2H), 6.83 (d, *J* = 7.9 Hz, 3H), 4.66 (dd, *J* = 10.3, 5.3 Hz, 1H), 4.30 (m, 1H), 3.78 (m, 3H), 3.69 (s, 3H), 2.99 – 2.91 (m, 1H), 2.82 (s, 3H), 2.69 – 2.79 (m, 1H) 1.42 (s, 9H).

$^{13}\text{C}$  NMR (150 MHz,  $\text{CDCl}_3$ )  $\delta$  171.11, 155.20, 144.50, 129.59, 127.93, 126.74, 79.73, 77.24, 77.03, 76.82, 66.69, 61.56, 49.75, 34.14, 32.16, 28.36.

IR ( $\text{CHCl}_3$ ) 832 (w), 1034 (w), 1161 (s), 1248 (s), 1302 (s), 1324 (w), 1368 (w), 1393 (w), 1456 (w), 1481 (w), 1512 (s), 1610 (w), 1685 (s), 1734 (s), 2976 (w), 3474 (b)

$[\alpha]_D^{25}$  -459

HRMS: ( $\text{ES}^+$ ) Found: 356.1527 (+0.31),  $\text{C}_{17}\text{H}_{26}\text{NO}_5\text{S}$  ( $\text{M}^+$ ) requires: 356.1526



**Methyl-L-cysteine (2.17)** N-Boc-N-methyl-S-PMB-L-cysteine (1.73 g, 4.8 mmol) was dissolved in ice-cold neat TFA (4 mL). To this, mercury acetate (1.71 g, 5.38 mmol) was added as a solid and the mixture was allowed to sit at room temperature under argon for 30 minutes. The reaction was quenched with water (36 mL), followed by addition of dithiothreitol (5 w/v%, 2.00 g). Which resulted in a thick white/gray precipitate. The reaction was stirred for an additional 30 minutes. Then, the mixture was centrifuged (20 minutes, 3900 RPM) and the clarified aqueous mixture was decanted and extracted with chloroform (10 x 20 mL). The aqueous layer was concentrated by rotary evaporation and lyophilization to give a white solid (1.04 g, 4.08 mmol, 85% yield).

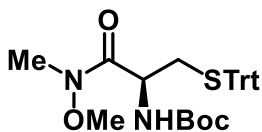
$^1\text{H}$  NMR: (400 MHz,  $\text{D}_2\text{O}$ )  $\delta$  4.14 (t,  $J$  = 4.4 Hz, 1H), 3.21 (dd,  $J$  = 15.4, 4.2 Hz, 1H), 3.07 (dd,  $J$  = 15.4, 4.5 Hz, 1H), 2.73 (s, 3H)

$^{13}\text{C}$  NMR: (100 MHz,  $\text{D}_2\text{O}$ )  $\delta$  169.90, 73.46, 69.78, 62.19, 42.30, 31.21, 29.32, 26.89, 26.59, 23.37, 22.43

IR (neat): 721 (s), 797 (w), 1048 (w), 1131 (s), 1192 (s), 1422 (w), 1662 (s), 1729 (w), 3034 (b)

$[\alpha]_D^{25}$  +42 (in water)

HRMS: ( $\text{ES}^+$ ): Found: 136.0421 (-3.79 ppm),  $\text{C}_4\text{H}_{10}\text{NO}_2\text{S}$  ( $\text{M}^+$ ) requires: 136.0426



**tert-butyl (S)-(1-(methoxy(methyl)amino)-1-oxo-3-(tritylthio)propan-2-yl)carbamate (2.38)** A flame dried flask was charged with argon, to which *N*-(*tert*-butoxycarbonyl)-*S*-trityl-*D*-cysteine (1 g, 2.16 mmol) was added and dissolved in DMF (8.6 mL). *N,O*-dimethylhydroxylamine hydrochloride (442 mg, 4.53 mmol) was added to the reaction mixture, followed by the addition of EDCI (1.7 g, 8.63 mmol) and DMAP (1.1 g, 8.63 mmol). The reaction was allowed to stir under argon overnight. Once it was determined complete by TLC, the reaction was condensed. The resulting solid was redissolved in EtOAc (30 mL) and washed with 10%  $\text{NaHSO}_4$  (1 x 30 mL), 10%  $\text{NaHCO}_3$  (1 x 30 mL), and brine (1 x 30 mL). The organic layer was dried over sodium sulfate, filtered and concentrated. Flash column purification (10% to 70% EtOAc in hexanes) afforded the product as a white solid (946 mg, 86%).

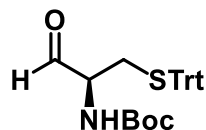
$^1\text{H}$  NMR (600 MHz,  $\text{CDCl}_3$ )  $\delta$  7.44 – 7.39 (m, 6H), 7.31 – 7.26 (m, 6H), 7.25 – 7.20 (m, 3H), 5.13 (d,  $J$  = 8.8 Hz, 1H), 4.77 (s, 1H), 3.66 (s, 3H), 3.16 (s, 3H), 2.57 (dd,  $J$  = 12.2, 4.6 Hz, 1H), 2.40 (dd,  $J$  = 12.0, 7.9 Hz, 1H), 1.64 (s, 2H), 1.45 (s, 9H)

$^{13}\text{C}$  NMR (150 MHz,  $\text{CDCl}_3$ )  $\delta$  171.11, 155.20, 144.50, 129.59, 127.93, 126.74, 79.73, 77.24, 77.03, 76.82, 66.69, 61.56, 49.75, 34.14, 32.16, 28.36.

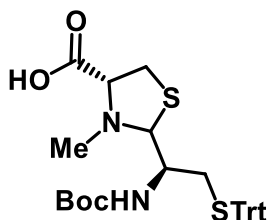
IR (neat): 700 (s), 743 (s), 1168 (s), 1250 (w), 1366 (w), 1390 (w), 1444(w), 1490 (s), 1490 (s), 1663 (s), 1714 (s), 2939 (w), 2976 (w), 3063 (w), 3322 (b), 3427 (b)

$[\alpha]_D^{25}$  112

HRMS (ES<sup>+</sup>): Found: 507.2297 (-2.93 ppm), C<sub>29</sub>H<sub>33</sub>O<sub>4</sub>N<sub>2</sub>S (M<sup>+</sup>) requires: 507.2312



**tert-butyl (S)-(1-oxo-3-(tritylthio)propan-2-yl)carbamate (2.39)** To a flame dried flask under argon, protected weinreb (**2.38**) (451 mg, 0.890 mmol) was added in THF (1.8 mL). The solution was then cooled to -40°C with a few pieces of dry ice in isopropanol. Meanwhile, to a flame dried vial under argon, a suspension of lithium aluminum hydride (40.5 mg, 1.068 mmol) in THF (1 mL) was prepared and also cooled to -40°C. Once a stable temperature was reached, the LAH/THF suspension was added to the reaction flask slowly over several minutes. The reaction was allowed to gradually warm to -20°C and stirred for 2.5 hours. The reaction was warmed to 0°C and quenched with alternating addition of saturated NH<sub>4</sub>Cl (11.1 mL) and 10% NaHSO<sub>4</sub> (4.0 mL). This was allowed to stir for 30 minutes. The reaction mixture was then transferred to a separatory funnel and the aqueous layer was extracted. This layer was then washed with EtOAc (3 x 20 mL). The organic layers were combined and washed with brine, dried with Na<sub>2</sub>SO<sub>4</sub>, filtered and concentrated. The crude oil was then carried through immediately to the next reaction.



**(4R)-2-((R)-1-((tert-butoxycarbonyl)amino)-2-(tritylthio)ethyl)-3-ethylthiazolidine-4-carboxylic acid (2.40)** N-methyl cysteine salt (**2.17**) (244 mg, 0.979 mmol) was added to a solution of Boc-Trt-aldehyde (398 mg, 0.890 mmol) in ethanol (30 mL) and water (13 mL). To this reaction sodium acetate (358 mg, 3.649 mmol) was added and allowed to stir under argon for 18 hours. Once the reaction was complete, the solvents were concentrated and the resulting solids were suspended in water (20 mL). Citric acid was added until a pH of 2 was achieved. At this point, EtOAc was added (20 mL) and used to extract (3 x 20 mL). The combined organic layers were washed with brine, dried with Na<sub>2</sub>SO<sub>4</sub>, filtered and concentrated. The resulting oil was purified by flash chromatography (10% to 70% EtOAc in hexanes) afforded a clear oil (340 mg, 68%) as a mixture of diastereomers.

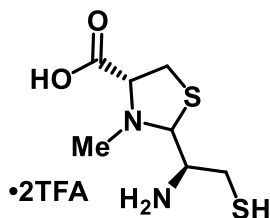
<sup>1</sup>H NMR (400 MHz, CD<sub>3</sub>OD) δ 7.38 (d, *J* = 7.4 Hz, 8H), 7.29 (t, *J* = 7.5 Hz, 8H), 7.21 (t, *J* = 7.2 Hz, 4H), 3.87 (d, *J* = 6.3 Hz, 1H), 3.53 (dt, *J* = 13.7, 7.3 Hz, 3H), 3.03 (dd, *J* = 11.2, 6.0 Hz, 2H), 2.97 – 2.89 (m, 1H), 2.46 (d, *J* = 7.2 Hz, 3H), 2.42 (s, 3H), 2.16 (s, 2H), 1.46 (s, 10H)

<sup>13</sup>C NMR (100 MHz, CD<sub>3</sub>OD) δ 220.90, 188.27, 172.64, 144.09, 129.65, 128.27, 127.18, 99.49, 77.37, 77.16, 76.95, 70.10, 44.14, 34.42, 28.45

IR (neat) 698 (s), 7226 (s), 906 (s), 1159 (w), 1492 (w), 1689 (w), 2980 (w), 3066(w), 3408 (b)

$[\alpha]_D^{25}$  -693

HRMS (ES<sup>+</sup>): Found: 565.2187 (-0.42 ppm), C<sub>31</sub>H<sub>37</sub>N<sub>2</sub>O<sub>4</sub>S<sub>2</sub> (M<sup>+</sup>) requires: 565.2189



**(4R)-2-((R)-1-ammonio-2-mercaptoethyl)-4-carboxy-3-methylthiazolidin-3-ium (2.31)** A 10 mL solution of 50% trifluoroacetic acid in DCM was made, to which 3% v/v triisopropyl silane was added. The protected thiazolidine (**2.40**) (100 mg, 0.177 mmol) was charged to a reaction flask and then dissolved in the freshly made solution (2 mL). This reaction was stirred for 30 minutes at which point only product mass was observed on LCMS. The reaction was condensed. To this water (5 mL) was added to dissolve the product. Insoluble impurities were filtered out and washed with water (5 mL). The resulting water solution was concentrated to about 2 mL, frozen in dry ice and isopropanol bath and lyophilize to a white solid. This was carried through without further purification.

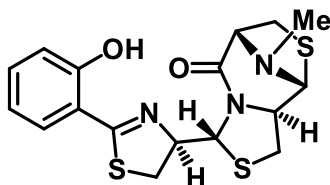
<sup>1</sup>H NMR (400 MHz, D<sub>2</sub>O) δ 4.32 (d, *J* = 10.1 Hz, 1H), 4.11 (dt, *J* = 14.9, 7.4 Hz, 1H), 3.61 (s, 1H), 3.48 (dd, *J* = 11.8, 7.9 Hz, 1H), 3.33 (dd, *J* = 11.9, 5.3 Hz, 1H), 3.20 (ddd, *J* = 10.8, 7.4, 3.6 Hz, 1H), 3.01 (dd, *J* = 15.2, 3.6 Hz, 1H), 2.72 (dd, *J* = 15.1, 7.4 Hz, 1H), 2.55 (s, 3H)

<sup>13</sup>C NMR (100 MHz, D<sub>2</sub>O) δ 176.30, 75.97, 72.65, 57.16, 44.50, 33.88, 23.72

IR (neat) 1136 (s), 1199 (s), 1668 (s), 2819 (w), 2913 (w), 2958 (w), 3370 (b)

[α]<sub>D</sub><sup>25</sup> -127 (in water)

HRMS (ES<sup>+</sup>): Found: 223.0569 (+0.20 ppm), C<sub>7</sub>H<sub>15</sub>N<sub>2</sub>O<sub>2</sub>S<sub>2</sub> (M<sup>+</sup>) requires: 223.0569



**(3R,6R,9R,9aR)-3-((R)-2-(2-hydroxyphenyl)-4,5-dihydrothiazol-4-yl)-10-methyltetrahydro-1H,3H,5H-6,9-epiminothiazolo[4,3-*c*][1,4]thiazepin-5-one (2.23)**

**Procedure A:**

Deprotected thiazolidine 2 x TFA salt (**2.31**) (136 mg, 0.302 mmol) was dissolved in 3:1 ethanol:water and added to a flask containing freshly prepared thiazoline aldehyde **2.16** (38 mg, 0.187 mmol). Sodium acetate trihydrate was added until the reaction measured pH=7 (1.41 g, 10.7 mmol) and the reaction was stirred under argon for 16 hours (overnight). The reaction was concentrated and resuspended in water (50 mL). The reaction was brought to pH=3 with solid citric acid. The acidic aqueous layer was extracted with 3 x 100 mL EtOAc. The combined organic layers were washed with brine, dried over Na<sub>2</sub>SO<sub>4</sub>, filtered and concentrated. The crude was then dissolved in EtOAc/Methanol and gently heated (50 °C) while stirring until the reaction was complete by LC-MS. The reaction was concentrated, and the resulting oil was purified by silica gel flash chromatography (100% DCM) to afford a yellow oil (340 mg, 68%) as a mixture of diastereomers (**2.23** and **2.41**), which were purified by preparative HPLC (45% to 95% acetonitrile in water, 0.1% formic acid) to afford the product as a white solid (17.6 mg, 24% yield).

**Procedure B:**

Deprotected tricycle **2.47** 79 mg, 0.272 mmol) was dissolved in methanol (1.4 mL) and pH 6.4 phosphate buffer (1.4 mL). 2-hydroxybenzothiazole (30.7 mg, 0.258 mmol) was added to the reaction, which was then heated to 35°C and monitored. When the reaction was complete, the reaction was concentrated, then dissolved in deionized water. The organic layer was extracted with dichloromethane (3 x 5 mL), washed

with brine (5 mL), dried with sodium sulfate, filtered, concentrated, and HPLC purified to yield **2.23** in 2.8% yield (3.02 mg, 1.19 mmol)

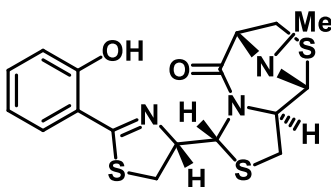
$^1\text{H NMR}$  (600 MHz,  $\text{CDCl}_3$ )  $\delta$  7.38 (dd,  $J = 7.8, 1.5$  Hz, 1H), 7.37 – 7.32 (m, 1H), 6.98 (dd,  $J = 8.3, 0.9$  Hz, 1H), 6.87 (td,  $J = 7.8, 1.1$  Hz, 1H), 5.75 (d,  $J = 6.0$  Hz, 1H), 4.86 (ddd,  $J = 8.5, 7.2, 6.0$  Hz, 1H), 4.61 (s, 1H), 4.03 (d,  $J = 6.9$  Hz, 1H), 3.83 (dd,  $J = 10.9, 5.2$  Hz, 1H), 3.45 – 3.39 (m, 2H), 3.32 (d,  $J = 10.7$  Hz, 1H), 3.22 (dd,  $J = 10.8, 6.4$  Hz, 1H), 2.99 (ddd,  $J = 14.6, 10.2, 7.3$  Hz, 2H), 2.28 (s, 3H)

$^{13}\text{C NMR}$  (150 MHz,  $\text{CDCl}_3$ )  $\delta$  173.93, 167.89, 159.35, 133.43, 130.88, 118.99, 117.37, 116.35, 80.79, 77.37, 77.16, 76.95, 73.21, 71.29, 69.53, 60.71, 40.22, 35.16, 34.66, 33.84

**IR** ( $\text{CHCl}_3$ ) 752 (w), 1029 (s), 1423 (w), 1668 (w), 2851 (w), 2923 (w), 3374 (b)

$[\alpha]_D^{25} +131$

**HRMS:** ( $\text{ES}^+$ ): Found: 394.0715 (+0.92 ppm),  $\text{C}_{17}\text{H}_{20}\text{O}_2\text{N}_2\text{S}_3$  ( $\text{M}^+$ ) requires: 394.0712



**(3R,6R,9R,9aR)-3-((S)-2-(2-hydroxyphenyl)-4,5-dihydrothiazol-4-yl)-10-methyltetrahydro-1H,2H,5H-6,9-epiminothiazolo[4,3-c][1,4]thiazepin-5-one (2.41)**

See **procedure A** for **2.23**. The product was isolated as a white solid (11.5 mg, 16% yield).

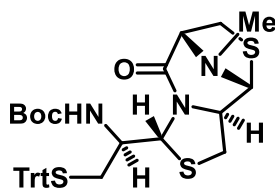
$^1\text{H NMR}$  (600 MHz,  $\text{CDCl}_3$ )  $\delta$  7.43 (dd,  $J = 7.8, 1.6$  Hz, 1H), 7.38 (ddd,  $J = 8.7, 7.3, 1.6$  Hz, 1H), 7.03 (dd,  $J = 8.3, 0.9$  Hz, 1H), 6.90 (td,  $J = 7.8, 1.1$  Hz, 1H), 5.65 (d,  $J = 7.7$  Hz, 1H), 4.92 (dd,  $J = 16.2, 8.2$  Hz, 1H), 4.74 (s, 1H), 4.11 (td,  $J = 3.5, 1.4$  Hz, 1H), 3.99 (dd,  $J = 11.2, 4.8$  Hz, 1H), 3.39 (dd,  $J = 11.2, 8.6$  Hz, 1H), 3.34 – 3.30 (m, 3H), 3.06 (dd,  $J = 11.2, 9.6$  Hz, 1H), 2.93 (dd,  $J = 9.5, 4.8$  Hz, 1H), 2.35 (s, 3H)

$^{13}\text{C NMR}$  (150 MHz,  $\text{CDCl}_3$ )  $\delta$  174.38, 168.31, 159.27, 133.53, 130.88, 119.09, 117.36, 116.31, 81.10, 77.37, 77.16, 76.95, 73.39, 71.43, 69.53, 61.27, 40.13, 35.41, 34.46, 34.18

**IR** ( $\text{CHCl}_3$ ) 754 (w), 1029 (s), 1466 (w), 1646 (w), 2850 (w), 2944 (w), 3397 (b)

$[\alpha]_D^{25} +135$

**HRMS:** ( $\text{ES}^+$ ): Found: 394.0714 (+0.70 ppm),  $\text{C}_{17}\text{H}_{20}\text{O}_2\text{N}_2\text{S}_3$  ( $\text{M}^+$ ) requires: 394.0712



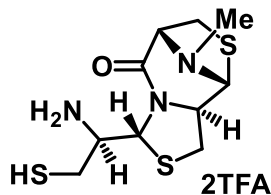
**tert-butyl((R)-1-((3R,6R,9R,9aR)-10-methyl-5-oxotetrahydro-1H,3H,5H-6,9-epiminothiazolo[4,3-c][1,4]thiazepin-3-yl)-2-(tritylthio)ethyl)carbamate (2.46)** To a reaction flask, aldehyde **2.39** (389 mg, 0.870 mmol) and deprotected thiazolidine **2.31** (392 mg, 0.870 mmol) were added and dissolved in ethanol (29 mL) and water (12 mL). The reaction vessel was wrapped in foil and sodium acetate was added (355 mg, 2.61 mmol). The reaction was allowed to stir overnight at which point it was concentrated, redissolved in deionized water and acidified with citric acid to pH 2. The organics were extracted with ethyl acetate (3 x 15 mL), washed with brine (15 mL), dried with sodium sulfate, filtered through celite, concentrated, and column purified (0 to 100 % ethyl acetate in hexanes) to yield tricycle **2.46** in 21% yield (114 mg, 72.3 mmol).

**<sup>1</sup>H NMR** (600 MHz, CDCl<sub>3</sub>) δ 7.43 – 7.40 (m, 6H), 7.30 (dd, *J* = 10.5, 5.0 Hz, 6H), 7.24 – 7.21 (m, 3H), 5.39 (d, *J* = 10.0 Hz, 1H), 4.94 (d, *J* = 9.3 Hz, 1H), 4.62 (s, 1H), 4.01 (d, *J* = 6.0 Hz, 1H), 3.89 – 3.84 (m, 1H), 3.80 (dd, *J* = 11.1, 5.4 Hz, 1H), 3.23 (dd, *J* = 10.6, 6.3 Hz, 1H), 3.15 (d, *J* = 10.7 Hz, 1H), 3.00 – 2.96 (m, 1H), 2.84 (dd, *J* = 9.3, 5.3 Hz, 1H), 2.49 (dd, *J* = 12.4, 3.8 Hz, 1H), 2.34 (dd, *J* = 12.4, 6.0 Hz, 1H), 2.30 (s, 3H), 1.46 (s, 9H)

**<sup>13</sup>C NMR** (151 MHz, CDCl<sub>3</sub>) δ 144.63 (s), 129.77 (d, *J* = 3.7 Hz), 128.08 (d, *J* = 6.1 Hz), 126.87 (d, *J* = 4.9 Hz), 77.37 (s), 77.16 (s), 76.95 (s), 28.66 (s)

**IR (neat)** 700 (s), 742 (w), 1162 (w), 1366 (w), 1445 (w), 1491 (w), 1676 (w), 1709 (w), 2851 (w), 2925 (w), 3060 (w), 3370 (br)

**[α]<sub>D</sub><sup>20</sup>** + 0.1



**(3R,6R,9R,9aR)-3-((R)-1-amino-2-mercaptoethyl)-10-methyltetrahydro-1H,3H,5H-6,9-**

**epiminothiazolo[4,3-c][1,4]thiazepin-5-one (2.47)** A solution of 1:1 dichloromethane (4.5 mL) and trifluoroacetic acid (4.5 mL) with 3% v/v triisopropylsilane (0.3 mL) was made, and then poured over tricycle **2.46** (112 mg, 0.177 mmol). The reaction was allowed to stir for 40 minutes at which point it was concentrated, dissolved in water and chloroform. The aqueous layer was extracted and lyophilized to yield the deprotected TFA salt in 86% yield (79 mg, 38.4 mmol).

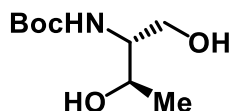
**<sup>1</sup>H NMR** (300 MHz, D<sub>2</sub>O) δ 5.61 (d, *J* = 8.7 Hz, 1H), 5.02 (s, 1H), 4.20 (s, 1H), 3.96 (dd, *J* = 11.0, 5.5 Hz, 1H), 3.53 (d, *J* = 8.8 Hz, 1H), 3.34 (d, *J* = 2.8 Hz, 2H), 3.14 – 3.06 (m, 1H), 3.02 (d, *J* = 4.7 Hz, 1H), 2.97 (d, *J* = 10.5 Hz, 1H), 2.83 (dd, *J* = 15.3, 6.9 Hz, 1H), 2.31 (s, 3H)

**<sup>13</sup>C NMR** (151 MHz, D<sub>2</sub>O) δ 163.13 (s), 117.30 (s), 115.37 (s), 70.19 (s), 69.13 (s), 54.22 (s), 38.62 (s), 34.01 (s), 33.30 (s), 33.08 (s)

**IR (neat)** 722 (w), 799 (w), 1132 (s), 1200 (s), 1430 (w), 1673 (s), 2879 (br), 2952 (br), 3202 (br), 3427 (br)

**[α]<sub>D</sub><sup>20</sup>** + 5.4

**HRMS:** (APCI<sup>+</sup>): Found: 292.06032 (-1.12 ppm), C<sub>10</sub>H<sub>18</sub>ON<sub>3</sub><sup>32</sup>S<sub>3</sub> (M<sup>+</sup>) requires: 292.06065



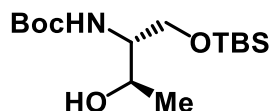
**tert-butyl((2R,3R)-1,3-dihydroxybutan-2-yl)carbamate (2.101)** A reaction flask and stir bar were base-bathed and flame dried under argon, then charged with methyl (*tert*-butoxycarbonyl)-*L*-threoninate (8.46 g, 36.3 mmol). Ethanol that had been dried over three angstrom molecular sieves, filtered through celite and magnesium sulfate, was added to the reaction flask (64 mL). The reaction was cooled in an ice bath to 0°C. Once cooled, sodium borohydride (2.88 g, 76.2 mmol) was added in small portions and stirred for 4.5 hours at which point the reaction was quenched with saturated ammonium chloride and diluted with ethyl acetate (30 mL). The organic layer was then washed with 1M hydrochloric acid (2 x 20 mL) and brine (2 x 20 mL), dried with magnesium sulfate, filtered through celite, and concentrated to yield **2.101** (5.92 g, 28.8 mmol) in 71%.

**<sup>1</sup>H NMR** (400 MHz, CDCl<sub>3</sub>) δ 5.39 (d, *J* = 9.1 Hz, 1H), 4.10 – 4.00 (m, 1H), 3.89 (s, 1H), 3.67 (dd, *J* = 5.0, 2.2 Hz, 2H), 3.45 (d, *J* = 5.7 Hz, 1H), 2.13 (d, *J* = 0.8 Hz, 1H), 1.39 (s, 9H), 1.15 (d, *J* = 6.4 Hz, 3H)  
**<sup>13</sup>C NMR** (126 MHz, CDCl<sub>3</sub>) δ 156.88 (s), 79.73 (s), 77.41 (s), 77.16 (s), 76.91 (s), 67.90 (s), 64.10 (s), 56.01 (s), 30.95 (s), 28.43 (s), 20.19 (s)

**IR (neat)** 752 (s), 1041 (w), 1063 (w), 1163 (s), 1247 (w), 1366 (w), 1503 (w), 1684 (s), 2885 (w), 2939 (w), 2976 (w), 3376 (br), 3436 (br)

**[α]<sub>D</sub><sup>20</sup>** -20

**HRMS:** (APCI<sup>+</sup>): Found: 206.1386 (-0.29 ppm), C<sub>9</sub>H<sub>20</sub>O<sub>4</sub>N (M<sup>+</sup>) requires: 206.1387



***Tert*-butyl((2*R*,3*R*)-1-((*tert*-butyldimethylsilyloxy)-3-hydroxybutan-2-yl)carbamate (2.102)** To a flame dried round-bottom flask, a stir bar compound **2.101** (1.30 g, 6.32 mmol) and dichloromethane (16 mL) was added. Then, freshly distilled triethylamine (1.8 mL, 12.6 mmol) and 4-dimethylaminopyridine (77.6 mg, 0.632 mmol) were added. The reaction was cooled to 0°C and then *tert*-butyldimethylsilyl chloride (1.00 g, 6.64 mmol) was added. The reaction was allowed to stir and warm to room temperature overnight. It was then quenched with 1M hydrochloric acid (15 mL) and diluted with ethyl acetate. The organic phase was separated and washed with 1M hydrochloric acid (15 mL) and brine (2 x 15mL), dried with magnesium sulfate, filtered through celite, and concentrated. The product was then purified through column chromatography (0 to 50% ethyl acetate in hexanes) to yield **2.102** (1.16 g, 3.62 mmol) in 90%.

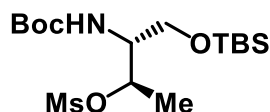
**<sup>1</sup>H NMR** (400 MHz, CDCl<sub>3</sub>) δ 5.18 (d, *J* = 8.4 Hz, 1H), 4.15 (d, *J* = 6.3 Hz, 1H), 3.88 (dd, *J* = 10.3, 3.3 Hz, 1H), 3.81 (dd, *J* = 10.3, 2.6 Hz, 1H), 3.47 – 3.42 (m, 1H), 3.33 (s, 1H), 1.44 (s, 9H), 1.17 (d, *J* = 6.4 Hz, 3H), 0.91 – 0.86 (m, 9H), 0.13 – 0.01 (m, 6H)

**<sup>13</sup>C NMR** (126 MHz, CDCl<sub>3</sub>) δ 156.38 (s), 79.47 (s), 77.41 (s), 77.15 (s), 76.90 (s), 69.56 (s), 66.54 (s), 55.00 (s), 28.53 (s), 25.95 (s), 20.04 (s), 18.28 (s), -5.49 (s)

**IR (neat)** 754 (s), 776 (w), 835 (s), 1099 (w), 1167 (w), 1252 (w), 1366 (w), 1499 (w), 1692 (w), 2857 (w), 2929 (w), 2955(w), 3443 (br)

**[α]<sub>D</sub><sup>20</sup>** -50

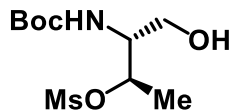
**HRMS:** (APCI): Found: 318.2110 (1.27 ppm), C<sub>15</sub>H<sub>32</sub>O<sub>4</sub>NSi (M<sup>+</sup>) requires: 318.2106



**(2*R*,3*R*)-3-((*tert*-butoxycarbonyl)amino)-4-((*tert*-butyldimethylsilyloxy)butan-2-yl methanesulfonate (2.99)** To a flame dried flask under argon, compound **2.102** (1.46 g, 4.56 mmol) was added and dissolved in dichloromethane (1.5 mL). Then freshly distilled triethylamine (11 mL, 9.58 mmol) and 4-dimethylaminopyridine (55.7 mg, 0.456 mmol) were added and the reaction was cooled to 0°C. Once cool, mesyl chloride (1.01 mL, 13.7 mmol) was added and allowed to stir for 2.5 hours. The reaction was quenched with 1 M hydrochloric acid (10 mL) and diluted with ethyl acetate (15 mL). The organic layer was separated and washed with 1 M hydrochloric acid (10 mL), sodium bicarbonate (2 x 10 mL), and brine (10 mL). The organic layer was then dried with magnesium sulfate, filtered through celite, concentrated to yield **2.102** in 89 % carried through crude due to instability.

**<sup>1</sup>H NMR** (400 MHz, CDCl<sub>3</sub>) δ 5.03 (dd, *J* = 6.4, 3.4 Hz, 1H), 4.74 (d, *J* = 9.6 Hz, 1H), 3.79 – 3.71 (m, 1H), 3.69 (dd, *J* = 10.1, 4.6 Hz, 1H), 3.53 (dd, *J* = 10.1, 7.8 Hz, 1H), 3.04 (s, 3H), 1.50 – 1.42 (m, 12H), 0.89 (s, 9H), 0.08 (d, *J* = 3.7 Hz, 6H)





**(2R,3R)-3-((tert-butoxycarbonyl)amino)-4-hydroxybutan-2-yl methanesulfonate (2.103) 2.99** (1.83 g, 4.60 mmol) was added to a flame dried round bottom flask under argon and dissolved in THF (23 mL). To this solution, 1M tetrabutylammonium fluoride (11.5 mL, 11.5 mmol) was added. After one hour, the reaction was quenched with saturated ammonium chloride (15 mL). The organic layer was washed with saturated ammonium chloride (3 x 10 mL) and brine (15 mL), dried with magnesium sulfate, filtered through celite, concentrated, and column purified (0 to 50% ethyl acetate in hexanes) to yield a clear, light yellow oil in 64% yield (0.832 g, 2.94 mmol).

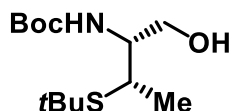
$^1\text{H NMR}$  (400 MHz,  $\text{CDCl}_3$ )  $\delta$  5.10 (dt,  $J = 6.4, 3.2$  Hz, 1H), 4.80 (d,  $J = 8.9$  Hz, 1H), 3.74 (dd,  $J = 19.9, 8.1$  Hz, 2H), 3.64 – 3.53 (m, 1H), 3.06 (s, 3H), 2.51 (s, 1H), 2.17 (s, 2H), 1.50 – 1.40 (m, 12H)

$^{13}\text{C NMR}$  (126 MHz,  $\text{cdCl}_3$ )  $\delta$  155.90 (s), 80.10 (s), 77.94 (s), 77.26 (s), 77.01 (s), 76.75 (s), 61.59 (s), 55.31 (s), 38.32 (s), 30.90 (s), 28.27 (s), 18.31 (s)

**IR (neat)** 751 (s), 904 (s), 974 (w), 1165 (s), 1331 (w), 1515 (w), 1692 (s), 2882 (br), 2939 (w), 2983 (w), 3383 (br)

$[\alpha]_D^{20} +3$

**HRMS:** (APCI<sup>+</sup>): Found: 284.1158 (-1.63 ppm),  $\text{C}_{10}\text{H}_{22}\text{O}_6\text{N}^{32}\text{S}$  ( $\text{M}^-$ ) requires: 284.1162



**tert-butyl ((2R,3R)-3-(tert-butylthio)-1-hydroxybutan-2-yl)carbamate (2.104)** A reaction flask was base bathed and flame dried under argon. To the flask, sodium hydride (60% in mineral oil, 0.532 g, 13.3 mmol) was added and suspended in DMF (5.5 mL). The suspension was then cooled to 0°C and *tert*-butyl thiol (1.75 mL, 15.5 mmol) was added dropwise. The reaction was warmed to room temperature and stirred for 10 minutes, then cooled to -13°C in a salt/ice bath. Then **2.103** (2.51 g, 8.87 mmol) was dissolved in DMF (5.5 mL) and added with the assistance of a syringe pump at a rate of 0.35 mL/min. Once the addition was complete, the reaction was allowed to warm to room temperature overnight. The reaction was quenched with saturated ammonium chloride (5 mL) and diluted with ethyl acetate (5 mL). The aqueous phase was extracted with ethyl acetate (1 x 10 mL). The organic phases were combined and washed with deionized water (10 mL) and brine (2 x 10 mL), dried with magnesium sulfate, filtered through celite, concentrated, and column purified (0 to 40 % ethyl acetate in hexanes) to yield **2.104** in 67 % (1.68 g, 6.06 mmol).

$^1\text{H NMR}$  (400 MHz,  $\text{CDCl}_3$ )  $\delta$  4.51 (d,  $J = 9.3$  Hz, 1H), 4.35 (dd,  $J = 10.0, 5.1$  Hz, 1H), 4.29 (ddd,  $J = 9.1, 6.8, 2.1$  Hz, 1H), 3.64 (ddd,  $J = 12.4, 10.1, 5.8$  Hz, 1H), 3.41 (td,  $J = 11.9, 5.1$  Hz, 1H), 2.65 (ddd,  $J = 11.2, 5.8, 2.1$  Hz, 1H), 1.41 (s, 9H), 1.29 (d,  $J = 6.9$  Hz, 12H)

$^{13}\text{C NMR}$  (126 MHz,  $\text{CDCl}_3$ )  $\delta$  157.06 (s), 80.28 (s), 77.41 (s), 77.16 (s), 76.91 (s), 64.62 (s), 50.42 (s), 44.67 (s), 42.74 (s), 31.70 (s), 28.40 (s), 19.43 (s)

**IR (neat)** 1017(s), 1090 (w), 1165 (s), 1280 (s), 1364 (w), 1536 (w), 1546 (s), 1672 (s), 2936 (w), 2965 (w), 2980 (w), 3246 (w), 3360 (w)

$[\alpha]_D^{20} -3.5$

**HRMS:** (APCI<sup>+</sup>): Found: 278.1782 (-0.74 ppm),  $\text{C}_{13}\text{H}_{28}\text{O}_3\text{NS}$  ( $\text{M}^+$ ) requires: 278.1784

## 7.2 Experimental Spectra

